Precise Design and Surface Modification of Poly(ε-caprolactone)-based 2D Assemblies

Tianlai Xia



A thesis submitted to the University of Birmingham for the degree of

MASTER OF SCIENCE BY RESEARCH

Supervisors: Prof. Rachel O'Reilly and Prof. Andrew Dove

School of Chemistry

University of Birmingham

February 2021

UNIVERSITY OF
BIRMINGHAM

University of Birmingham Research Archive

e-theses repository

This unpublished thesis/dissertation is copyright of the author and/or third parties. The intellectual property rights of the author or third parties in respect of this work are as defined by The Copyright Designs and Patents Act 1988 or as modified by any successor legislation.

Any use made of information contained in this thesis/dissertation must be in accordance with that legislation and must be properly acknowledged. Further distribution or reproduction in any format is prohibited without the permission of the copyright holder.

This thesis is dedicated to my parents Weihong and Xiangping for their unconditional love, constant encouragement and invaluable support.

Table of Contents

Table of Contents II

List of Schemes VII

List of Figures IX

List of Tables XVII

Acknowledgments XVIII

Declaration of Authorship XX

Publication XXI

Thesis Summary XXII

List of Abbreviations XXIV

Chapter One - Introduction 1

1.1 Synthetic Polymer Building Block 2

1.1.1 Living Polymerisation 3

1.1.2 Reversible-Deactivation Radical Polymerisation 4

1.1.2.1 Persistent Radical Effect 5

1.1.2.2 Degenerative Transfer Effect 5

1.1.2.3 Choice of RAFT Agent and Monomer 7

1.1.3 Light Mediated Polymerisation 10

1.1.4 Ring Opening Polymerisation 12

1.2 Self-Assembly of Block Copolymers 14

1.2.1 Polymer Solution Self-Assembly 15

1.2.2 Crystallisation-Driven Self-Assembly 17
1.2.3 Precise Morphology and Size Control by CDSA 20
1.2.3.1 Length Control of 1D Structures 20
1.2.3.2 Size Control of 2D Structures 23
1.2.3.3 Spatial Control of Hierarchical Structures 29
1.3 Surface Modification of Nanomaterials 31
1.3.1 Traditional Physical and Chemical Routes 31
1.3.2 Surface-Initiated Functionalisation 32
1.4 Summary 35
1.5 References 36
Chapter Two – Uniform two-dimensional poly(ε-caprolactone)-based platelets *via* crystallisation-driven self-assembly 49
2.1 Abstract 50
2.2 Introduction 51
2.3 Results and Discussion 54
2.3.1 Synthesis of Dual Head Chain Transfer Agent (CTA) 54
2.3.2 Synthesis of Homopolymer and Block Copolymer 56
2.3.2.1 Ring Opening Polymerisation of Poly(*ε*-Caprolactone) (PCL) 57
2.3.2.2 RAFT Polymerisation of PCL-*b*-PDMA 61
2.3.2.3 Fluorescent Functionalisation of PCL and PCL-*b*-PDMA 63
2.3.3 Crystallisation-Driven Self-Assembly (CDSA) of PCL-*b*-PDMA 65
2.3.4 Two-Dimensional Epitaxial Growth 67

2.3.4.1 Effect of Homopolymer Amounts on Assemblies Morphologies.....67

2.3.4.2 2D 'living' CDSA.....68

2.3.5 Sequential Growth of Multi-Layered Platelet.....73

2.3.6 Fluorescent Multi-Layered Platelet.....74

2.4 Conclusions.....77

2.5 Experimental.....78

2.5.1 Materials.....78

2.5.2 Instrumentation.....78

2.5.3 Experimental Procedures.....82

2.5.3.1 Synthesis of 4-cyano-4-(((ethylthio)carbonothioyl)thio)pentanoic acid (CEPA).....82

2.5.3.2 Synthesis of 2-cyano-5-hydroxypentan-2-yl ethyl carbonotrithioate (CHPET).....83

2.5.3.3 Synthesis of Poly(ε-Caprolactone) (PCL).....84

2.5.3.4 Synthesis of PCL-*b*-PDMA.....85

2.5.3.5 Synthesis of PCL-ACM.....85

2.5.3.6 Synthesis of PCL-*b*-PDMA-ACM.....85

2.5.3.7 Crystallisation-Driven Self-Assembly of PCL-*b*-PDMA Cylinder.....86

2.5.3.8 Preparation of PCL-*b*-PDMA Seeds Solution.....86

2.5.3.9 Living Epitaxial Growth of 2D Platelet.....86

2.5.3.10 Sequential Growth of Multi-Layered Platelet.....87

2.5.3.11 Growth of Fluorescent Multi-Layered Platelet.....87

2.6 References 88

Chapter three – Precision surface modification of poly(ε-caprolactone) assemblies *via* photo RAFT polymerisation 93

3.1 Abstract 94

3.2 Introduction 95

3.3 Results and Discussion 99

3.3.1 Photo RAFT Polymerisation on Platelets Surface 99

3.3.2 Photo RAFT of Fluorescent Monomer 101

3.3.3 Photo RAFT with Different DMA Monomer Concentration 102

3.3.4 Photo RAFT with Different Monomers 104

3.3.5 Spatial Selective Modification on the Surface of Platelets 105

3.3.5.1 Removal of Trithiocarbonate End Group 106

3.3.5.2 Growth of Multi-Layered Platelets 109

3.3.5.3 Photo RAFT on the Surface of Multi-Layered Platelets 110

3.3.5.4 Photo RAFT with Fluorescent Dye on the Surface of Multi-Layered Platelets 112

3.4 Conclusions 114

3.5 Experimental 115

3.5.1 Materials 115

3.5.2 Instrumentation 115

3.5.3 Experimental procedures 116

3.5.3.1 Photo RAFT polymerisation on platelets surface 116

3.5.3.2 Synthesis of PCL-H 117

3.5.3.3 Synthesis of PCL-*b*-PDMA-H 117

3.5.3.4 Epitaxial growth of platelets 118

3.5.3.5 Sequential growth of multi-layered platelets 118

3.6 References 119

Chapter Four – Conclusions and Outlook 124

List of Schemes

Scheme 1.1 Mechanism of RAFT polymerisation.[51] 6

Scheme 1.2 Representative mechanisms for photo mediated polymerisation involving an intramolecular photochemical process and a photoredox process. Adapted from ref.[67] 10

Scheme 1.3 Overview of the iniferter mechanism for photo mediated polymerisation.[67, 73] 11

Scheme 1.4 Ring opening polymerisation of lactones using DPP as a catalyst.[90, 91] 14

Scheme 1.5 Basic mechanism of crystallisation-driven self-assembly.[104] 18

Scheme 2.1 Synthetic strategy of multi-layered platelets with controlled dimensions. 53

Scheme 2.2 Three-step synthesis of dual-head RAFT chain transfer agent CHPET. 54

Scheme 2.3 Synthesis of PCL macro CTA and PCL-*b*-PDMA block copolymer by ROP and RAFT polymerisation. 57

Scheme 2.4 Design of fluorescent functionalised homopolymer and block copolymer. 63

Scheme 2.5 Mechanism of preparing multi-layered platelets by sequential seeded growth. 73

Scheme 2.6 Mechanism of preparing fluorescent modified multi-layered platelets by sequential seeded growth. 74

Scheme 3.1 Strategy of surface modification of platelets prepared by CDSA via photo-RAFT polymerisation. Red dots: Light responsive group for photo RAFT. Yellow line: Extended corona after photo RAFT. 98

Scheme 3.2 Strategy of fluorescence modification of PCL/PCL-*b*-PDMA platelet via photo RAFT polymerisation. 101

Scheme 3.3 Route of spatial selective modification on the surface of platelets..... 106

Scheme 3.4 Design of RAFT group removed homopolymer and block copolymer. 107

Scheme 3.5 Design of alternate RAFT or nonRAFT layered platelet..... 109

Scheme 3.6 Route of spatial selective functionalisation with fluorescent dye on the surface of platelets. 112

List of Figures

Figure 1.1 Main polymer characteristics that can be modulated to control the polymer architecture and properties. Adapted from ref.[26] 2

Figure 1.2 A brief timeline representing the development of living polymerisation. Figure adapted from ref.[28] 4

Figure 1.3 Structure of RAFT chain transfer agents with different Z groups (dithioester Z=R', trithiocarbonate Z=SR', dithiocarbamate Z=NR'R'', xanthate Z=OR').[54] 8

Figure 1.4 General guidelines for RAFT agent R and Z group for various monomer classes. Addition rate decreases (fragmentation rate increases) from left to right. Dashed lines indicate partial control.[51] 9

Figure 1.5 Chemical structure of selected iniferters used in photo mediated polymerisation. Adapted from refs.[60, 67] 12

Figure 1.6 Schematic illustration of possible self-assembled morphologies obtained by different packing parameters, p.[21] 16

Figure 1.7 TEM micrographs of (left) crystal platelets of PEO-PS copolymer,[105] (right) long rod-like micelles of PFS-*b*-PDMS.[106] 18

Figure 1.8 Chemical structures of the semi-crystalline core-forming block commonly reported in the literature. Adapted from ref.[139] 19

Figure 1.9 Living PI-CDSA (at 10% w/w solids) of PIP-b-PFDMS with a block ratio of approximately 5.3:1 in 10% v/v THF/n-hexanes. (a) Schematic representation of the preparation of near monodisperse PIP-b-PFDMS cylindrical micelles via living PI-CDSA. TBP was used as a quenching agent. PI-CDSA seeded growth of PIP-b-PFDMS cylindrical micelles was carried out at 10% w/w solids in 10% v/v THF/n-hexanes. (b–i) TEM micrographs of dried near monodisperse cylindrical micelles of PIP-b-PFDMS

prepared by living PI-CDSA. (b) Small seed micelles prepared by the ultrasonication of long polydisperse micelles. PIP-to-seed ratios of (c to i) 3:1 - 21:1. Adapted from ref.[101] 22

Figure 1.10 (a) Schematic representation of epitaxial growth in water using PCL_{50}-b-$PMMA_{20}$-b-$PDMA_{200}$ triblock copolymer. TEM micrographs of cylindrical micelles epitaxially grown from seed micelles in water with an unimer/seed ratio of (b-e) 1, 5, 9, and 15. (f) TEM micrograph and (g) confocal image of fluorescently labeled cylindrical micelles epitaxially grown from seed micelles in water with an unimer/seed ratio of 15. (h) Length dispersity of cylindrical micelles. (i) Plot showing a linear epitaxial growth regime of cylinders with narrow length dispersities in comparison to the theoretical length. Adapted from ref.[130] 23

Figure 1.11 Uniform diamond platelet micelles prepared by seeded growth of $PLLA_{24}[PPh_2Me]I$. **(a)** Schematic representation of the formation of diamond platelets through seeded growth. (**b**–**e**) TEM images of uniform diamond platelets formed through seeded growth from a 1D seed with m_{unimer}/m_{seed} of 5:1-20:1. (**f**) AFM image of a diamond platelet micelle. (**g**) Height profile of the diamond platelet. (**h**) Linear dependence of micelle area on the m_{unimer}/m_{seed}. (**i**) Schematic diagram showing the formation of fluorescent concentric diamond block co-micelles in two dimensions from a non-fluorescent diamond platelet by the sequential addition of fluorescent blend and non-fluorescent $PLLA_{24}[PPh_2Me]I$ in $CHCl_3$ and visualised by LSCM. (**j**, **k**) LSCM images of diblock (**j**) and tetra-block (**k**) co-micelles with segregated regions comprised of non-fluorescent blocks and fluorescent blocks. Adapted from ref.[110] 25

Figure 1.12 Patchy and hollow rectangular platelet micelles. Concentric rectangular platelet block co-micelles can be prepared through the sequential, alternate addition of PFS_{36}-b-$P2VP_{502}/PFS_{20}$ and PFS_{28}-b-$PDMS_{560}/PFS_{20}$ blend unimers. (A) Schematic

diagram illustrating this process. (B) TEM, AFM height, and AFM 3D images of triblock co-micelles formed through the sequential addition of the PFS_{36}-b-$P2VP_{502}/PFS_{20}$, PFS_{28}-b-$PDMS_{560}/PFS_{20}$, and PFS_{36}-b-$P2VP_{502}/PFS_{20}$ blend unimers to a solution of the PFS_{28}-b-$PDMS_{560}$ seeds in a mixture of hexane and iPrOH. (C) TEM image of platelets after cross-linking of the P2VP coronas. (D and E) TEM and AFM height images of a mixture of perforated rectangular platelets and well-defined hollow rectangular rings formed after redispersal in THF. Adapted from ref.[99] 27

Figure 1.13 (A) Schematic illustration of seeded growth of 2D platelets used as precursors upon the addition of BCP unimers resulting in the significant increase in the lateral dimension of preformed platelets. TEM images of a representative sample prepared by the seeded growth of (B) PCL_{101}-b-PF_{178} platelet seed precursors in aqueous solution by the addition of the corresponding BCP PCL_{101}-b-PF_{178} unimers aged at 3-4 °C led to the formation of (C, D) supersized 2D hexagonal platelets (Scale bar = 2 μm). Adapted from ref.[98] 28

Figure 1.14 TEM images and schematic representations of supermicelles. (a) Side-by-side stacking of P-H-P triblock co-micelles including PFS-b-P2VP (green) and PFS-b-PDMS (red); (b) End-to-end stacking of P-H-P triblock comicelles including PFS-b-P2VP (green) and PFS-b-PDMS (red); (c) End-to-end stacking of H-P-H triblock comicelles consists of PFS-b-P2VP (green) and PFS-b-PDMS (red). Adapted from ref.[103] 29

Figure 1.15 Pictorial representations and corresponding TEM images of (a, c) the M(PFDMS-b-PDMS)-b-M(PFDMS-b-XLPI)@PFDMS and (b, d) the M(PFDMS-b-XLPI)-b-M(PFDMS-b-PDMS)@PFDMS multiarmed diblock co-micelles. Adapted from ref.[147] 30

Figure 1.16 Conventional surface decoration methods. (a) spray; (b) spin-coating; (c) electrochemical deposition; (d) heat treatment.[150-153] 31

Figure 1.17 Seeded growth of hydrophilic PFS-b-P2VP and segmented micellar brushes on a silicon wafer. (A) Schematic illustration of the growth process for PFS_{20}-b-$P2VP_{140}$ micellar brushes. (B to D) AFM height images of (C) PFS_{36}-b-$P2VP_{502}$ seed-coated silicon wafer and PFS_{20}-b-$P2VP_{140}$ micellar brushes formed by the addition of (B, D) 4 and 10 ml unimers solution, respectively. (E) Schematic illustration of the growth process for PFS_{30}-b-$P2VP_{226}$ micellar brushes and segmented micellar brushes. (F to H) AFM height images of (G) short PFS_{30}-b-$P2VP_{226}$ micellar brushes formed by the addition of 3 ml unimer solution, (F) elongated micellar brushes formed by further addition of 3 mL of PFS_{30}-b-$P2VP_{226}$ unimer solution to the short micellar brushes shown in (G), and (H) segmented micellar brushes formed by further addition of 3 ml of PFS_{32}-b-$PDMS_{385}$ unimer solution to the short micellar brushes shown in (G). Adapted from ref.[108] 33

Figure 1.18 Patterning of polymer brushes from substrates uniformly functionalised with trichlorosilane-substituted a-bromoisobutyrate based initiators (a) using b) a photomask for patterns or c) a neutral density filter for gradient structures. DMF = N,N-dimethylformamide, ppy = 2-phenylpyridine. Adapted from ref.[70] 34

Figure 2.1 ^{1}H NMR (400 MHz) and ^{13}C NMR (100 MHz) spectra of 4-cyano-4-(((ethylthio)carbonothioyl)thio)pentanoic acid (CEPA) in $CDCl_3$. 55

Figure 2.2 ^{1}H NMR (400 MHz) and ^{13}C NMR (100 MHz) spectra of 2-cyano-5-hydroxypentan-2-yl ethyl carbonotrithioate (CHPET) in $CDCl_3$. 56

Figure 2.3 Kinetic for the ROP of ε-caprolactone. Top: ^{1}H NMR of ROP kinetic of ε-caprolactone at different reaction time. Bottom: plot of ln of initial monomer

concentration by monomer concentration (ln([M_0]/[M_t])) against time for the ROP of ε-caprolactone. 58

Figure 2.4 ^{1}H NMR spectrum of PCL_{50} in $CDCl_3$ (400 MHz). 59

Figure 2.5 SEC chromatogram (RI and UV 309 nm trace) of PCL_{50} using $CHCl_3$ with 0.5% TEA as an eluent. Poly(methyl methacrylate) (PMMA) was used as a standard. 59

Figure 2.6 MALDI-TOF mass spectrum of PCL_{50}. Minor distribution corresponds to sodium ion of the fragmentation of the trithiocarbonate.[60] 60

Figure 2.7 ^{1}H NMR spectrum of PCL_{50}-b-$PDMA_{198}$ in $CDCl_3$ (400 MHz). 62

Figure 2.8 SEC chromatogram (RI and UV 309 nm trace) of PCL_{50}-b-$PDMA_{198}$ using $CHCl_3$ with 0.5% TEA as an eluent (PMMA standard). 62

Figure 2.9 ^{1}H NMR spectra of PCL_{50} homopolymer before and after coupling with fluorescent molecule ACM in $CDCl_3$ (400 MHz). 64

Figure 2.10 SEC chromatogram (UV trace, 360 nm) of PCL_{50} homopolymer before and after coupling with fluorescent molecule ACM using $CHCl_3$ with 0.5% TEA as an eluent with PMMA standards. 64

Figure 2.11 SEC chromatogram (UV trace, 360 nm) of block copolymer PCL_{50}-b-$PDMA_{198}$ before and after coupling with fluorescent molecule ACM using $CHCl_3$ with 0.5% TEA as an eluent with PMMA standards. 65

Figure 2.12 Transmission electron microscopy (TEM) images of cylindrical micelles (0.5 mg mL^{-1}) prepared using PCL_{50}-b-$PDMA_{198}$ in ethanol, heating at 70 °C for 3 h and subsequently cooling down to room temperature (stained with 1 wt. % uranyl acetate in water). (TEM images collected by Mr. Bo Li.) 66

Figure 2.13 TEM micrographs of PCL_{50}-b-$PDMA_{198}$ cylinders assembled in ethanol after sonication at 0 °C for 20 min using a sonic probe (stained with 1 wt. % uranyl acetate in water). (TEM images collected by Mr. Bo Li). 67

Figure 2.14 Effect of PCL homopolymer concentration on the assemblies by seeded epitaxial growth. m_{PCL}: $m_{PCL\text{-}b\text{-}PDMA}$=0.25, 0.5, 0.75, 1, 1.25, 2, 3 and 5; The crystalline seeds are prepared from PCL_{50}-b-$PDMA_{198}$ cylinder. The unimer-to-seed ratio is fixed as 10. Top: AFM images of PCL_{50}/PCL_{50}-b-$PDMA_{198}$ blending platelets; Bottom: Plots of 2D assemblies' length versus m_{unimer}/m_{seed}. 68

Figure 2.15 (a) AFM images and (b) CLSM images of PCL_{50}/PCL_{50}-b-$PDMA_{198}$ (mass ratio=1) blending platelets grown from PCL_{50}-b-$PDMA_{198}$ crystalline seeds with m_{unimer}/m_{seed} of 1, 3, 6, 9, 12, 20, 30, 40, 50, 60, 70 and 80; (c) graph showing the linear dependence of 2D platelet length, width, ratio of length-to-width and area upon the unimer-to-seed ratio. (Normally, the concentration of unimers is 10 mg mL^{-1}, when the ratio of unimers to seeds above 20, it changes to 50 mg mL^{-1}) (CLSM images collected by Dr. Yujie Xie.) 71

Figure 2.16 AFM (top) and TEM (bottom) images of multi-layered platelets of (a) single, (b) double, (c) triple and (d) quadruple layered after sequential seeded growth. (TEM images collected by Mr Bo Li).....74

Figure 2.17 CLSM images of fluorescent modified multi-layered platelets by sequential epitaxial growth. (scale bar = 2 μm) (CLSM images collected by Dr. Yujie Xie.) 75

Figure 2.18 CLSM images of fluorescent platelets after different period of time (2, 10 and 35 days). (scale bar = 2 μm) (CLSM images collected by Dr. Yujie Xie.) 76

Figure 3.1 The applications of surface modified materials. (a) CO_2 catalysis,[46] (b) adhesion,[41] (c) lubrication,[40] and (d) energy storage.[33].....96

Figure 3.2 AFM images and height profiles of platelet before (left) and after (right) photo RAFT polymerisation; below: height measured at selected region (line). 99

Figure 3.3 SEC chromatogram of PCL/PCL-b-PDMA platelets before and after photo RAFT polymerisation using $CHCl_3$ with 0.5% TEA as an eluent with PMMA standards. (Blue line present the molecular weight distribution of original platelets; Red line presents the molecular weight distribution of platelets after photo RAFT).....100

Figure 3.4 CLSM images of platelets after photo RAFT with fluorescent dye. Left: confocal field; Right: bright field. (Scale bar = 3 μm) (CLSM images collected by Dr. Yujie Xie.).....102

Figure 3.5 AFM images of platelets reacted with different concentration of DMA (0, 10, 25, 50, 75, 100, 200 and 400 equivalent) before and after photo RAFT. 103

Figure 3.6 Plots of platelets height against the concentration of DMA monomer....103

Figure 3.7 SEC chromatogram of PCL/PCL-b-PDMA platelets reacted with different monomer (a) DMA, (b) NIPAm, (c) 4VP, and (d) DMAEMA before and after photo RAFT polymerisation using $CHCl_3$ with 0.5% TEA as an eluent with PMMA standards. 105

Figure 3.8 ^1H NMR spectrum of PCL_{50} homopolymer before and after removing end group in $CDCl_3$ (400 MHz).....107

Figure 3.9 SEC chromatogram (UV trace, 309 nm) of PCL_{50} homopolymer before and after removing end group using $CHCl_3$ with 0.5% TEA as an eluent with PMMA standards. 108

Figure 3.10 SEC chromatogram (UV trace, 309 nm) of block copolymer PCL_{50}-b-$PDMA_{198}$ before and after removing end group using $CHCl_3$ with 0.5% TEA as an eluent with PMMA standards. 108

Figure 3.11 AFM images and height profiles of double-layered platelet. Top: inner layer - RAFT layer, outer layer - nonRAFT layer; Bottom: inner layer - nonRAFT layer, outer layer - RAFT layer. 110

Figure 3.12 AFM images and height profiles of double-layered platelet (inner layer: RAFT layer, outer layer: nonRAFT layer) before and after photo RAFT with DMA. 111

Figure 3.13 AFM images and height profiles of double-layered platelet (inner layer: nonRAFT layer, outer layer: RAFT layer) before and after photo RAFT with DMA. 111

Figure 3.14 CLSM images of double-layered platelet before and after photo RAFT with fluorescent dye. (a) Inner layer: RAFT layer, outer layer: nonRAFT layer; (b) Inner layer: nonRAFT layer, outer layer: RAFT layer. (CLSM images collected by Dr. Yujie Xie.) 113

List of Tables

Table 2.1 MALDI-TOF data of PCL_{50}.[a] 60

Table 2.2 Length, width and area dispersity of platelet micelles.[a] 72

Acknowledgments

Firstly, I would like to thank Professor Rachel O'Reilly for having me in our warm O'DOVEILLY group and giving me the opportunity to conduct a research project. Rachel's high scientific standards, attention to detail and willingness to teach these to me, are qualities that I hope to possess. I am truly grateful for Rachel's guidance, encouragement, patience, understanding and support in both my research and my life! It would be impossible to count all the ways that Rachel has helped me!

I would also like to thank Prof. Andrew Dove, whose advice and guidance have been of help to me as well as his enthusiasm towards the progress of my work. A massive thanks go to Dr. Maria Chiara Arno as well for her countless help, kind advice and patient guidance. I will miss our weekly meeting for programme discussion.

I would like to express my gratitude to all members of the O'DOVEILLY group, past and present, who have made my Master experience a very enjoyable and unforgettable time. My thank-you goes to Dr. Amanda Pearce, Dr. Josh Worch, Dr. Kayla Delle Chiaie and Mr. Simon Dale for their countless help in answering my stupid questions and sorting my problems. A special gratitude goes to the "Chinese Mafia": Massive thanks to Dr. Wei Yu for his advice and selfless support throughout the year. I would like to thank Dr. Yujie Xie for providing massive help, invaluable suggestions, and discussions in my project. And huge thanks go to Mr. Bo Li, for his constant help and patience on training me and all the skills I learnt from him, from using Schlenk line to synthesising polymer. Massive thanks go also to Dr. Maria Chiara Arno, Dr. Yujie Xie and Mr. Simon Dale for proof-reading my thesis.

Finally, I am forever grateful to my parents, Weihong Xia and Xiangping Li for their endless support and encouragement which has kept me going.

Declaration of Authorship

This thesis is submitted to the University of Birmingham in support of my application for the degree of Master of Science by research. It has been composed by myself and has not been submitted in any previous application for any degree. The work presented (including data generated and data analysis) was carried out by myself, except in the following cases which are outlined below:

Chapter 2: Confocal laser scanning microscopy analysis were conducted by Dr. Yujie Xie. Transmission electron microscopy images were acquired by Mr. Bo Li.

Chapter 3: Confocal laser scanning microscopy analysis were conducted by Dr. Yujie Xie.

Publication

Precise Design and Surface Modification of Poly(ε-caprolactone)-based 2D Assemblies. (Manuscript in preparation)

Thesis Summary

This thesis investigates the precise design of poly(ε-caprolactone)-based 2D assemblies and their selective surface modification.

Chapter One provides a broad introduction of the research, discussing the importance of achieving morphology and size control over nanostructures, polymerisation techniques, self-assembly methods, and surface modification approaches.

Chapter Two demonstrates a controlled fabrication approach of uniform poly(*ε*-caprolactone)-based 2D assemblies utilizing seeded epitaxial crystallisation methods. Exquisite control over the multiblock co-micelles in morphology and dimensions was achieved by altering the amount of added unimers. Moreover, fluorescent labelling was achieved by polymer modification with fluorophores, providing a platform for future applications such as fluorescent imaging or biocompatible and biodegradable carriers.

Chapter Three reports a facile method for the preparation of poly(*ε*-caprolactone)-based platelets *via* crystallisation-driven self-assembly (CDSA), in which the height can be finely tuned by *in situ* photo-RAFT polymerisation. Furthermore, a fluorescent monomer could be synthesised and polymerised on the surface of such platelets allowing confocal microscopic imaging. More importantly, the prepared 2D platelet micelles could be selectively functionalised on the surface with different monomers through selective photo RAFT polymerisation, achieving spatial control over the platelet height. Such strategy has opened the possibility of highly controlled surface functionalisation for soft materials, providing potential applications in material science and polymer chemistry.

Chapter Four summarises the research presented in Chapter Two and Three, providing key conclusions as well as discussing the scope for future directions in this area of research.

List of Abbreviations

1D	One-dimensional
2D	Two-dimensional
3D	Three-dimensional
4VP	4-vinylpyridine
Å	Angstrom(s)
a_0	Contacting area of the hydrophilic headgroup interface
ABM	Aminobromomaleimide
ACM	Aminochloromaleimide
AFM	Atomic force microscopy
AIBN	2,2-Azobis(2-methylpropionitrile)
AM	Acrylamide
AN	Acrylonitrile
A_n	Number-average area
ATRP	Atom transfer radical polymerisation
A_w	Weight-average area
BCP	Block copolymer
c	Concentration

CDCl3	Deuterated chloroform
CDSA	Crystallisation-driven self-assembly
CEPA	4-cyano-4-(((ethylthio)carbonothioyl)thio)pentanoic acid
CHPET	2-cyano-5-hydroxypentan-2-yl ethyl carbonotrithioate
CLSM	Confocal laser scanning microscopy
CRP	Controlled radical polymerisation
CSIRO	Commonwealth scientific and industrial research organisation
CTA	Chain transfer agent
d	Diameter
d	Doublet
DBDS	Dibenzoyl disulfide
DBU	1,8-diazabicyclo[5.4.0]undec-7-ene
DCC	Dicyclohexylcarbodiimide
DCM	Dichloromethane
$Đ_M$	Molar-mass dispersity
DMA	*N*,*N*-dimethlyacrylamide
DMAEMA	2-(dimethylamino)ethyl methacrylate
DMAP	4-dimethylaminopyridine

DMF	N,N-Dimethyl formamide
DP	Number average degree of polymerisation
DPP	Diphenyl phosphate
DSC	Differential scanning calorimetry
eq	Equivalents
EtOH	Ethanol
GO	Graphene oxide
HPAM	N-(2-hydroxypropyl)methacrylamide
I	Initiator
iniferter	Initiator-transfer-agent-terminator
IR	Infrared
kDa	Kilodaltons
LAM	Less activated monomer
l_c	Length of hydrophobic block
L_i	Length of each counted particle
L_n	Number-average length
LP	Living polymerisation
L_w	Weight-average length
m	Multiplet

m/z	Mass to charge ratio
MA	Methyl acrylate
MALDI-ToF	Matrix-assisted laser desorption ionisation – time of flight
MAM	More activated monomer
MeOH	Methanol
mg	Milligram(s)
mL	Millilitre(s)
MMA	Methyl methacrylate
mmol	Millimole(s)
M_n	Number average molecular weight
mol	Mole(s)
MS	Mass spectrometry
M_w	Weight average molecular weight
N_i	Number of micelles of length L_i
NIPAm	N-isopropylacrylamide
NMP	Nitroxide-mediated polymerisation
NMR	Nuclear magnetic resonance
NVC	N-vinyl carbazole
NVP	N-vinyl pyrrolidone

OPV	Oligo(p-phenylenevinylene)
p	Packing parameter
P[F-co-BMDO])	Poly[(1-O-acryloyl-D-fructopyranose)-co-(5,6-benzo-2-methylene-1,3-dioxepane)]
P2VP	Poly(2-vinylpyridine)
P3DSe	Poly(3-decylselenophene)
P3HT	Poly(3-hexylthiophene)
PAA	Poly(acrylic acid)
PC	Photoredox catalyst
PCL	Poly(ε-caprolactone)
PDHF	Poly(di-n-hexylfluorene)
PDMA	Poly(N,N-dimethlyacrylamide)
PDMAEMA	Poly(2-(dimethylamino)ethyl methacrylate)
PDMS	Poly(dimethylsiloxane)
PE	Poly(ethylene)
PEG	Poly(ethylene glycol)
PEO	Poly(ethylene oxide)
PET	Poly(ethylene terephthalate)
PFS	Poly(ferrocenyldimethylsilane)

PFTMC	Poly(spiro[fluorene-9,5'-[1,3]-dioxan]-2'-one)
PI-CDSA	Polymerisation-induced and crystallisation driven self-assembly
PIP	Polyisoprene
PiPrOx	Poly(2-isopropyl-2-oxazoline)
PISA	Polymerisation-induced self-assembly
PLA	Poly(lactide)
PLLA	Poly(L-lactide)
PMMA	Poly(methyl methacrylate)
P_n	Polymer with a degree of polymerisation of n
ppm	Parts per million
PS	Polystyrene
PtBA	Poly(tert-butyl acrylate)
q	Quartet
RAFT	Reversible addition-fragmentation chain transfer
RDRP	Reversible deactivation radical polymerisation
RI	Refractive index
ROMP	Ring-opening metathesis polymerisation
ROP	Ring-opening polymerisation

RT	Room temperature
s	Singlet
SEC	Size exclusion chromatography
St	Styrene
t	Time
t	Triplet
TBD	1,5,7-triazabicyclo[4.4.0]dec-5-ene
T_c	Crystallisation temperature
TEA	Triethanolamine
TEM	Transmission electron microscopy
T_g	Glass transition temperature
THF	Tetrahydrofuran
T_m	Melting temperature
TMS	Trimethylsilane
TTC	Trithiocarbonates
TTDS	Tetraethylthiuram disulfide
UA	Uranyl acetate
UV	Ultraviolet
v	Volume of hydrophobic segment

VAc	Vinyl acetate
W_n	Number-average width
wt. %	Weight percent
W_w	Weight-average width
δ-VL	δ-valerolactone
ε-CL	ε-caprolactone
θ	Angle
λ	Wavelength
$\lambda_{abs.}$	Wavelength of absorption
µg	Microgram(s)
µL	Microlitre(s)
µmol	Micromole(s)
l_c	Length of a hydrophobic block
v	Volume
γ	Interfacial tension

Chapter One - Introduction

1.1 Synthetic Polymer Building Block

Polymers are large molecules composed of a variable number of small units and are essential in almost every aspect of our modern life, from transportation, to healthcare and technology.[1-7] Polymeric materials have distinct properties depending on the chemistry of the monomers used as building blocks, the overall stereochemistry, the monomer sequence (*e.g.* statistical copolymers or block copolymers), and molecular weight.[8-14] Additionally, the packing of polymer chains in 3D space, *i.e.* the polymer topology, allows to achieve a diverse range of morphologies.[15-21] Furthermore, the incorporation of functional units within selective domains, for example in a hydrophobic or hydrophilic region, is of great importance for the synthesis of (multi)functional polymers, where the additional feature can impart specific properties that are essential for the application of the resultant materials.[22-25] The ability to simultaneously modulate polymer composition, topology, and functionalisation allows sophisticated structures to be readily achieved and tailored for a wide variety of applications (**Figure 1.1**).[26]

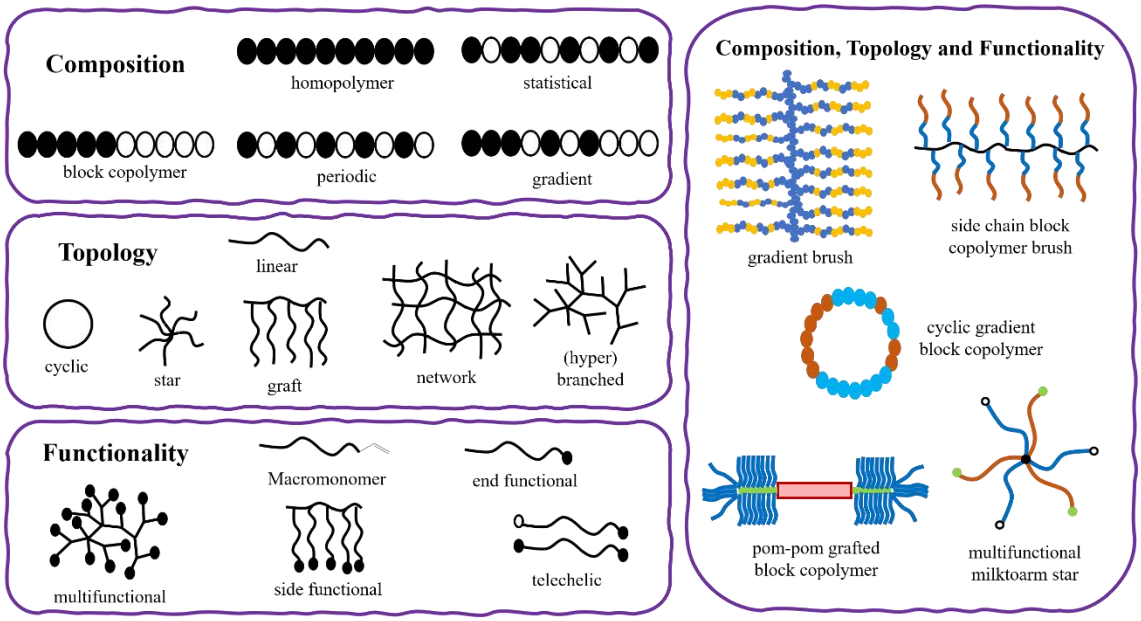


Figure 1.1 Main polymer characteristics that can be modulated to control the polymer architecture and properties. Adapted from ref.[26]

To precisely control these three elements, it is essential to understand the polymerisation mechanism in order to be able to predict polymer composition. Living polymerisation (LP) is considered as the most promising mechanism by which to achieve a high level of control over polymer composition.[27, 28]

1.1.1 Living Polymerisation

Compared to other conventional polymerisation methods, such as step growth polymerisation, chain growth polymerisation has been widely explored in modern synthetic polymer chemistry.[9, 29, 30] LP is a critical class of chain growth polymerisation without chain transfer and termination processes. For the polymerisation to be considered "living" in nature, a linear relationship should exist between the number average degree of polymerisation (DP) and the monomer conversion. This is an indication that the polymer chain keeps growing by sustained monomer addition, leading to a continuous polymerisation. Therefore, polymers produced by living polymerisation exhibit well-defined topologies, with narrow molecular weight distributions and controlled lengths. Since the concept of a 'polymer' was invented by Berzelius in 1833, and the first report on living anionic polymerisation published in 1956,[31] various types of LP have been investigated, such as living cationic polymerisation and ring-opening metathesis polymerisation (ROMP) (**Figure 1.2**).[32, 33] However, these methods require extremely stringent conditions, normally involving complete exclusion of oxygen or water from the reaction vessel to ensure that high monomer conversion is achieved, which restricts the wide use and scale up of such polymerisations in commercial applications.

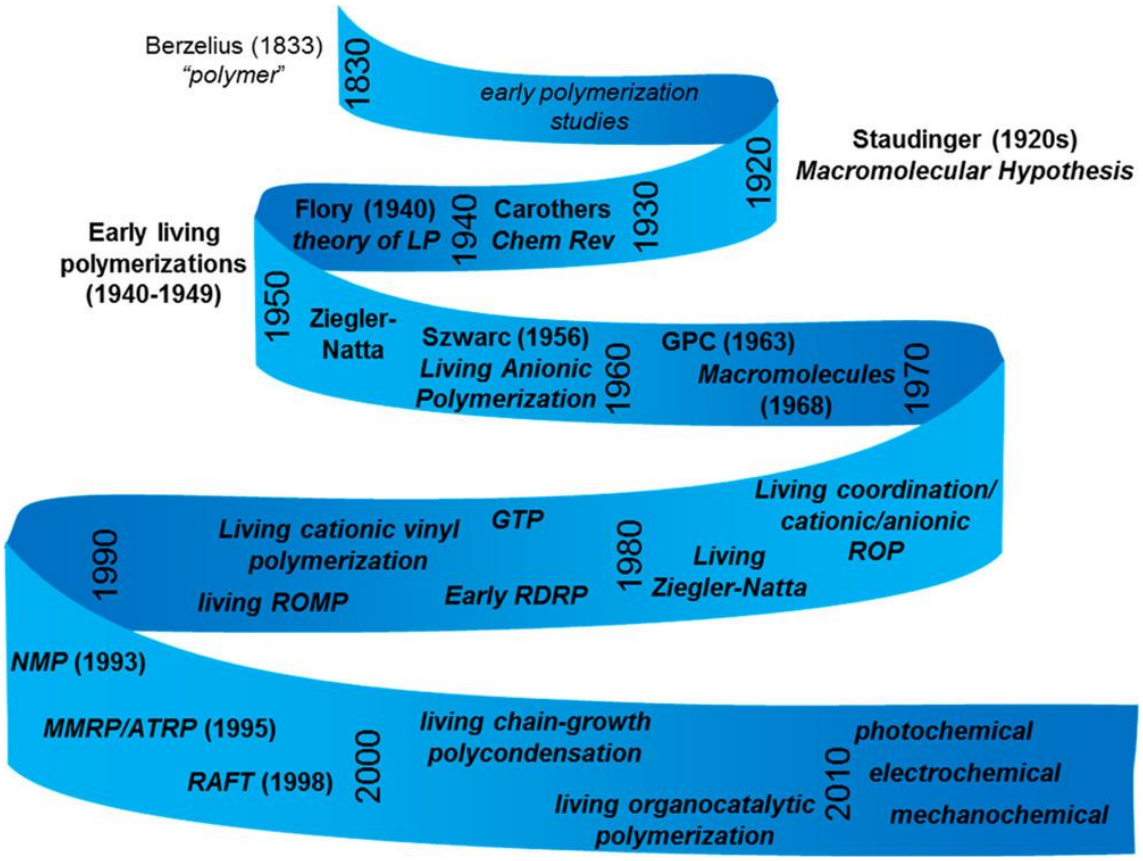


Figure 1.2 A brief timeline representing the development of living polymerisation. Figure adapted from ref.[28]

1.1.2 Reversible-Deactivation Radical Polymerisation

Compared to other polymerisation approaches, controlled radical polymerisation (CRP) can be used to synthesise block copolymers with precise molecular weights and tailored architectures, and with high tolerance for a broad range of functional groups.[29, 30] The most widely used CRP approach is reversible-deactivation radical polymerisation (RDRP), which is based on a dynamic equilibrium between a dormant chain and propagating species. This process decreases the concentration of radicals, thereby lowering the rate of chain transfer and termination, as well as increasing the average lifetime of the propagating species.[34, 35] This dynamic equilibrium in RDRP can be achieved by two mechanistic routes: the persistent radical effect, involving the reversible

deactivation of propagating chains that subsequently can be reactivated, and the degenerative chain transfer process between propagating chains and dormant radicals.[36, 37]

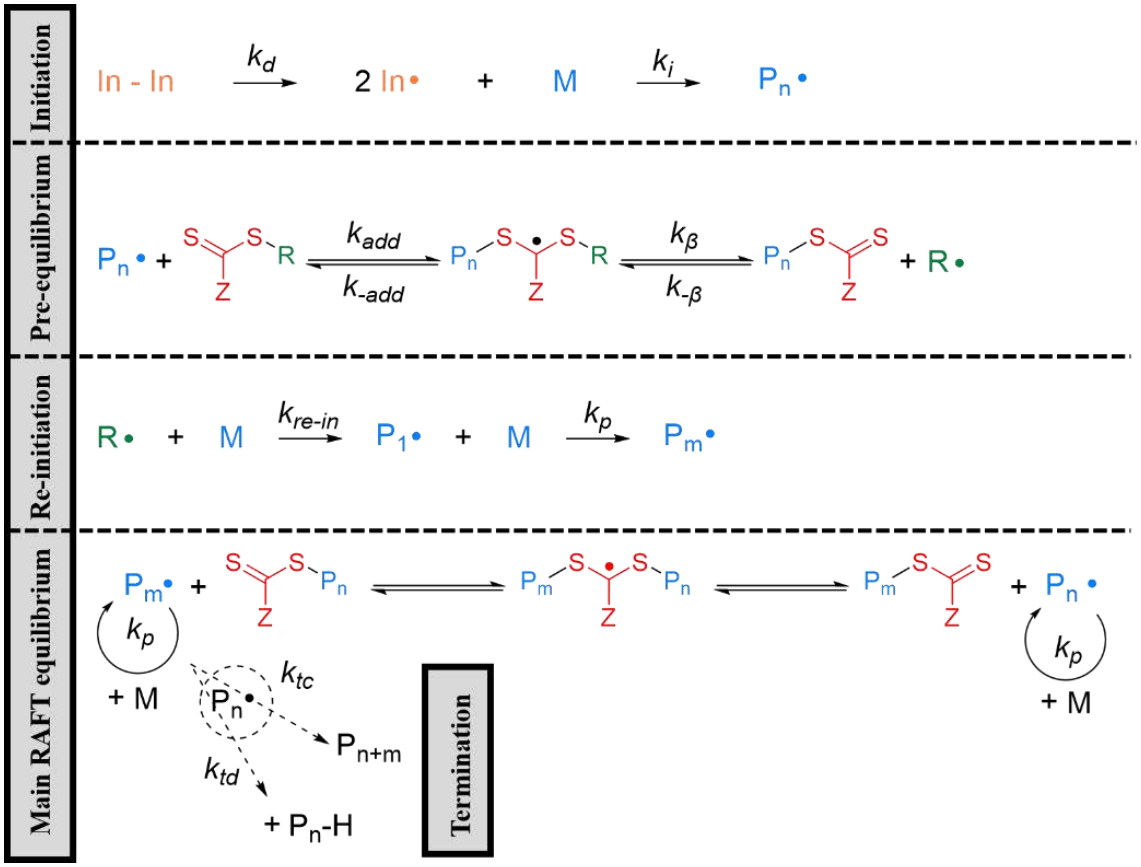
1.1.2.1 Persistent Radical Effect

The persistent radical effect is observed in both nitroxide-mediated polymerisation (NMP) and atom transfer radical polymerisation (ATRP).[38-40] Due to the fact persistent radicals cannot self-terminate with each other, radicals can only cross couple with the propagating species. Each technique has both application-specific advantages as well as divergent characteristics, although most monomers that are used with free radical polymerisation can be applied. NMP relies on alkoxyamines to function as initiators, and is mediated by nitroxide radicals.[39, 40] Compared to ATRP and reversible addition fragmentation chain transfer (RAFT), NMP still exists several intrinsic drawbacks, containing slow polymerisation kinetics, high polymerisation temperatures, and a narrow range of monomers, limiting its application in polymer synthesis. ATRP was separately reported by Matyjaszewski *et al.* and Sawamoto *et al.* in 1995. They demonstrated the polymerisation of styrene and methyl methacrylate, respectively, in the presence of halogen-containing initiators using transition metal/ligand complexes that act as catalysts. A variety of monomers can be polymerised *via* ATRP technique under mild conditions and in a broad range of solvents, thus demonstrating high potential for many applications.[38, 41-43]

1.1.2.2 Degenerative Transfer Effect

In stark contrast to the persistent radical effect, the degenerative transfer mechanism, where an active polymer radical is in equilibrium with a dormant polymer radical, is intended to minimise the effect of radical-radical termination.[44-46] RAFT polymerisation

was first reported by Thang and co-workers in 1998,[47] which is based on this type of mechanism through the reversible addition/fragmentation by shifting between active species and dormant, including five steps: initiation, pre-equilibrium, re-initiation, main equilibrium and termination process (depicted in **Scheme 1.1**).[48-50]



Scheme 1.1 Mechanism of RAFT polymerisation.[51]

In the initiation phase, radicals are generated by decomposition of an initiator molecule that reacts with a monomer, leading to the formation of oligomer radicals (P_n•) which react with the chain transfer agent (CTA). P_n• is now associated with the CTA, transforming into macromolecular CTA and generating a new radical R•, this process is termed as the pre-equilibrium stage. In the re-initiation process, a new propagating chain (P_m•) is formed through the reaction between radical R• and free monomer. The reaction then proceeds to main equilibrium, where the exchange between the dormant chains and

the active chains enables identical polymer growth rates whilst minimising termination. In the termination process, two polymeric radicals react with each other through disproportionation or recombination, resulting in dead polymer chains that cannot propagate further.

1.1.2.3 Choice of RAFT Agent and Monomer

RAFT polymerisation represents one of the most versatile and effective strategies for controlling macromolecular polymer architecture, owing to its good tolerance towards functional monomers and its compatibility with a broad range of monomer classes without requiring tedious optimisation steps.[52] A careful selection of the RAFT agent and monomer is imperative to achieve excellent control over the RAFT polymerisation. Well-defined polymers can be achieved with narrow polymer dispersity and predictable molecular weights, as well as retaining functionality of the end group.

The Z and R group are the substituents around the C=S group, which can be tailored to satisfy the monomer used.[53] The main functionality of the Z group is to activate the C=S bond, leading to radical addition and stabilising the intermediate radical formed. The stability of the intermediate thiocarbonylthio compound is strongly determined by its electron density. As the RAFT equilibrium proceeds, a CTA with an electron withdrawing Z group will form the intermediate, As a consequence of its higher stability compared to the propagating radical, in contrast to electron donating Z groups, which disfavour the formation of the radical intermediate. By varying the Z group, the four main types of CTA can be achieved simply by changing the substituent next to the reactive double bond (C=S): dithioester, trithiocarbonate, dithiocarbamate, xanthate (**Figure 1.3**). The selection of R group is as important as the choice of Z group. Compared to the propagating species, R group should act as a good homolytic leaving group, whilst also being capable of initiating radical polymerisation. Thus, by tuning these parameters, RAFT

polymerisation offers the ability to polymerise a wide range of functional monomers whilst avoiding many of the problems associated with RAFT polymerisation through careful consideration of the CTA and the monomer.

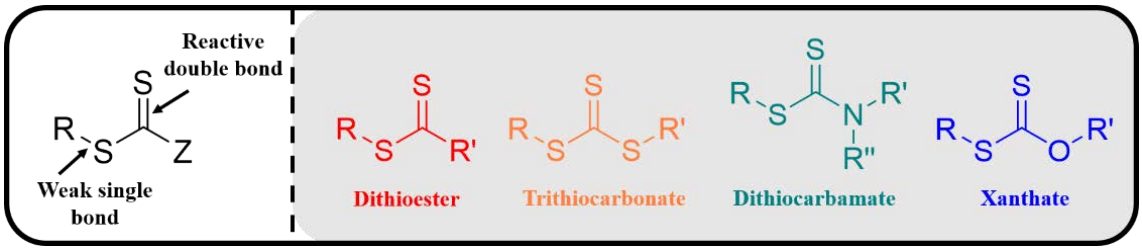


Figure 1.3 Structure of RAFT chain transfer agents with different Z groups (dithioester Z=R', trithiocarbonate Z=SR', dithiocarbamate Z=NR'R'', xanthate Z=OR').[54]

In 2009, Moad *et al.* proposed an empirical guide to select suitable Z and R groups based on the design of CTA, and categorised monomers into two classes based on their reactivity (**Figure 1.4**).[55] For more activated monomers (MAMs), such as methyl methacrylate (MMA), styrene (St), N-(2-hydroxypropyl)methacrylamide (HPAM), acrylamide (AM), methyl acrylate (MA), and acrylonitrile (AN), an active CTA with an electron withdrawing or weakly electron donating Z group should be selected. On the contrary, less activated monomers (LAMs), such as vinyl acetate (VAc), N-vinyl pyrrolidone (NVP) and N-vinyl carbazole (NVC), require a less active CTA with a strong electron donating Z group.

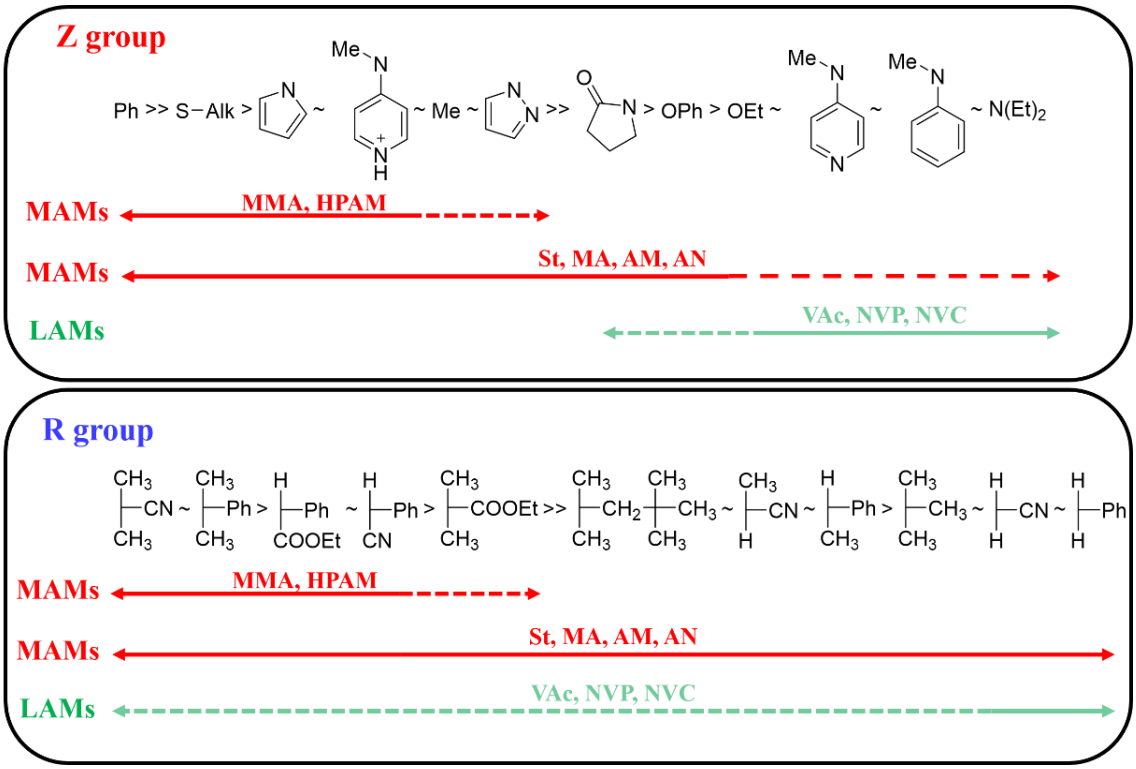


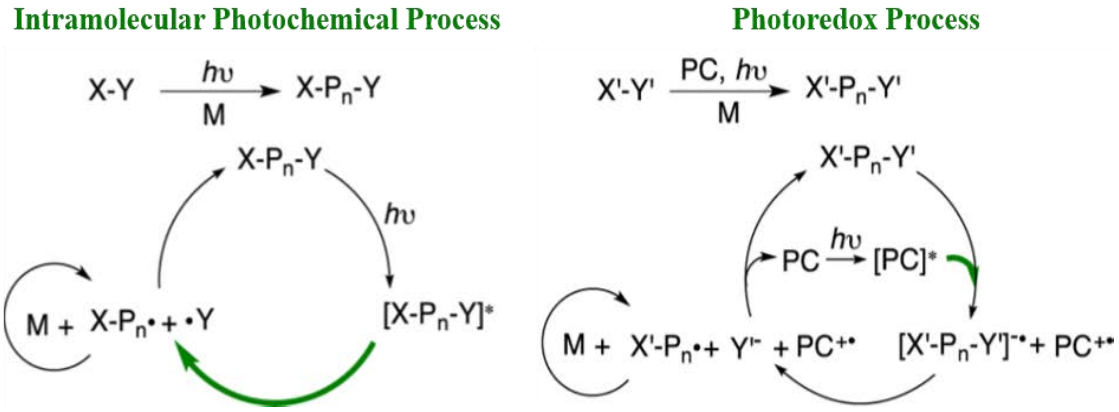
Figure 1.4 General guidelines for RAFT agent R and Z group for various monomer classes. Addition rate decreases (fragmentation rate increases) from left to right. Dashed lines indicate partial control.[51]

Compared with NMP, RAFT polymerisation generally requires lower polymerisation temperatures and faster polymerisation kinetics, while allowing versatile monomers to be polymerized in the same initiation system. RAFT polymerisation also avoids the need of metal catalysts which might limit the use of the resultant materials for biological and medical applications. The major disadvantage of RAFT polymerisation is that it typically requires an inert atmosphere owing to its extreme sensitivity towards oxygen. Because peroxy radicals and hydroperoxides could be produced by reacting with the carbon-centred radicals under oxygen containing environment, lowering the rate of re-initiation.[56] Another drawback is the use of thiol-containing alkyls and carbon disulfide to synthesise CTAs, which can generate unpleasant smells and coloured products. Despite these disadvantages, RAFT polymerisation is one of the most promising CRP techniques, as a

consequence of its compatibility with various functionalities and the mild reaction conditions.

1.1.3 Light Mediated Polymerisation

Over recent years, light-mediated controlled radical polymerisation has become a powerful strategy for a controlled and efficient polymer synthesis, owing to fewer side reactions, relatively low energy requirements, and the ability to exert temporal and spatial control over the polymerisation by simply switching the light to the desired wavelength.[57-72] By varying the photochemical mechanism, two types of light-mediated polymerisations have been reported, involving an intramolecular photochemical or a photoredox process (**Scheme 1.2**).

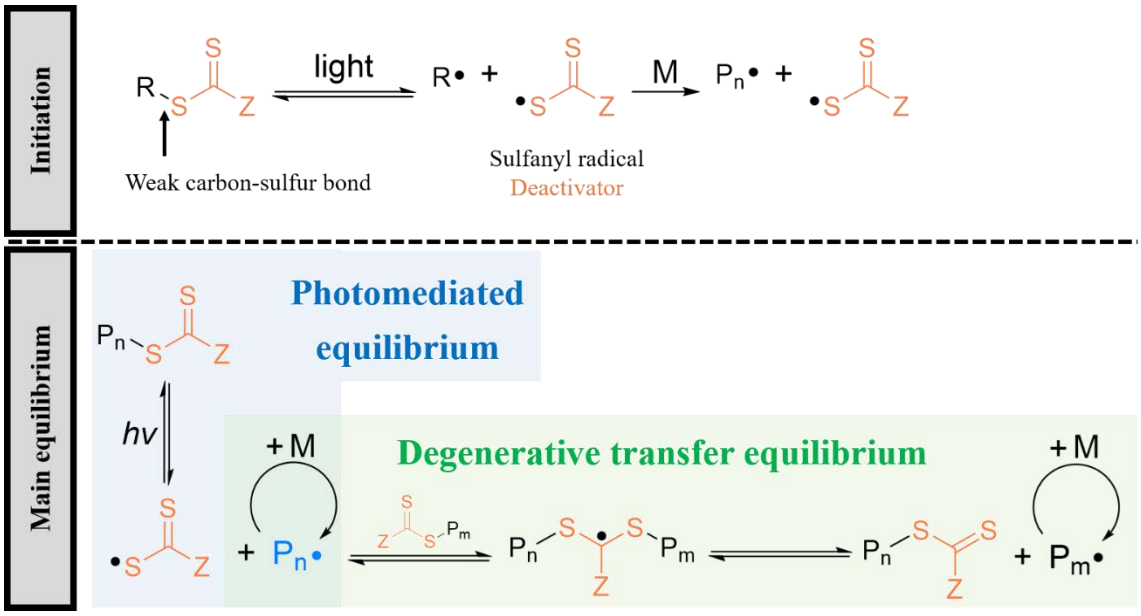


Scheme 1.2 Representative mechanisms for photo mediated polymerisation involving an intramolecular photochemical process and a photoredox process. Adapted from ref.[67]

In the photoredox process, the absorbing species photoredox catalyst (PC) undergoes photoinduced single electron transfer to form an initiator, producing radical species for propagation. Contrastingly, in an intramolecular photochemical process without catalyst, the initiator and the reversible terminator are originated from the absorbing species X-Y. Homolytic cleavage of the polymeric or excited initiator can generate radicals for propagation or recombination. Thus, the first step of the photochemical process is the

cleavage of homolytic bond in the light absorbing species followed by its direct incorporation into the polymer chain.

In the case of photo iniferter polymerisation, thiocarbonylthio compounds are served as initiator-transfer-agent-terminator (iniferter) in the intramolecular photochemical process. The iniferters undergo homolytic cleavage of the carbon-sulfur bond when under irradiation to produce R• and the deactivator of surfanyl radicals that initiate polymerisation. The propagating species can then undertake degenerative chain transfer with iniferters and maintains the equilibrium, similarly to the RAFT equilibrium process (**Scheme 1.3**). Based on the mechanism, it is known that no exogenous radical initiator is needed in iniferter systems, as the cleavage of the iniferter occurs through photo radiation.



Scheme 1.3 Overview of the iniferter mechanism for photo mediated polymerisation.[67, 73]

In 1982, Otsu *et al.* reported the first example of a photo-controlled radical polymerisation and introduced the concept of iniferter.[74] They reported the synthesis of iniferter tetraethylthiuram disulfide (TTDS) and dibenzoyl disulfide (DBDS) and applied them in the polymerisation of St and MMA monomers under irradiation, exhibiting a linear

relationship between monomer conversion and M_n, with a well-controlled polymerisation process. Over the last four decades, many researchers made tremendous efforts in this field and explored a range of photo iniferters to suit different monomers, such as popular trithiocarbonate (TTC) based iniferters,[66, 75-77] pursuing to reach universal conditions for a wide range of monomers while achieving predictable molecular weights and narrow dispersities. (**Figure 1.5** summarised by Johnson and co-workers).[67]

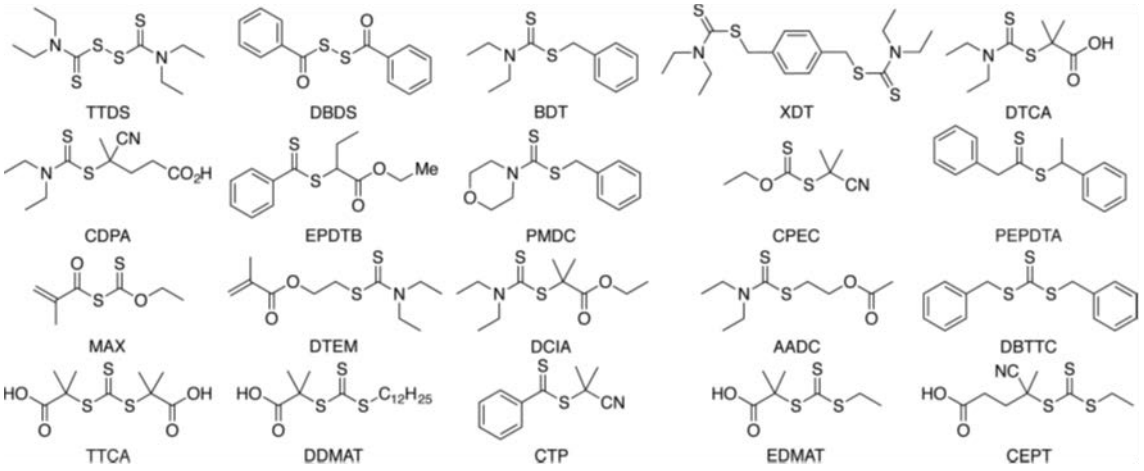


Figure 1.5 Chemical structure of selected iniferters used in photo mediated polymerisation. Adapted from refs.[60, 67]

1.1.4 Ring Opening Polymerisation

Recently, a large amount of research in the field of polyesters, including poly(lactide) (PLA) and poly(caprolactone) (PCL), has been conducted to investigate potential biorelevant applications of these polymers as a consequence of their superior biodegradability and biocompatibility. Thus, it's critical to fabricate well defined polyesters with narrowed dispersities and predictable molecular weights. Among various polymerisation approaches, ring opening polymerisation (ROP) is a good candidate to achieve this purpose, which relies on the mechanism of chain growth polymerisation. In the ROP process, the terminus of the active chains reacts with cyclic monomers by

opening their ring system and keeping the end activity of combined chain to form a longer polymer, which can be divided into three main types (anionic, cationic and radical) based on the reaction mechanism.[78-82]

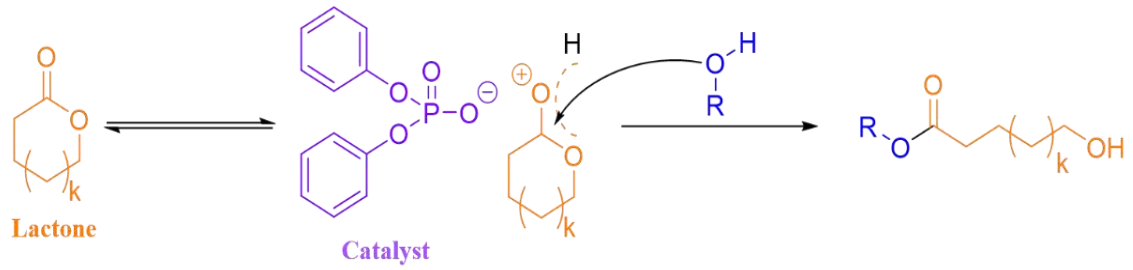
Lactone is a form of cyclic carboxylic ester which includes a 1-oxacycloalkan-2-one structure (−(C=O)−O−). Aliphatic poly(lactones) represent a class of materials with significant benefits, including biodegradability and biocompatibility. As a result of these interesting and desirable features, these polymers can be used for biomedical applications, including drug delivery and tissue engineering. Ring opening polymerisation is now a commonly employed method to synthesise poly(lactones), as it offers excellent polymerisation control and high-end group fidelity, allowing to achieve well-defined poly(lactones) with predictable molecular weights and narrow dispersities.[80]

Generally, a broad range of catalysts can be used to start a ROP, including organometallic catalysts, organocatalysts, and enzymes. Organocatalysis has been commonly used to control the ROP of lactones, offering several benefits of low toxicity, low costs, and less sensitivity to water and oxygen.[83] Since the first ROP organocatalyst, 4-dimethylaminopyridine (DMAP), was reported by Hedrick and co-workers,[84] great advances have been achieved in this field with a diverse range of organic catalysts shown to be active for the polymerisation of cyclic lactones and carbonates.

One of the most popular class of organocatalysts applied to the ROP of cyclic monomers is the one of superbases with amidine and guanidine substructures.[85-88] In 2006, Lohmeijer *et al.* described the use of a guanidine-based catalyst 1,5,7-triazabicyclo[4.4.0]dec-5-ene (TBD) and an amidine-based catalyst 1,8-diazabicyclo[5.4.0]undec-7-ene (DBU) for the organocatalytic ring-opening of cyclic esters.[89] Both catalysts showed excellent activity for the polymerisation of lactide,

generating polymers with very narrow molecular weight distributions. To further minimise transesterification reactions, the thiourea-amine bifunctional catalyst was designed by Dove *et al.* in 2005.[87] This catalyst possesses bifunctionality for monomer and initiator activation. The thiourea serves as a hydrogen-bond donor to the carbonyl in the monomer, while the tertiary amine acts as a hydrogen-bond acceptor to the alcohol/propagating chain end.

A series of acids have demonstrated superior catalytic ability for the ROP of ε-caprolactone (ε-CL). For instance diphenyl phosphate (DPP), first reported by Kakuchi and co-workers, is an Brønsted acid with high chemical stability and commercial availability, widely used for the ring opening of lactones.[90] An activated monomer mechanism was postulated (**Scheme 1.4**), where DPP coordinates with the carbonyl of the lactone and promotes a nucleophilic attack by an alcohol initiator, with resultant polymers exhibiting negligible transesterification. In addition, the linear relationship of M_n with monomer conversion was achieved, exhibiting a controlled nature of the polymerisations. Even at high monomer conversions, the dispersity remained very low.[83, 90]



Scheme 1.4 Ring opening polymerisation of lactones using DPP as a catalyst.[90, 91]

1.2 Self-Assembly of Block Copolymers

As previously discussed, huge developments of 'living' polymerisation techniques have allowed access to polymers with various compositions, topologies and functions,

including amphiphilic block copolymers (BCPs). Self-assembly of amphiphilic BCPs involving at least one soluble (solvophilic) and one insoluble (solvophobic) block connected by covalent linkage occurs in selective solvents spontaneously. A core-corona micellar structure can be obtained through BCP chains self-assembly, composed of a hydrophobic core block and hydrophilic corona block in a selective solvent, in order to minimise the unfavourable ordering in entropy and the unfavourable interaction between the core segment and the selective solvent.[92, 93]

1.2.1 Polymer Solution Self-Assembly

The morphology of the aggregates formed by polymers in solution can be mainly ascribed to the linkage of the core block chain, repulsion of the corona forming block, and the interfacial tension with the solvent.[21, 94] All these properties are affected by the composition of the polymer and the conditions under self-assembly process, including temperature and solvent. Thus, each kind of polymer topology can self-organize into assemblies of diverse structures by simply changing the assembly conditions.

In 1976, Israelachvili and co-workers proposed an equation of packing parameter ($p = \frac{v}{a_0 l_c}$) that can be used as a guide to predict the potential morphology of assemblies, where v is the volume of hydrophobic segment, a_0 represents the contacting area of the hydrophilic headgroup interface, and l_c is the length of hydrophobic block.[95] Typically, there are three main classes of structures followed by the rule of packing parameter value. Spherical micelles are formed when $p \leq \frac{1}{3}$, cylinders (fibre-like or worm-like) are favoured when $\frac{1}{3} < p \leq \frac{1}{2}$, and vesicles are observed when $\frac{1}{2} < p \leq 1$. Hence, all different structures can be achieved by regulating the ratio of the core and corona blocks.

Cylindrical morphologies occupy a narrow window ($\frac{1}{3} < p \leq \frac{1}{2}$) of the packing parameter, where it is difficult to modulate the block composition (**Figure 1.6**).

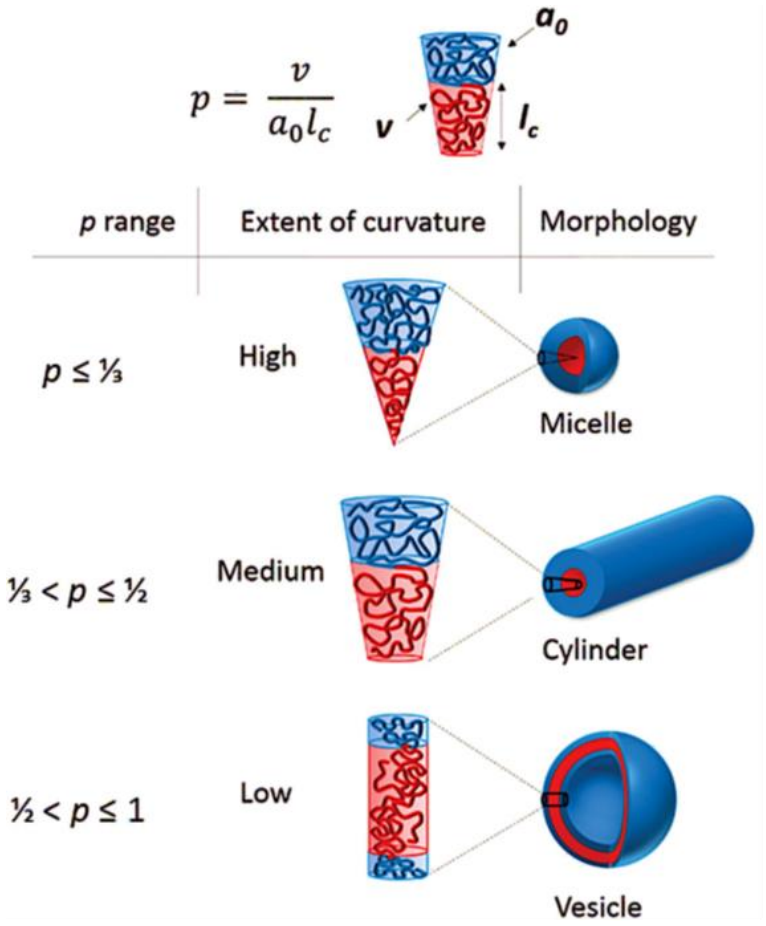


Figure 1.6 Schematic illustration of possible self-assembled morphologies obtained by different packing parameters, *p*.[21]

Over several decades of investigation of amorphous block copolymers self-assembly in solution, a large number of researchers have focussed on controlling the micelle morphology. However, generating the high order of one-dimensional (1D) cylindrical[96, 97] and two-dimensional (2D) platelet assemblies[98-100] is extremely challenging to achieve in a controlled fashion. For 1D structure, it's difficult to obtain pure cylindrical micelles only in a narrow window of the amorphous BCPs phase diagram.[101] Owing to the colloidal instability and lack of directionality of the building blocks, 2D assemblies

cannot be accessed easily through traditional self-assembly.[102] Semi-crystalline block copolymers have attracted increasing attention and have shown to be able to address these issues during self-assembly, favourably forming the structures with minimal interfacial curvature at the core-corona interface *via* the crystallisation of the core-forming block. This is in balance with a free energy penalty associated with solvated inter-chain coronal steric repulsions.[103] Thus, crystallisation of the semi-crystalline block leads to the preference for 1D cylindrical structures or 2D lamellae structures with controlled morphology and dimensions.[104]

1.2.2 Crystallisation-Driven Self-Assembly

Crystallisation-driven self-assembly (CDSA) can be dated back to mid-1960s, when Lotz *et al.* reported the formation of crystal platelet micelles involving chain folded crystalline poly(ethylene oxide) (PEO) sandwiched between amorphous polystyrene (PS) in solution.[105] In 1998, Manners and Winnik demonstrated an interesting organometallic-inorganic BCP poly(ferrocenyldimethylsilane)-*b*-poly(dimethylsiloxane) (PFS-*b*-PDMS), forming a cylindrical structure in hexane consisting of a crystallisable PFS block attached by an extended corona of PDMS chains. Nowadays, CDSA has grown into one of the most burgeoning and powerful self-assembly strategies in solution phase for the formation of complex polymeric architectures[106] (**Figure 1.7**).

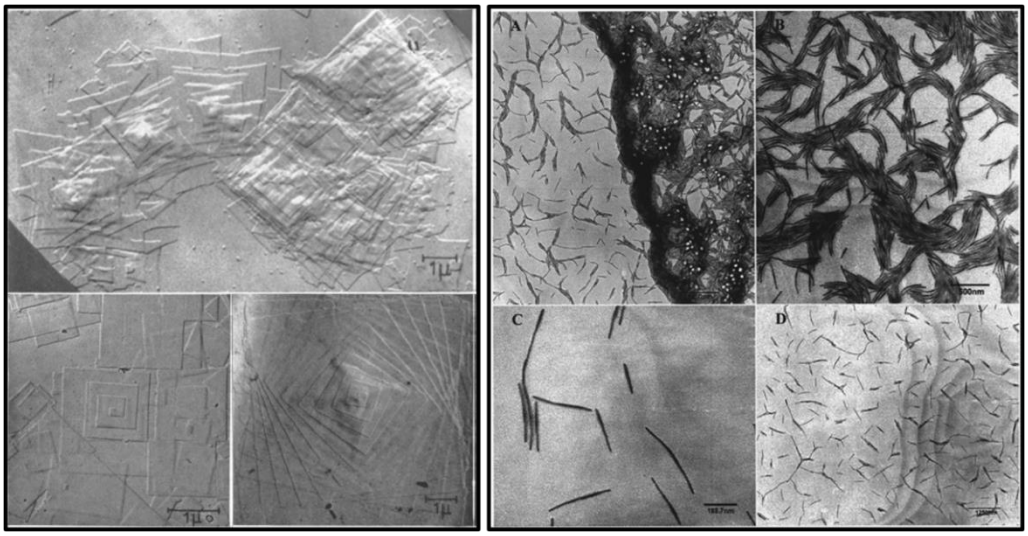
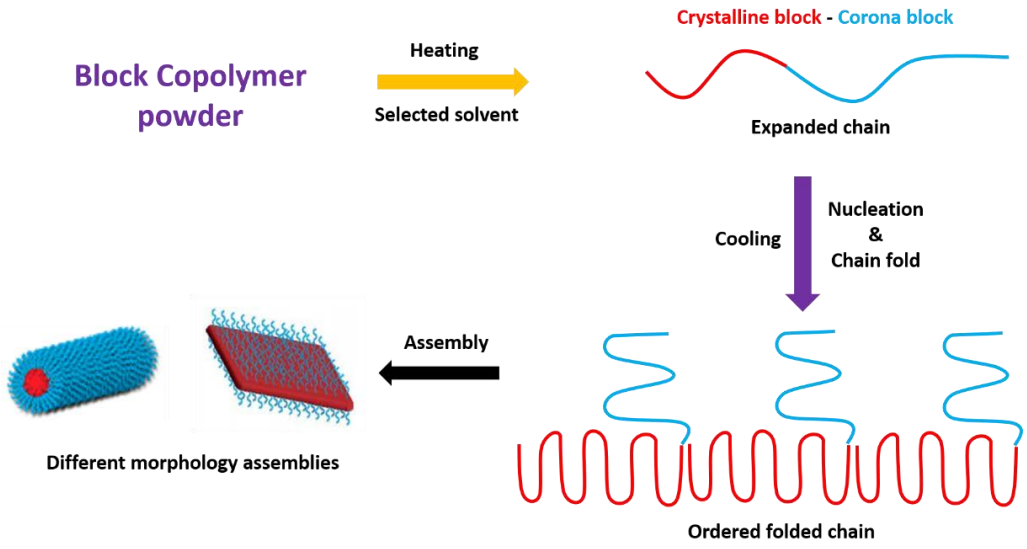


Figure 1.7 TEM micrographs of (left) crystal platelets of PEO-PS copolymer,[105] (right) long rod-like micelles of PFS-*b*-PDMS.[106]

In the general mechanism of CDSA, bulk BCP powders with at least one crystalline block are dissolved in a selected solvent that is favourable for the corona segment and unsuitable for the crystalline chain block. The solution is heated to above the melting temperature (T_m) of the crystalline block, allowing sufficient time for the polymer to dissolve completely. The crystalline chains folded and formed micelles by homogenous nucleation when cooled below the crystallisation temperature (shown in **Scheme 1.5**).



Scheme 1.5 Basic mechanism of crystallisation-driven self-assembly.[104]

Currently, crystalline core forming BCPs have demonstrated to exhibit excellent flexibility in the preparation of crystalline materials, accompanied by a variety of building blocks. A range of both organometallic and organic crystallisable core forming blocks have been explored to date, such as poly(ferrocenyldimethylsilane) (PFS),[96, 99, 102, 103, 106-117] poly(spiro[fluorene-9,5'-[1,3]-dioxan]-2'-one) (PFTMC),[118] poly(ethylene) (PE),[119-121] poly(L-lactide) (PLLA),[122-125] poly(ethylene oxide) (PEO),[105, 126] poly(di-n-hexylfluorene) (PDHF),[127, 128] poly(3-hexylthiophene) (P3HT),[97] poly(2-isopropyl-2-oxazoline) (PiPrOx),[129] poly(ε-caprolactone) (PCL),[126, 130-133] oligo(p-phenylenevinylene) (OPV)[134-137] and Poly(3-decylselenophene) (P3DSe),[138] (**Figure 1.8**).

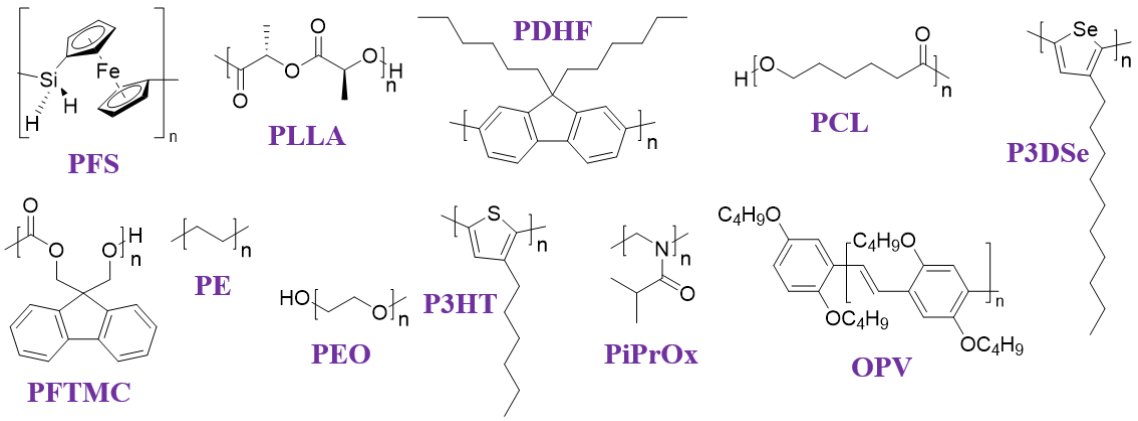


Figure 1.8 Chemical structures of the semi-crystalline core-forming block commonly reported in the literature. Adapted from ref.[139]

CDSA is a pivotal technique in the preparation of colloidally stable assemblies, exploring an impressive range of hierarchical nanostructures with controlled spatial dimensions and uniform dispersity.[104] Importantly, precision controlled living growth of CDSA systems has been demonstrated that the size could be predicted by altering the ratio of unimer-to-seed through further addition of unimers, realising the precise morphological control on scales from the nano- to micro-meter.[140]

1.2.3 Precise Morphology and Size Control by CDSA

In the process of CDSA of semi-crystalline BCPs, the relationship between morphology and core crystallinity of assemblies can be related to a range of features, such as block copolymer composition, additives, solvent choice, temperature and many others.[104, 133, 135, 141] For example, although the crystallisation of the core-forming block favourably generating low curvature structures, the core-corona block ratio still wields a great influence over the micellar morphology.[138] Usually, 1D cylindrical structures can be accessed by employing BCPs with a high ratio of corona-to-core block (solvophilic : solvophobic $\gg 3$).[115, 130, 142] 2D platelet structures can be obtained under a low ratio of corona-to-core block (≤ 1).[143] These 1D, 2D and even more complex hierarchical structures are regarded attractive candidates for potential applications in the biomedical field as well as electronics.[122, 144, 145] Therefore, optimal conditions of precise living growth are important for building up the desired structure for specific applications.

1.2.3.1 Length Control of 1D Structures

The fabrication of 1D structures is a considerable challenge by self-assembly of amorphous BCPs.[146] In CDSA systems, as the core of 1D block copolymer micelles are crystalline, it's possible for further unimers to grow from exposed active sites through an epitaxial growth mechanism.[130] Moreover, it is possible to fragment long 1D BCPs micelles into short "seed" micelles by imposing shear forces through vigorous sonication. These seed micelles can initiate epitaxial crystallisation with the addition of further BCP unimers, through a process called seeded growth.[133] Due to the epitaxial growth suppressing the self-nucleation effectively, the final micelle length is linearly dependent on the amount of BCP unimers added to the seed initiators, and is termed as "living" CDSA in analogy to a living covalent polymerisation.[96, 123] Furthermore, the crystallinity of insoluble core forming segments inhibits the exchange between unimers in the micelle

with unimers in solution and the micelles exist within a deep kinetic trap.[112] Thus, the critical micelle concentration of BCPs with crystalline core-forming blocks is effectively zero, which means that 100% of the unimers added to the seeds is consumed by living CDSA process, and high level control over the final lengths can be expected.[104]

Manners and co-workers reported a rapid and convenient method for preparing scalable and uniform 1D cylindrical micelles through the synchronous coupling of polymerisation-induced and crystallisation driven self-assembly (PI-CDSA), which is a one-pot method from polymerisation to self-assembly. This approach can be used to access the scalable fabrication of cylinders of controlled length up to 3 mm with low dispersity, while demonstrating the formation of micelles from monomers at high weight percentage of solids using a one-pot approach.[101] The PI-CDSA of polyisoprene-*b*-poly(ferrocenyldimethylsilane) (PIP-*b*-PFDMS, PFDMS block is insoluble in THF) BCPs have been observed in a THF/n-hexane solvent mixture (**Figure 1.9**). Significantly, the concept of living PI-CDSA has demonstrated the superior ability to rapidly prepare monodisperse cylinders with excellent level of control in the presence of small seeds by altering the PIP-to-seed ratio. This method is expected to expand endowing novel properties for a wide range of areas from nanomedicine to composite toughening.

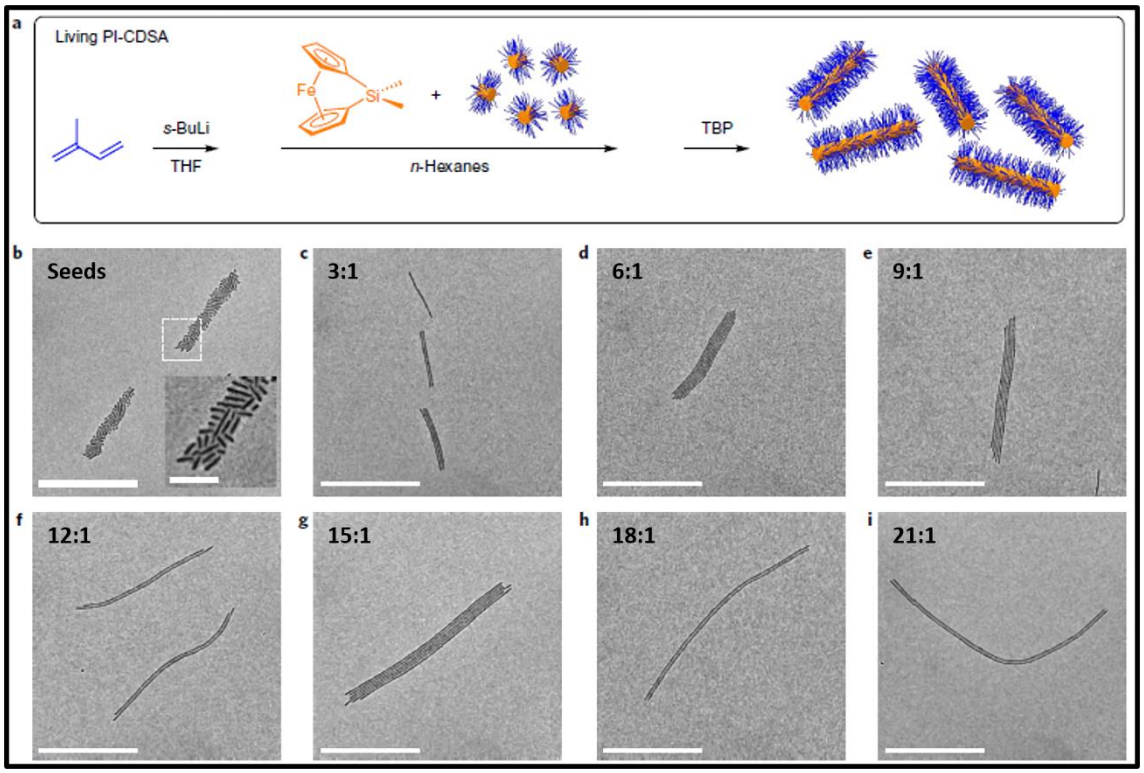


Figure 1.9 Living PI-CDSA (at 10% w/w solids) of PIP-*b*-PFDMS with a block ratio of approximately 5.3:1 in 10% v/v THF/n-hexanes. (a) Schematic representation of the preparation of near monodisperse PIP-*b*-PFDMS cylindrical micelles *via* living PI-CDSA. TBP was used as a quenching agent. PI-CDSA seeded growth of PIP-*b*-PFDMS cylindrical micelles was carried out at 10% w/w solids in 10% v/v THF/n-hexanes. (b–i) TEM micrographs of dried near monodisperse cylindrical micelles of PIP-*b*-PFDMS prepared by living PI-CDSA. (b) Small seed micelles prepared by the ultrasonication of long polydisperse micelles. PIP-to-seed ratios of (c to i) 3:1 - 21:1. Adapted from ref.[101]

In order to further investigate CDSA behaviour in water, the epitaxial growth in aqueous solvent was first reported by O'Reilly and co-workers, who achieved precise control over 1D cylinders in aqueous solvent.[130] The cylindrical structures fragment when the PCL_{50}-*b*-$PDMA_{180}$ (PDMA: poly(N,N-dimethyl acrylamide)) micelles were transferred into water from alcoholic solvent, which could be ascribed to the swelling of the corona block causing stress to the crystalline structure. Through the introduction of a short glassy block of poly(methyl(methacrylate)) (PMMA) to protect the PCL core, water stable triblock

copolymers of PCL_{50}-*b*-$PMMA_{20}$-*b*-$PDMA_{200}$ could be synthesised, as the highly hydrophobic polymer effectively prevents disassembly. Importantly, cylindrical micelles with controlled epitaxial growth were obtained *via* adding different unimers-to-seeds ratio to achieve desired and stable structures directly in water, paving the way for bio-relevant applications (**Figure 1.10**).

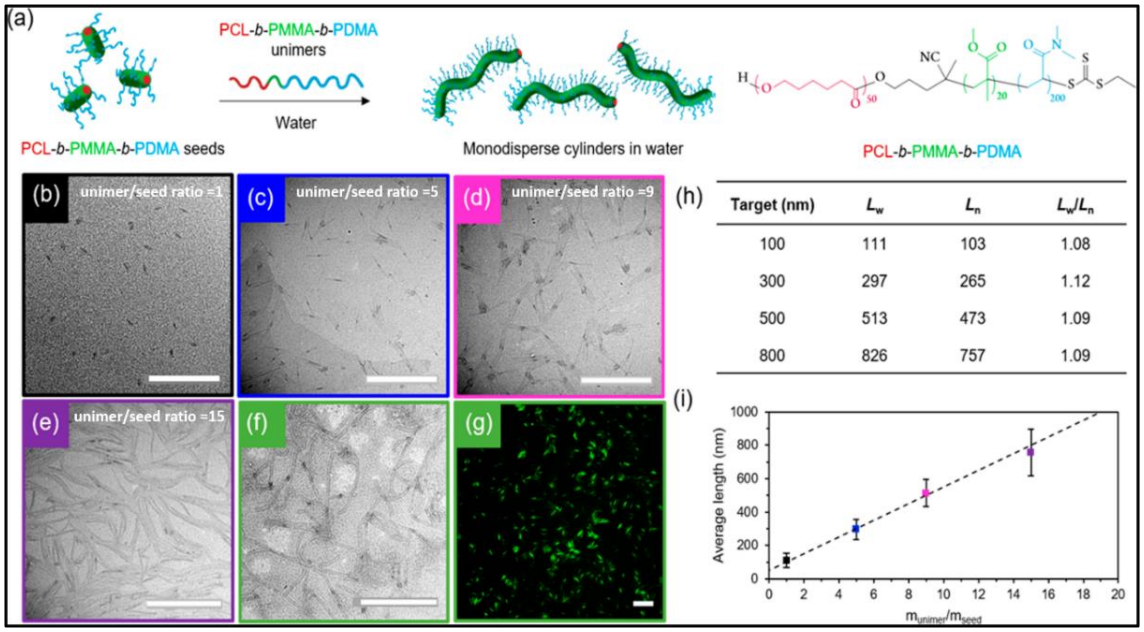


Figure 1.10 (a) Schematic representation of epitaxial growth in water using PCL_{50}-*b*-$PMMA_{20}$-*b*-$PDMA_{200}$ triblock copolymer. TEM micrographs of cylindrical micelles epitaxially grown from seed micelles in water with an unimer/seed ratio of (b-e) 1, 5, 9, and 15. (f) TEM micrograph and (g) confocal image of fluorescently labeled cylindrical micelles epitaxially grown from seed micelles in water with an unimer/seed ratio of 15. (h) Length dispersity of cylindrical micelles. (i) Plot showing a linear epitaxial growth regime of cylinders with narrow length dispersities in comparison to the theoretical length. Adapted from ref.[130]

1.2.3.2 Size Control of 2D Structures

Despite these remarkable examples of 1D BCP micelles with length control in one-dimension, fewer examples of living CDSA in the fabrication of precise 2D structures have been investigated. He *et al.* reported the use of surface charge to stabilise self-

assembled planar structures that are formed from crystallizable polymer precursors by a seeded growth approach on PFS-containing system[110]. Addition of homopolymers with charged end groups to seeds generated by the sonication of block copolymer micelles with crystalline core yields uniform, colloidally stable 2D platelet micelles with controlled dimensions. This strategy has also been explored using the semicrystalline biodegradable organic polymer PLLA. Using $PLLA_{24}[PPh_2Me]I$ and $PLLA_{34}[PPh_2Me]I$, 2D diamond-platelets were prepared with controlled size by adjusting the unimer-to-seed ratio (**Figure 1.11**). This type of 2D platelets with lipophilic charged surfaces provides a potential platform for bio-nanoparticles and therapeutic agents as well as adhesives for composite reinforcement.

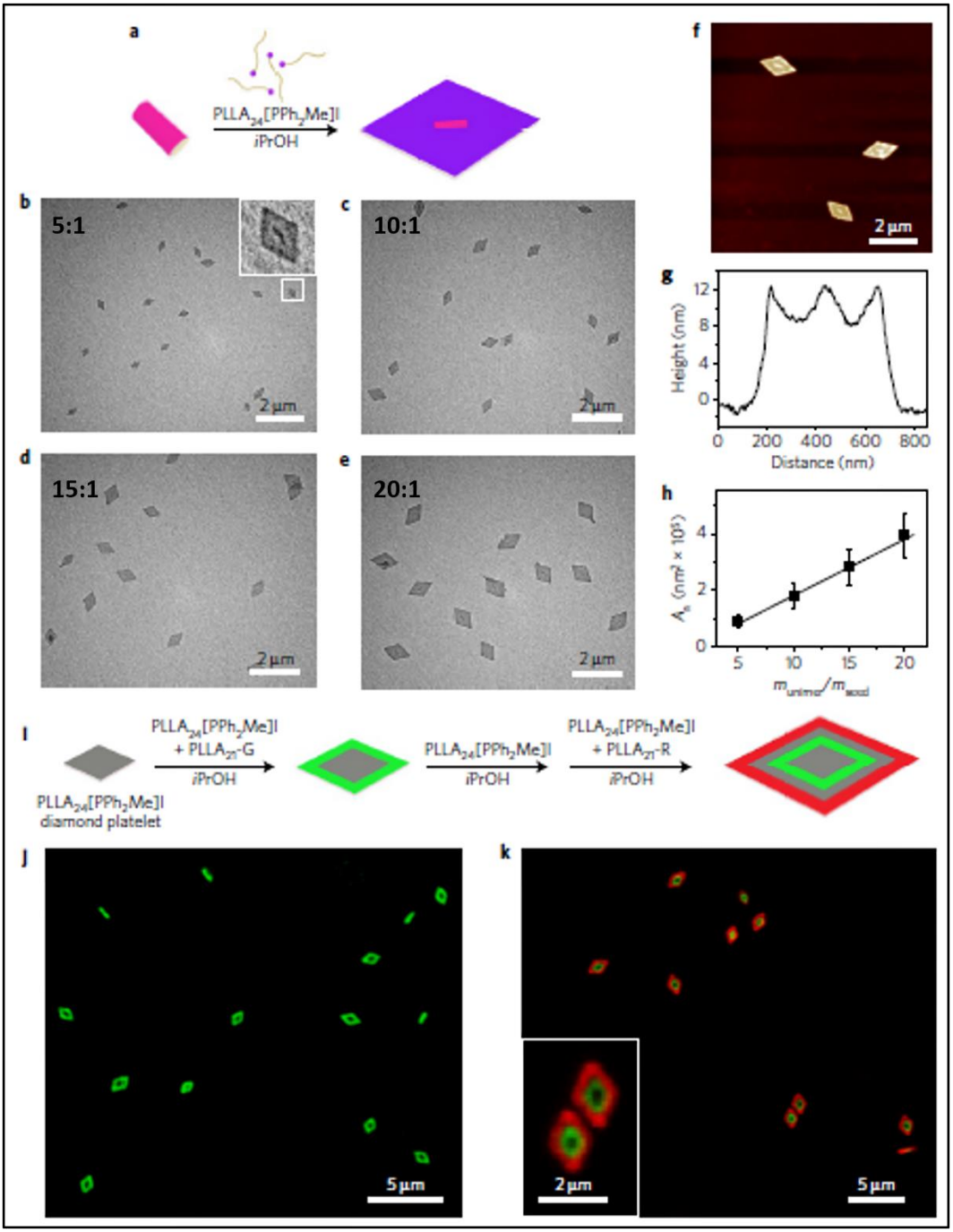


Figure 1.11 Uniform diamond platelet micelles prepared by seeded growth of $PLLA_{24}[PPh_2Me]I$. **(a)** Schematic representation of the formation of diamond platelets through seeded growth. (**b**–**e**) TEM images of uniform diamond platelets formed through seeded growth from a 1D seed with m_{unimer}/m_{seed} of 5:1-20:1. (**f**) AFM image of a diamond platelet micelle. (**g**) Height profile of the diamond platelet. (**h**) Linear dependence of micelle area on the m_{unimer}/m_{seed}. (**i**) Schematic diagram showing the formation of fluorescent concentric diamond block co-micelles in two dimensions from a non-fluorescent diamond platelet by the sequential addition of fluorescent

blend and non-fluorescent $PLLA_{24}[PPh_2Me]I$ in $CHCl_3$ and visualised by LSCM. (**j**, **k**) LSCM images of diblock (**j**) and tetra-block (**k**) co-micelles with segregated regions comprised of non-fluorescent blocks and fluorescent blocks. Adapted from ref.[110]

Manners and co-workers investigated a seeded growth method to prepare monodisperse and uniform rectangular platelets micelles with controlled size through adding blends of BCP (PFS_{36}-*b*-$P2VP_{502}$) (P2VP: poly(2-vinylpyridine)) and homopolymer (PFS_{20}) to cylindrical micelle seeds[99]. Interestingly, sequential addition of homopolymer and BCP blends with different corona chemistries (P2VP or PDMS corona block) yields concentric rectangular platelet block co-micelles, which could be selectively crosslinked in spatially specific regions, allowing the disassembly of un-cross-linked regions to form hollow rectangular platelets in a good solvent (**Figure 1.12**). Furthermore, 2D micelles with spatially defined dye functionality were obtained and characterized by fluorescence microscopy. This work opens the door for building up complex 2D micelles with exceptional level of control and provides a tuneable platform for further functionalisation on soft matter.

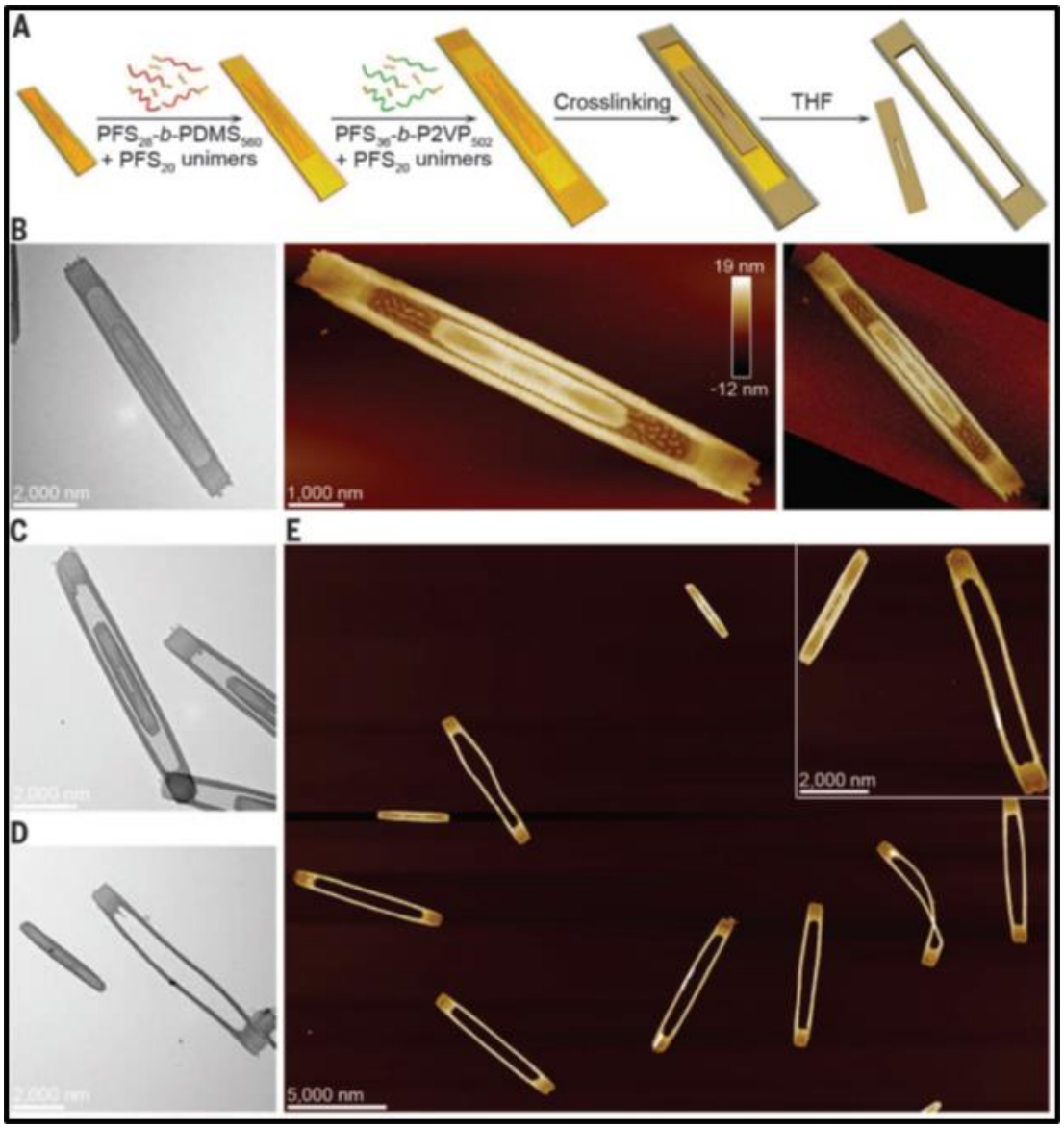


Figure 1.12 Patchy and hollow rectangular platelet micelles. Concentric rectangular platelet block co-micelles can be prepared through the sequential, alternate addition of PFS_{36}-*b*-$P2VP_{502}$/PFS_{20} and PFS_{28}-*b*-$PDMS_{560}$/PFS_{20} blend unimers. (A) Schematic diagram illustrating this process. (B) TEM, AFM height, and AFM 3D images of triblock co-micelles formed through the sequential addition of the PFS_{36}-*b*-$P2VP_{502}$/PFS_{20}, PFS_{28}-*b*-$PDMS_{560}$/PFS_{20}, and PFS_{36}-*b*-$P2VP_{502}$/PFS_{20} blend unimers to a solution of the PFS_{28}-*b*-$PDMS_{560}$ seeds in a mixture of hexane and iPrOH. (C) TEM image of platelets after cross-linking of the P2VP coronas. (D and E) TEM and AFM height images of a mixture of perforated rectangular platelets and well-defined hollow rectangular rings formed after redispersal in THF. Adapted from ref.[99]

In 2017, Stenzel and co-workers demonstrated that the dimensions of 2D platelet particles could be controlled from nano- to micro-meter, by changing the composition of the corona-forming segment and modulating the polymeric chain length.[98] Furthermore, biodegradable diblock glycopolymers of poly(ε-caprolactone)-*b*-poly[(1-O-acryloyl-D-fructopyranose)-co-(5,6-benzo-2-methylene-1,3-dioxepane)] (PCL-*b*-P[F-co-BMDO]) were used as a model system. Through the addition of unimers, super-sized hexagonal 2D platelets were formed by epitaxial growth, likely as a consequence of the stronger repulsion of corona-chain and chains stretching, leading to a higher free-energy cost (**Figure 1.13**). As a result, this system drives more chains folding, therefore favourably generating larger-sized lamellar aggregates.

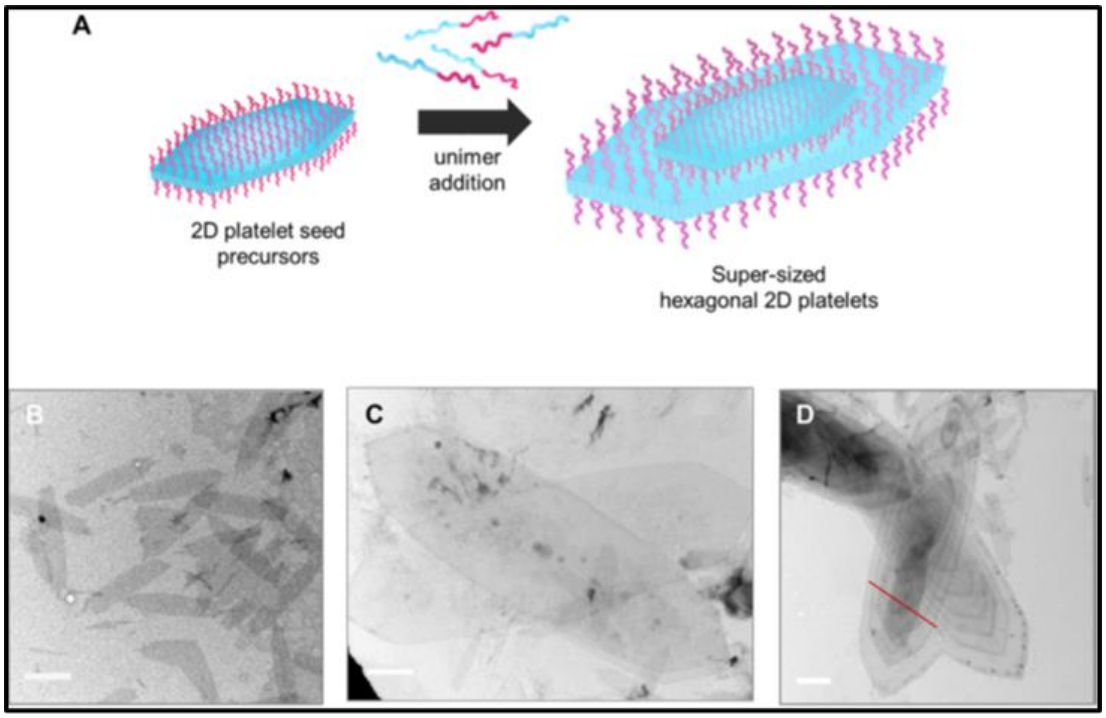


Figure 1.13 (A) Schematic illustration of seeded growth of 2D platelets used as precursors upon the addition of BCP unimers resulting in the significant increase in the lateral dimension of preformed platelets. TEM images of a representative sample prepared by the seeded growth of (B) PCL_{101}-*b*-PF_{178} platelet seed precursors in aqueous solution by the addition of the corresponding BCP PCL_{101}-*b*-PF_{178} unimers aged at 3-4 °C led to the formation of (C, D) supersized 2D hexagonal platelets (Scale bar = 2 μm). Adapted from ref.[98]

1.2.3.3 Spatial Control of Hierarchical Structures

Living CDSA has also shown the ability to create complex higher order structures, owing to the epitaxial nature of seeded growth. A good example to illustrate the hierarchical system using the living CDSA was reported by Manners and co-workers.[103] The super-micelles were fabricated by modulating the hydrophobic interactions in the system based on the building block - polar (P) blocks or hydrophobic (non-polar, H) segments, where P represents PFS-*b*-P2VP BCP, and H represents PFS-*b*-PDMS BCP. First, 1D micelles are prepared directly (**Figure 1.14 a**). Then, a multi-step self-assembly of each diblock copolymer into uniform P-H-P triblock co-micelles with nonpolar middle segment and polar outer segment was obtained *via* side-by-side or end-to-end stacking (**Figure 1.14 b**). Finally, multidimensional superstructures are prepared by the end-to-end self-assembly of H-P-H triblock co-micelles by altering the solvent (**Figure 1.14 c**). These assemblies could be reached on a micrometre length scale through the combination of multiple levels of structural hierarchy.

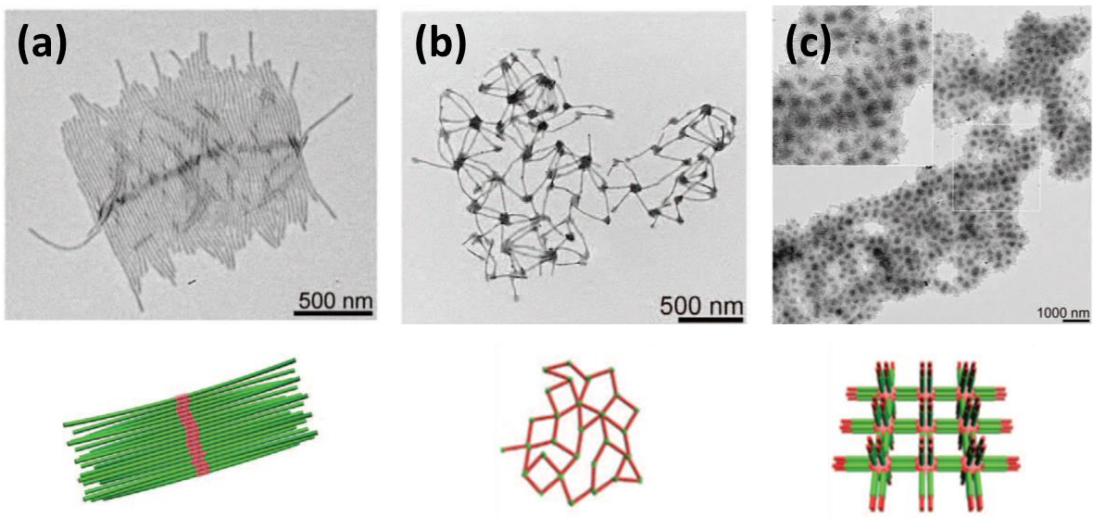


Figure 1.14 TEM images and schematic representations of supermicelles. (a) Side-by-side stacking of P-H-P triblock co-micelles including PFS-*b*-P2VP (green) and PFS-*b*-PDMS (red); (b) End-to-end stacking of P-H-P triblock comicelles including PFS-*b*-P2VP (green) and PFS-*b*-

PDMS (red); (c) End-to-end stacking of H-P-H triblock comicelles consists of PFS-*b*-P2VP (green) and PFS-*b*-PDMS (red). Adapted from ref.[103]

Though strategic manipulation of seeded growth based on PFS nanocrystals, the branched structures such as multi-armed nanostructures were accessed. Qiu *et al.* created multi-armed micelles using this approach (**Figure 1.15**),[147] where a suitable time window exists for PFS colloids to co-assemble, similarly to how surfactants are used to stabilise emulsions. The number of arms was observed to increase with increasing nanocrystal size. Furthermore, segmented multi-armed diblock co-micelles were also achieved through adding unimers with different corona chemistries.

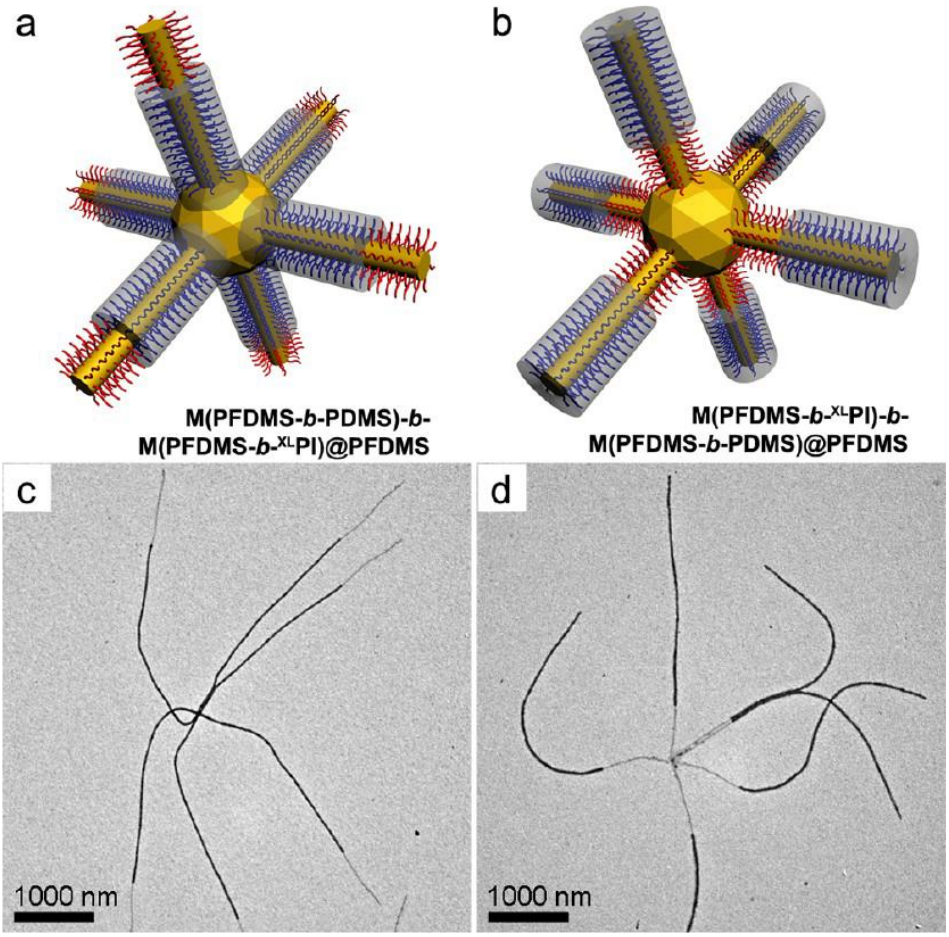


Figure 1.15 Pictorial representations and corresponding TEM images of (a, c) the M(PFDMS-*b*-PDMS)-*b*-M(PFDMS-*b*-XLPI)@PFDMS and (b, d) the M(PFDMS-*b*-XLPI)-*b*-M(PFDMS-*b*-PDMS)@PFDMS multiarmed diblock co-micelles. Adapted from ref.[147]

1.3 Surface Modification of Nanomaterials

Many applications of functional materials require the modification of their surface for use in composite materials, electronics, membranes, semi-conductive sensors, microfluidic, and biomedical devices. Surface functionalisation endows new properties independent from those of the original substrate and protects the material from unusual environmental damage.

1.3.1 Traditional Physical and Chemical Routes

A broad range of traditional methods including physical techniques and chemical routes, such as spray, spin-coating, electrochemical deposition and heat treatment (**Figure 1.16**) have been investigated to tailor materials surfaces with an extensive range of desired properties for electrolysis, energy storage, and nanomorphology manufacture.[148-153]

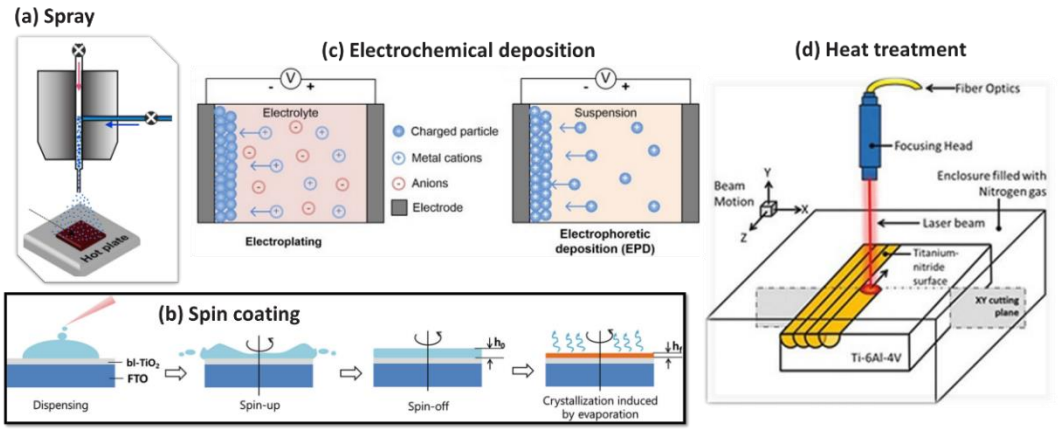


Figure 1.16 Conventional surface decoration methods. (a) spray; (b) spin-coating; (c) electrochemical deposition; (d) heat treatment.[150-153]

To date, a large number of research groups working to improve energy conversion have paid particular attention to functionalising and protecting such substrate interface through surface modification techniques. In 2018, Hao and co-workers fabricated a superior Cu_2ZnSnS_4 solar cell with efficiency of 11% and high open-circuit voltage of 730 mV,

which was achieved *via* surface heterojunction heat treatment.[153] This work uses the surface treatment to fastens elemental inter-diffusion of Cd atoms, directly occupying the lattice sites of Zn or Cu. It could facilitate the accumulation of Na, accompanied by local Cu deficiency within the heterojunction area. As a result, non-radiative recombination was decreased in the hetero-interface, due to new phases generated and more favourable conduction band alignment obtained. However, traditional physical and chemical methods are still limited by some practical conditions in reality.

1.3.2 Surface-Initiated Functionalisation

Together with traditional surface decoration approaches, surface-initiated functionalisation with polymer brushes is one of promising approach, tailoring the novel chemical and physical properties of polymeric interfaces.[154-157] The use of polymer brushes has been mostly focused to the modification of surfaces for adhesion,[158, 159] biocompatibility,[160] lubrication,[161, 162] wetting,[163, 164] and colloidal stabilisation applications.[165-167]

Recently, Manners and co-workers demonstrated endowed multifunctional micellar brushes on a silicon surface through crystallisation-driven growth.[108] They selected PFS-*b*-P2VP as small seeds to immobilise on a silicon wafer substrate, owing to the tenacious attachment between silanol groups and P2VP corona *via* hydrogen bonding. Upon addition, unimers grew at the termini of the immobilised seeds, eventually generating a layer of fibre-like nanoscopic brushes with lengths of ~1 mm on the surface (**Figure 1.17**). Moreover, the coronal block, density, and length of the micellar brushes can be exquisitely modulated. More importantly, post-growth decorated nanostructures can be implemented in antibacterial materials and catalysis. This method has also been extended to other material surfaces, and micellar brushes anchored on graphene oxide (GO) sheets

were obtained. This work provided a versatile bottom-up strategy for the precisely controlled functionalisation of BCP micellar brushes on the surfaces through crystallisation-driven growth in a precisely controlled fasion, which has great potential to be applied in a variety of fields including super hydrophobicity and lithography.

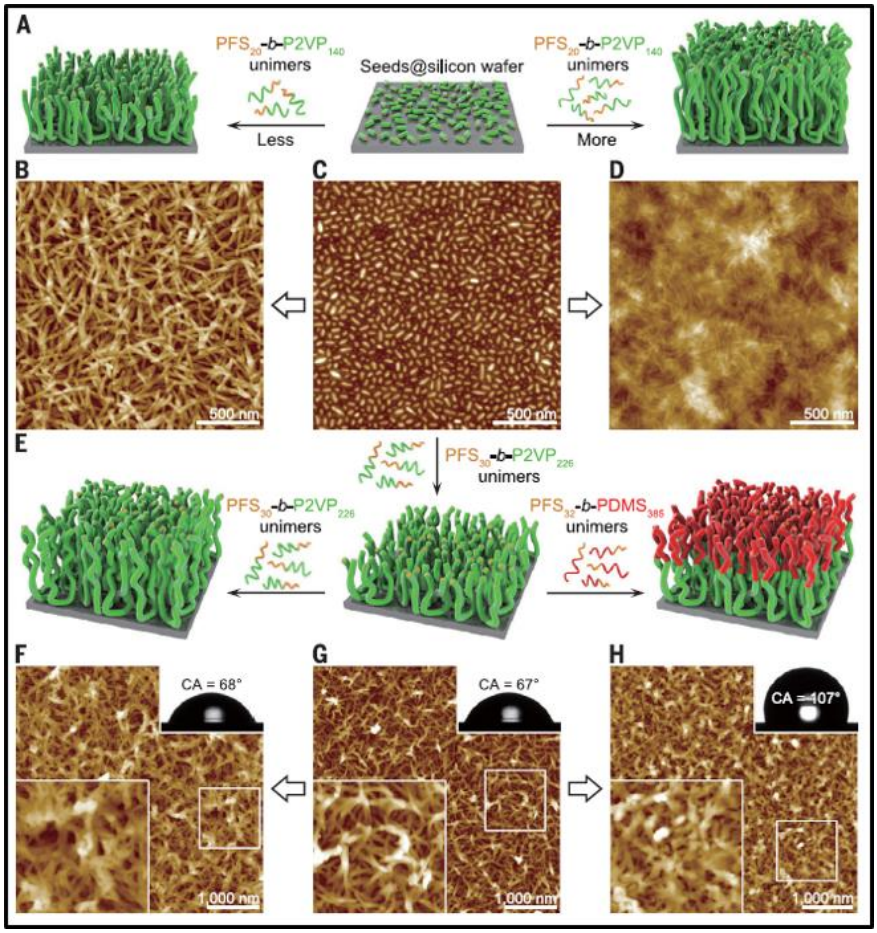


Figure 1.17 Seeded growth of hydrophilic PFS-*b*-P2VP and segmented micellar brushes on a silicon wafer. (A) Schematic illustration of the growth process for PFS_{20}-*b*-$P2VP_{140}$ micellar brushes. (B to D) AFM height images of (C) PFS_{36}-*b*-$P2VP_{502}$ seed-coated silicon wafer and PFS_{20}-*b*-$P2VP_{140}$ micellar brushes formed by the addition of (B, D) 4 and 10 ml unimers solution, respectively. (E) Schematic illustration of the growth process for PFS_{30}-*b*-$P2VP_{226}$ micellar brushes and segmented micellar brushes. (F to H) AFM height images of (G) short PFS_{30}-*b*-$P2VP_{226}$ micellar brushes formed by the addition of 3 ml unimer solution, (F) elongated micellar brushes formed by further addition of 3 mL of PFS_{30}-*b*-$P2VP_{226}$ unimer solution to the short

micellar brushes shown in (G), and (H) segmented micellar brushes formed by further addition of 3 ml of PFS_{32}-*b*-$PDMS_{385}$ unimer solution to the short micellar brushes shown in (G). Adapted from ref.[108]

Hawker and co-workers reported a facile method to fabricate three dimensional (3D) polymer brushes based on a uniform initiating layer *via* light mediated living radical polymerisation.[70] The propagating polymeric chains can be controlled by switching on/off the light, returning to dormant state efficiently when the light is switched off, while continuing reinitiation upon exposing to the light. Moreover, brush growth also could be selectively defined to specific expose regions by using a traditional photomask, affording temporal and spatial control over chain growth (**Figure 1.18**). Excitingly, the patterning process is non-destructive with regards to initiator activity, providing the ability to achieve sequential polymerisation of monomers from the former initiating layer and fabricate 3D structures by manipulation of surface properties.

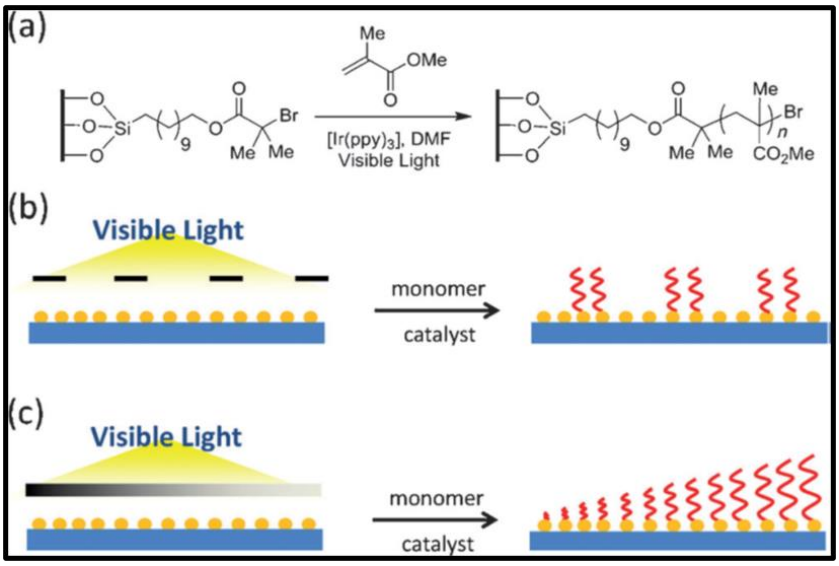


Figure 1.18 Patterning of polymer brushes from substrates uniformly functionalised with trichlorosilane-substituted a-bromoisobutyrate based initiators (a) using b) a photomask for patterns or c) a neutral density filter for gradient structures. DMF = *N*,*N*-dimethylformamide, ppy = 2-phenylpyridine. Adapted from ref.[70]

1.4 Summary

The primary advantage of precise nanostructure design relies in the control that can be achieved over the composition and structure of the resultant assemblies to afford unique morphologies. This introductory chapter outlines the principles discussed in this thesis.

The first section highlighted advanced living polymerisation techniques for the synthesis of macromolecules, such as RAFT polymerisation, light-mediated polymerisation and ring-opening polymerisation. This was followed by a discussion of traditional self-assembly strategies, the theory of block copolymer self-assembly and critical factors of this process. One of the most recently developed self-assembly approach, CDSA, has been described in detail. This platform allows the formation of well-defined 1D, 2D, and even complex hierarchical assemblies with exquisite dimension and spatial control. The self-assembly PCL-based 2D platelet micelles with the high level of control, including size manipulation, multilayer combination, and fluorescent dye incorporation, is investigated in Chapter 2.

Finally, several design strategies for surface modification of nanomaterials were summarised in this chapter, including conventional physical and chemical routes and surface-initiated functionalisation. In Chapter 3, photo RAFT polymerisation technique has been expanded to surface modification on the PCL-based platelets, to spatial tune in three dimensions.

1.5 References

1. Z. Wu, Y. Wu, W. He, X. Lin, J. Sun and Q. He, *Angew. Chem. Int. Ed.*, 2013, **52**, 7000-7003.
2. M. Sienkiewicz, H. Janik, K. Borzędowska-Labuda and J. Kucińska-Lipka, *J. Clean. Prod.*, 2017, **147**, 560-571.
3. G. Hong, Y. Zou, A. L. Antaris, S. Diao, D. Wu, K. Cheng, X. Zhang, C. Chen, B. Liu, Y. He, J. Z. Wu, J. Yuan, B. Zhang, Z. Tao, C. Fukunaga and H. Dai, *Nat. Commun.*, 2014, **5**, 4206.
4. J. H. Park, S. Lee, J.-H. Kim, K. Park, K. Kim and I. C. Kwon, *Prog. Polym. Sci.*, 2008, **33**, 113-137.
5. F. Hussain, M. Hojjati, M. Okamoto and R. E. Gorga, *J. Compos. Mater.*, 2006, **40**, 1511-1575.
6. G. Schwartz, B. C. Tee, J. Mei, A. L. Appleton, D. H. Kim, H. Wang and Z. Bao, *Nat. Commun.*, 2013, **4**, 1859.
7. X. Zhang, M. Fevre, G. O. Jones and R. M. Waymouth, *Chem. Rev.*, 2018, **118**, 839-885.
8. J. C. Worch, H. Prydderch, S. Jimaja, P. Bexis, M. L. Becker and A. P. Dove, *Nat. Rev. Chem.*, 2019, **3**, 514-535.
9. J. C. Foster and R. K. O'Reilly, *Science*, 2019, **363**, 1394.
10. N. G. Engelis, A. Anastasaki, G. Nurumbetov, N. P. Truong, V. Nikolaou, A. Shegiwal, M. R. Whittaker, T. P. Davis and D. M. Haddleton, *Nat. Chem.*, 2017, **9**, 171-178.
11. P. R. Judzewitsch, T. K. Nguyen, S. Shanmugam, E. H. H. Wong and C. Boyer, *Angew. Chem. Int. Ed.*, 2018, **57**, 4559-4564.

12. D. T. Gentekos, L. N. Dupuis and B. P. Fors, *J. Am. Chem. Soc.*, 2016, **138**, 1848-1851.

13. D. J. Walsh, D. A. Schinski, R. A. Schneider and D. Guironnet, *Nat. Commun.*, 2020, **11**, 3094.

14. J. C. Foster, S. Varlas, B. Couturaud, J. R. Jones, R. Keogh, R. T. Mathers and R. K. O'Reilly, *Angew. Chem. Int. Ed.*, 2018, **57**, 15733-15737.

15. T. Takata and D. Aoki, *Polym. J.*, 2017, **50**, 127-147.

16. Y. Gu, J. Zhao and J. A. Johnson, *Trends Chem.*, 2019, **1**, 318-334.

17. S. Yagai, Y. Kitamoto, S. Datta and B. Adhikari, *Acc. Chem. Res.*, 2019, **52**, 1325-1335.

18. E. B. Trigg, M. J. Stevens and K. I. Winey, *J. Am. Chem. Soc.*, 2017, **139**, 3747-3755.

19. P. Shieh, H. V. Nguyen and J. A. Johnson, *Nat. Chem.*, 2019, **11**, 1124-1132.

20. Y. Rokhlenko, K. Kawamoto, J. A. Johnson and C. O. Osuji, *Macromolecules*, 2018, **51**, 3680-3690.

21. K. E. B. Doncom, L. D. Blackman, D. B. Wright, M. I. Gibson and R. K. O'Reilly, *Chem. Soc. Rev.*, 2017, **46**, 4119-4134.

22. N. U. Dharmaratne, T. M. M. Jouaneh, M. K. Kiesewetter and R. T. Mathers, *Macromolecules*, 2018, **51**, 8461-8468.

23. M. Lucius, R. Falatach, C. McGlone, K. Makaroff, A. Danielson, C. Williams, J. C. Nix, D. Konkolewicz, R. C. Page and J. A. Berberich, *Biomacromolecules*, 2016, **17**, 1123-1134.

24. B. Qiao, G. M. Leverick, W. Zhao, A. H. Flood, J. A. Johnson and Y. Shao-Horn, *J. Am. Chem. Soc.*, 2018, **140**, 10932-10936.

25. Y. Gu, J. Zhao and J. A. Johnson, *Angew. Chem. Int. Ed.*, 2020, **59**, 5022-5049.

26. K. Matyjaszewski, *Science*, 2011, **333**, 1104-1105.
27. H. Sun, L. Yang, M. P. Thompson, S. Schara, W. Cao, W. Choi, Z. Hu, N. Zang, W. Tan and N. C. Gianneschi, *Bioconjug. Chem.*, 2019, **30**, 1889-1904.
28. R. B. Grubbs and R. H. Grubbs, *Macromolecules*, 2017, **50**, 6979-6997.
29. P. B. Zetterlund, S. C. Thickett, S. Perrier, E. Bourgeat-Lami and M. Lansalot, *Chem. Rev.*, 2015, **115**, 9745-9800.
30. W. A. Braunecker and K. Matyjaszewski, *Prog. Polym. Sci.*, 2007, **32**, 93-146.
31. M. Szwarc, M. Levy and R. Milkovich, *J. Am. Chem. Soc.*, 1956, **78**, 2656-2657.
32. S. Varlas, S. B. Lawrenson, L. A. Arkinstall, R. K. O'Reilly and J. C. Foster, *Prog. Polym. Sci.*, 2020, **107**.
33. W. Sang and Q. Yan, *Angew. Chem. Int. Ed.*, 2018, **57**, 4907-4911.
34. X. Wang, L. Shen and Z. An, *Prog. Polym. Sci.*, 2018, **83**, 1-27.
35. A. Sandeau, S. Mazières and M. Destarac, *Polymer*, 2012, **53**, 5601-5618.
36. H. Fischer, *Macromolecules*, 1997, **30**, 5666-5672.
37. H. Fischer, *Chem. Rev.*, 2001, **101**, 3581-3610.
38. K. Matyjaszewski, *Macromolecules*, 2012, **45**, 4015-4039.
39. J. Nicolas, Y. Guillaneuf, C. Lefay, D. Bertin, D. Gigmes and B. Charleux, *Prog. Polym. Sci.*, 2013, **38**, 63-235.
40. W. Tang, T. Fukuda and K. Matyjaszewski, *Macromolecules*, 2006, **39**, 4332-4337.
41. E. H. Discekici, A. Anastasaki, J. Read de Alaniz and C. J. Hawker, *Macromolecules*, 2018, **51**, 7421-7434.
42. J. Ran, L. Wu, Z. Zhang and T. Xu, *Prog. Polym. Sci.*, 2014, **39**, 124-144.
43. F. Seidi, H. Salimi, A. A. Shamsabadi and M. Shabanian, *Prog. Polym. Sci.*, 2018, **76**, 1-39.

44. B. M. Rosen and V. Percec, *Chem. Rev.*, 2009, **109**, 5069-5119.

45. S. Yamago, *Chem. Rev.*, 2009, **109**, 5051-5068.

46. S. G. Gaynor, J.-S. Wang and K. Matyjaszewski, *Macromolecules*, 1995, **28**, 8051-8056.

47. J. Chiefari, Y. K. Chong, F. Ercole, J. Krstina, J. Jeffery, T. P. T. Le, R. T. A. Mayadunne, G. F. Meijs, C. L. Moad, G. Moad, E. Rizzardo and S. H. Thang, *Macromolecules*, 1998, **31**, 5559-5562.

48. M. R. Hill, R. N. Carmean and B. S. Sumerlin, *Macromolecules*, 2015, **48**, 5459-5469.

49. X. Tian, J. Ding, B. Zhang, F. Qiu, X. Zhuang and Y. Chen, *Polymers*, 2018, **10**.

50. G. Moad, E. Rizzardo and S. H. Thang, *Polymer*, 2008, **49**, 1079-1131.

51. S. Perrier, *Macromolecules*, 2017, **50**, 7433-7447.

52. A. Gregory and M. H. Stenzel, *Prog. Polym. Sci.*, 2012, **37**, 38-105.

53. D. J. Keddie, G. Moad, E. Rizzardo and S. H. Thang, *Macromolecules*, 2012, **45**, 5321-5342.

54. D. J. Keddie, *Chem. Soc. Rev.*, 2014, **43**, 496-505.

55. G. Moad, E. Rizzardo and S. H. Thang, *Aust. J. Chem.*, 2009, **62**, 1402-1472.

56. J. Yeow, R. Chapman, A. J. Gormley and C. Boyer, *Chem. Soc. Rev.*, 2018, **47**, 4357-4387.

57. X. Pan, M. A. Tasdelen, J. Laun, T. Junkers, Y. Yagci and K. Matyjaszewski, *Prog. Polym. Sci.*, 2016, **62**, 73-125.

58. G. Yilmaz and Y. Yagci, *Prog. Polym. Sci.*, 2020, **100**.

59. N. Corrigan and C. Boyer, *Trends Chem.*, 2020, **2**, 689-706.

60. J. Yeow and C. Boyer, *Adv. Sci.*, 2017, **4**, 1700137.

61. T. Gruendling, M. Kaupp, J. P. Blinco and C. Barner-Kowollik, *Macromolecules*, 2011, **44**, 166-174.

62. E. E. Stache, V. Kottisch and B. P. Fors, *J. Am. Chem. Soc.*, 2020, **142**, 4581-4585.

63. Q. Fu, T. G. McKenzie, J. M. Ren, S. Tan, E. Nam and G. G. Qiao, *Sci. Rep.*, 2016, **6**, 20779.

64. M. Chen, S. Deng, Y. Gu, J. Lin, M. J. MacLeod and J. A. Johnson, *J. Am. Chem. Soc.*, 2017, **139**, 2257-2266.

65. S. Shin, F. Menk, Y. Kim, J. Lim, K. Char, R. Zentel and T. L. Choi, *J. Am. Chem. Soc.*, 2018, **140**, 6088-6094.

66. M. Chen, Y. Gu, A. Singh, M. Zhong, A. M. Jordan, S. Biswas, L. T. Korley, A. C. Balazs and J. A. Johnson, *ACS Cent. Sci.*, 2017, **3**, 124-134.

67. M. Chen, M. Zhong and J. A. Johnson, *Chem. Rev.*, 2016, **116**, 10167-10211.

68. M. Chen and J. A. Johnson, *Chem. Commun.*, 2015, **51**, 6742-6745.

69. T. Gegenhuber, L. De Keer, A. S. Goldmann, P. H. M. Van Steenberge, J. O. Mueller, M.-F. Reyniers, J. P. Menzel, D. R. D'hooge and C. Barner-Kowollik, *Macromolecules*, 2017, **50**, 6451-6467.

70. J. E. Poelma, B. P. Fors, G. F. Meyers, J. W. Kramer and C. J. Hawker, *Angew. Chem. Int. Ed.*, 2013, **52**, 6844-6848.

71. S. Shanmugam, J. Xu and C. Boyer, *J. Am. Chem. Soc.*, 2015, **137**, 9174-9185.

72. C. P. Easterling, Y. Xia, J. Zhao, G. E. Fanucci and B. S. Sumerlin, *ACS Macro Lett.*, 2019, **8**, 1461-1466.

73. N. Corrigan, J. Yeow, P. Judzewitsch, J. Xu and C. Boyer, *Angew. Chem. Int. Ed.*, 2019, **58**, 5170-5189.

74. T. Otsu and M. Yoshida, *Macromol. Rapid Commun.*, 1982, **3**, 127-132.

75. J. R. Lamb, K. P. Qin and J. A. Johnson, *Polym. Chem.*, 2019, **10**, 1585-1590.

76. M. Rubens, P. Latsrisaeng and T. Junkers, *Polym. Chem.*, 2017, **8**, 6496-6505.

77. A. Bagheri, C. Bainbridge and J. Jin, *ACS Appl. Polym. Mater.*, 2019, **1**, 1896-1904.

78. G. L. Gregory, E. M. Lopez-Vidal and A. Buchard, *Chem. Commun.*, 2017, **53**, 2198-2217.

79. Q. Song, J. Zhao, G. Zhang, F. Peruch and S. Carlotti, *Polym. J.*, 2019, **52**, 3-11.

80. M. Bednarek, *Prog. Polym. Sci.*, 2016, **58**, 27-58.

81. A.-L. Brocas, C. Mantzaridis, D. Tunc and S. Carlotti, *Prog. Polym. Sci.*, 2013, **38**, 845-873.

82. S. Penczek, M. Cypryk, A. Duda, P. Kubisa and S. Slomkowski, *Prog. Polym. Sci.*, 2007, **32**, 247-282.

83. K. Makiguchi, Y. Ogasawara, S. Kikuchi, T. Satoh and T. Kakuchi, *Macromolecules*, 2013, **46**, 1772-1782.

84. F. Nederberg, E. F. Connor, M. Möller, T. Glauser and J. L. Hedrick, *Angew. Chem. Int. Ed.*, 2001, **40**, 2712-2715.

85. L. Mespouille, O. Coulembier, M. Kawalec, A. P. Dove and P. Dubois, *Prog. Polym. Sci.*, 2014, **39**, 1144-1164.

86. P. Olsen, K. Odelius, H. Keul and A. C. Albertsson, *Macromolecules*, 2015, **48**, 1703-1710.

87. A. P. Dove, R. C. Pratt, B. G. Lohmeijer, R. M. Waymouth and J. L. Hedrick, *J. Am. Chem. Soc.*, 2005, **127**, 13798-13799.

88. H. Misaka, R. Kakuchi, C. Zhang, R. Sakai, T. Satoh and T. Kakuchi, *Macromolecules*, 2009, **42**, 5091-5096.

89. B. G. G. Lohmeijer, R. C. Pratt, F. Leibfarth, J. W. Logan, D. A. Long, A. P. Dove, F. Nederberg, J. Choi, C. Wade, R. M. Waymouth and J. L. Hedrick, *Macromolecules*, 2006, **39**, 8574-8583.

90. K. Makiguchi, T. Satoh and T. Kakuchi, *Macromolecules*, 2011, **44**, 1999-2005.

91. J. A. Wilson, Z. Ates, R. L. Pflughaupt, A. P. Dove and A. Heise, *Prog. Polym. Sci.*, 2019, **91**, 29-50.

92. X. Lian, D. Wu, X. Song and H. Zhao, *Macromolecules*, 2010, **43**, 7434-7445.

93. W. M. Jacobs and D. Frenkel, *J. Am. Chem. Soc.*, 2016, **138**, 2457-2467.

94. M. J. Derry, L. A. Fielding and S. P. Armes, *Prog. Polym. Sci.*, 2016, **52**, 1-18.

95. J. N. Israelachvili, D. J. Mitchell and B. W. Ninham, *J. Chem. Soc. Faraday Trans.*, 1976, **72**.

96. J. B. Gilroy, T. Gadt, G. R. Whittell, L. Chabanne, J. M. Mitchels, R. M. Richardson, M. A. Winnik and I. Manners, *Nat. Chem.*, 2010, **2**, 566-570.

97. J. B. Gilroy, D. J. Lunn, S. K. Patra, G. R. Whittell, M. A. Winnik and I. Manners, *Macromolecules*, 2012, **45**, 5806-5815.

98. S. Ganda, M. Dulle, M. Drechsler, B. Förster, S. Förster and M. H. Stenzel, *Macromolecules*, 2017, **50**, 8544-8553.

99. H. Qiu, Y. Gao, C. E. Boott, O. E. Gould, R. L. Harniman, M. J. Miles, S. E. Webb, M. A. Winnik and I. Manners, *Science*, 2016, **352**, 697-701.

100. S. Pearce, X. He, M.-S. Hsiao, R. L. Harniman, L. R. MacFarlane and I. Manners, *Macromolecules*, 2019, **52**, 6068-6079.

101. C. E. Boott, J. Gwyther, R. L. Harniman, D. W. Hayward and I. Manners, *Nat. Chem.*, 2017, **9**, 785-792.

102. A. Nazemi, X. He, L. R. MacFarlane, R. L. Harniman, M. S. Hsiao, M. A. Winnik, C. F. Faul and I. Manners, *J. Am. Chem. Soc.*, 2017, **139**, 4409-4417.

103. H. Qiu, Z. M. Hudson, M. A. Winnik and I. Manners, *Science*, 2015, **347**, 1329-1332.

104. S. Ganda and M. H. Stenzel, *Prog. Polym. Sci.*, 2020, **101**.

105. B. Lotz, A. J. Kovacs, G. A. Bassett and A. Keller, *Colloid Polym. Sci.*, 1966, **209**, 115-128.

106. J. Massey, K. N. Power, I. Manners and M. A. Winnik, *J. Am. Chem. Soc.*, 1998, **120**, 9533-9540.

107. C. E. Boott, E. M. Leitao, D. W. Hayward, R. F. Laine, P. Mahou, G. Guerin, M. A. Winnik, R. M. Richardson, C. F. Kaminski, G. R. Whittell and I. Manners, *ACS Nano*, 2018, **12**, 8920-8933.

108. J. Cai, C. Li, N. Kong, Y. Lu, G. Lin, X. Wang, Y. Yao, I. Manners and H. Qiu, *Science*, 2019, **366**, 1095-1098.

109. G. Guerin, M. Cruz and Q. Yu, *Sci. Adv.*, 2020, **6**, eaaz7301.

110. X. He, M. S. Hsiao, C. E. Boott, R. L. Harniman, A. Nazemi, X. Li, M. A. Winnik and I. Manners, *Nat. Mater.*, 2017, **16**, 481-488.

111. Z. M. Hudson, C. E. Boott, M. E. Robinson, P. A. Rupar, M. A. Winnik and I. Manners, *Nat. Chem.*, 2014, **6**, 893-898.

112. Z. M. Hudson, D. J. Lunn, M. A. Winnik and I. Manners, *Nat. Commun.*, 2014, **5**, 3372.

113. C. N. Jarrett-Wilkins, R. A. Musgrave, R. L. N. Hailes, R. L. Harniman, C. F. J. Faul and I. Manners, *Macromolecules*, 2019, **52**, 7289-7300.

114. A. M. Oliver, J. Gwyther, C. E. Boott, S. Davis, S. Pearce and I. Manners, *J. Am. Chem. Soc.*, 2018, **140**, 18104-18114.

115. X. Wang, G. Guerin, H. Wang, Y. Wang, I. Manners and M. A. Winnik, *Science*, 2007, **317**, 644-647.

116. Q. Zhang, Y. He, A. M. Oliver, S. Pearce, R. L. Harniman, G. R. Whittell, Y. Liu, S. Du, J. Leng and I. Manners, *Polym. Chem.*, 2019, **10**, 3973-3982.

117. R. L. Hailes, A. M. Oliver, J. Gwyther, G. R. Whittell and I. Manners, *Chem. Soc. Rev.*, 2016, **45**, 5358-5407.

118. J. R. Finnegan, X. He, S. T. G. Street, J. D. Garcia-Hernandez, D. W. Hayward, R. L. Harniman, R. M. Richardson, G. R. Whittell and I. Manners, *J. Am. Chem. Soc.*, 2018, **140**, 17127-17140.

119. J. Schmelz, A. E. Schedl, C. Steinlein, I. Manners and H. Schmalz, *J. Am. Chem. Soc.*, 2012, **134**, 14217-14225.

120. J. Schmelz, M. Karg, T. Hellweg and H. Schmalz, *ACS Nano*, 2011, **5**, 9523-9534.

121. J. Schöbel, M. Karg, D. Rosenbach, G. Krauss, A. Greiner and H. Schmalz, *Macromolecules*, 2016, **49**, 2761-2771.

122. M. C. Arno, M. Inam, A. C. Weems, Z. Li, A. L. A. Binch, C. I. Platt, S. M. Richardson, J. A. Hoyland, A. P. Dove and R. K. O'Reilly, *Nat. Commun.*, 2020, **11**, 1420.

123. Y. He, J. C. Eloi, R. L. Harniman, R. M. Richardson, G. R. Whittell, R. T. Mathers, A. P. Dove, R. K. O'Reilly and I. Manners, *J. Am. Chem. Soc.*, 2019, **141**, 19088-19098.

124. P. J. Hurst, A. M. Rakowski and J. P. Patterson, *Nat. Commun.*, 2020, **11**, 4690.

125. L. Sun, N. Petzetakis, A. Pitto-Barry, T. L. Schiller, N. Kirby, D. J. Keddie, B. J. Boyd, R. K. O'Reilly and A. P. Dove, *Macromolecules*, 2013, **46**, 9074-9082.

126. G. Rizis, T. G. van de Ven and A. Eisenberg, *Angew. Chem. Int. Ed.*, 2014, **53**, 9000-9003.

127. X. H. Jin, M. B. Price, J. R. Finnegan, C. E. Boott, J. M. Richter, A. Rao, S. M. Menke, R. H. Friend, G. R. Whittell and I. Manners, *Science*, 2018, **360**, 897-900.

128. H. Shaikh, X. H. Jin, R. L. Harniman, R. M. Richardson, G. R. Whittell and I. Manners, *J. Am. Chem. Soc.*, 2020, **142**, 13469-13480.

129. C. Legros, M. C. De Pauw-Gillet, K. C. Tam, D. Taton and S. Lecommandoux, *Soft Matter*, 2015, **11**, 3354-3359.

130. M. C. Arno, M. Inam, Z. Coe, G. Cambridge, L. J. Macdougall, R. Keogh, A. P. Dove and R. K. O'Reilly, *J. Am. Chem. Soc.*, 2017, **139**, 16980-16985.

131. Y. Cha, C. Jarrett-Wilkins, M. A. Rahman, T. Zhu, Y. Sha, I. Manners and C. Tang, *ACS Macro Lett.*, 2019, **8**, 835-840.

132. Z. Coe, A. Weems, A. P. Dove and R. K. O'Reilly, *J. Vis. Exp.*, 2019, DOI: 10.3791/59772, e59772.

133. W. Yu, J. C. Foster, A. P. Dove and R. K. O'Reilly, *Macromolecules*, 2020, **53**, 1514-1521.

134. Y. Cui, Z. Wang, X. Huang, G. Lu, I. Manners, M. A. Winnik and C. Feng, *Macromolecules*, 2020, **53**, 1831-1841.

135. D. Tao, Y. Cui, X. Huang, G. Lu, I. Manners, M. A. Winnik and C. Feng, *J. Colloid Interface Sci.*, 2020, **560**, 50-58.

136. D. Tao, C. Feng, Y. Cui, X. Yang, I. Manners, M. A. Winnik and X. Huang, *J. Am. Chem. Soc.*, 2017, **139**, 7136-7139.

137. D. Tao, Z. Wang, X. Huang, M. Tian, G. Lu, I. Manners, M. A. Winnik and C. Feng, *Angew. Chem. Int. Ed.*, 2020, **59**, 8232-8239.

138. E. L. Kynaston, A. Nazemi, L. R. MacFarlane, G. R. Whittell, C. F. J. Faul and I. Manners, *Macromolecules*, 2018, **51**, 1002-1010.

139. S. Ganda and M. H. Stenzel, *Prog. Polym. Sci.*, 2020, **101**, 101195.

140. L. R. MacFarlane, H. Shaikh, J. D. Garcia-Hernandez, M. Vespa, T. Fukui and I. Manners, *Nat. Rev. Mater.*, 2020, **6**, 7-26.

141. T. Vilgis and A. Halperin, *Macromolecules*, 1991, **24**, 2090-2095.

142. C. Ma, Z. Wang, X. Huang, G. Lu, I. Manners, M. A. Winnik and C. Feng, *Macromolecules*, 2020, **53**, 8009-8019.

143. X. Li, Y. Gao, R. Harniman, M. Winnik and I. Manners, *J. Am. Chem. Soc.*, 2016, **138**, 12902-12912.

144. T. Fukui, J. D. Garcia-Hernandez, L. R. MacFarlane, S. Lei, G. R. Whittell and I. Manners, *J. Am. Chem. Soc.*, 2020, **142**, 15038-15048.

145. J. Tian, Y. Zhang, L. Du, Y. He, X. H. Jin, S. Pearce, J. C. Eloi, R. L. Harniman, D. Alibhai, R. Ye, D. L. Phillips and I. Manners, *Nat. Chem.*, 2020, **12**, 1150-1156.

146. J. C. Foster, S. Varlas, B. Couturaud, Z. Coe and R. K. O'Reilly, *J. Am. Chem. Soc.*, 2019, **141**, 2742-2753.

147. H. Qiu, G. Cambridge, M. A. Winnik and I. Manners, *J. Am. Chem. Soc.*, 2013, **135**, 12180-12183.

148. Z. Han, R. Kortlever, H. Y. Chen, J. C. Peters and T. Agapie, *ACS Cent. Sci.*, 2017, **3**, 853-859.

149. F. Li, A. Thevenon, A. Rosas-Hernandez, Z. Wang, Y. Li, C. M. Gabardo, A. Ozden, C. T. Dinh, J. Li, Y. Wang, J. P. Edwards, Y. Xu, C. McCallum, L. Tao, Z. Q. Liang, M. Luo, X. Wang, H. Li, C. P. O'Brien, C. S. Tan, D. H. Nam, R. Quintero-Bermudez, T. T. Zhuang, Y. C. Li, Z. Han, R. D. Britt, D. Sinton, T. Agapie, J. C. Peters and E. H. Sargent, *Nature*, 2020, **577**, 509-513.

150. I. S. Yang, M. R. Sohn, S. D. Sung, Y. J. Kim, Y. J. Yoo, J. Kim and W. I. Lee, *Nano Energy*, 2017, **32**, 414-421.

151. T. Ozel, B. A. Zhang, R. Gao, R. W. Day, C. M. Lieber and D. G. Nocera, *Nano Lett.*, 2017, **17**, 4502-4507.

152. J. H. Heo, D. H. Song and S. H. Im, *Adv. Mater.*, 2014, **26**, 8179-8183.

153. C. Yan, J. Huang, K. Sun, S. Johnston, Y. Zhang, H. Sun, A. Pu, M. He, F. Liu, K. Eder, L. Yang, J. M. Cairney, N. J. Ekins-Daukes, Z. Hameiri, J. A. Stride, S. Chen, M. A. Green and X. Hao, *Nat. Energy*, 2018, **3**, 764-772.

154. J. M. Giussi, M. L. Cortez, W. A. Marmisolle and O. Azzaroni, *Chem. Soc. Rev.*, 2019, **48**, 814-849.

155. J. O. Zoppe, N. C. Ataman, P. Mocny, J. Wang, J. Moraes and H. A. Klok, *Chem. Rev.*, 2017, **117**, 1105-1318.

156. G. Sun, S. Cho, C. Clark, S. V. Verkhoturov, M. J. Eller, A. Li, A. Pavia-Jimenez, E. A. Schweikert, J. W. Thackeray, P. Trefonas and K. L. Wooley, *J. Am. Chem. Soc.*, 2013, **135**, 4203-4206.

157. W. Zong, G. W. Li, J. M. Cao, X. Lei, M. L. Hu, H. Sun, C. Griesinger and R. X. Tan, *Angew. Chem. Int. Ed.*, 2016, **55**, 3690-3693.

158. O. Roling, L. Stricker, J. Voskuhl, S. Lamping and B. J. Ravoo, *Chem. Commun.*, 2016, **52**, 1964-1966.

159. A. Synytska, E. Svetushkina, D. Martina, C. Bellmann, F. Simon, L. Ionov, M. Stamm and C. Creton, *Langmuir*, 2012, **28**, 16444-16454.

160. M. Krishnamoorthy, S. Hakobyan, M. Ramstedt and J. E. Gautrot, *Chem. Rev.*, 2014, **114**, 10976-11026.

161. R. A. Wright, K. Wang, J. Qu and B. Zhao, *Angew. Chem. Int. Ed.*, 2016, **55**, 8656-8660.

162. B. T. Seymour, R. A. E. Wright, A. C. Parrott, H. Gao, A. Martini, J. Qu, S. Dai and B. Zhao, *ACS Appl. Mater. Interfaces*, 2017, **9**, 25038-25048.

163. H. Yamaguchi, M. Kikuchi, M. Kobayashi, H. Ogawa, H. Masunaga, O. Sakata and A. Takahara, *Macromolecules*, 2012, **45**, 1509-1516.

164. O. Azzaroni, A. A. Brown and W. T. Huck, *Angew. Chem. Int. Ed.*, 2006, **45**, 1770-1774.

165. F. Polzer, D. A. Kunz, J. Breu and M. Ballauff, *Chem. Mater.*, 2010, **22**, 2916-2922.

166. B. A. Humphreys, E. J. Wanless and G. B. Webber, *J. Colloid Interface Sci.*, 2018, **516**, 153-161.

167. L. Jia, G. Zhao, W. Shi, N. Coombs, I. Gourevich, G. C. Walker, G. Guerin, I. Manners and M. A. Winnik, *Nat. Commun.*, 2014, **5**, 3882.

Chapter Two – Uniform two-dimensional poly(ε-caprolactone)-based platelets *via* crystallisation-driven self-assembly

2.1 Abstract

The construction of uniform two-dimensional (2D) structures with diverse morphologies and controlled size remains a significant challenge in the field of nanotechnology. Herein, we report a new approach to obtain uniform poly(*ε*-caprolactone) (PCL)-based 2D platelet micelles using epitaxial crystallisation growth, which involves the addition of blends unimers of PCL-based homopolymer and block copolymer to a solution of crystallite seeds. By sequential addition of different PCL-based blends unimers, exquisite control over the size of co-micelles could be achieved. Through fluorescent labelling, multi-layered co-micelles were further characterised using confocal microscopy. This study provides a suitable platform for precisely controlled nanostructure assembly.

2.2 Introduction

Self-assembly of BCPs into different spatial structures such as spheres,[1-3] cylinders,[4-8] lamellae,[9, 10] and vesicles[11-15] has been widely exploited over the past decades. 2D morphology is known to grant evolutionary benefits in a range of applications including nanotechnology, energy, bioengineering and many other areas.[16-18] Several different chemical and physical strategies have been investigated to achieve the 2D assemblies. However, it has been more challenging to fabricate 2D assemblies with spatial control over shape and size. In particular, the preparation of highly anisotropic and low curvature 2D assemblies driven by crystallisation of the core has been limited by uncontrolled crystallisation process.[19-30] The morphology of assemblies can be related to a range of features, such as block copolymers compositions, additives, solvent conditions, temperature, *etc*. For example, the ratio of core and corona is one of the key parameters for tailoring the compositional phase space, as well as the dimensionality of the 2D assemblies. It has been reported that 1D cylinders are generally originated from unsymmetrical BCPs, with significantly longer corona-forming blocks,[31-38] while 2D platelets are derived from an equal core to corona ratio.[18, 39, 40] Considering the potential applications of the 2D assemblies in in liquid crystals,[41, 42] emulsion[22] and composite reinforcement,[18] it is of great importance for researchers to fabricate 2D structures, especially with controlled size and shape.

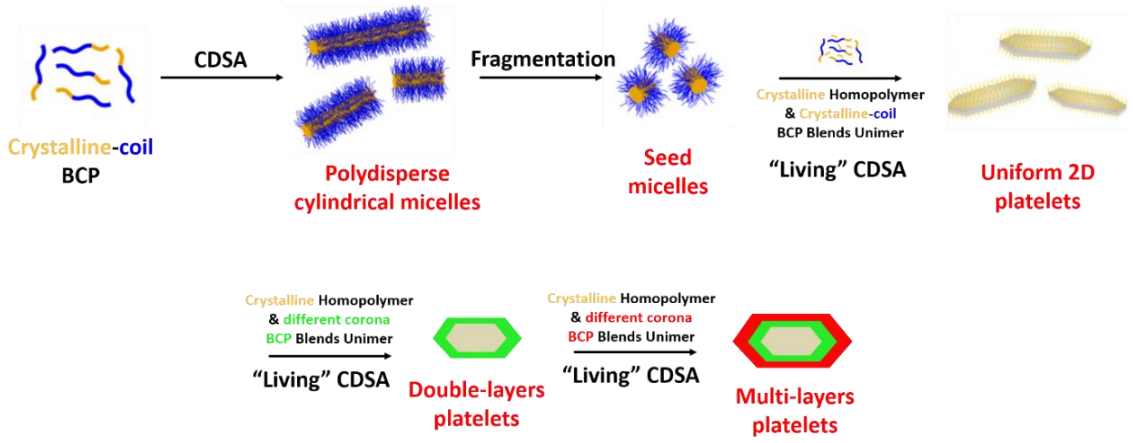
CDSA is a pivotal technique for the preparation of 2D nanostructures with different morphologies, controlled spatial dimensions, and uniform dispersity. To date, a series of BCPs with different crystalline core-forming blocks have been reported to fabricate BCP-based 2D platelets. In an early study, Cheng's group showed poly(ethylene oxide)-based (PEO) BCPs can readily form 2D PEO platelets by alternating addition of PEO-*b*-PS (PS: polystyrene) BCP and PEO homopolymer to the pre-existed 2D PEO crystals.[43] More

recently, Eisenberg and co-workers used PCL homopolymer to trigger the morphological transition from spherical micelles to 2D platelets of PCL-*b*-PEO and PCL-*b*-PAA (PAA: poly(acrylic acid)) in water.[44, 45] Xu and co-workers also prepared the 2D polyethylene (PE) single crystals by blending PE homopolymer and PE-*b*-PtBA (PtBA: poly(tert-butyl acrylate)) BCP.[46] Different from the general cases in which BCPs with low corona-to-core block ratios favour 2D structures, O'Reilly group successfully prepared different 2D platelets using poly(L-lactic acid)-*b*-poly(N,N-dimethylacrylamide) (PLLA-*b*-PDMA) BCPs with a high corona-to-core block ratio by taking advantage of the better solubility of a larger corona in a selective solvent.[47] Moreover, size controllable 2D platelets of PLLA-*b*-PDMAEMA (PDMAEMA: poly(2-dimethylaminoethyl methacrylate)) could be prepared through addition of good solvents to achieve good unimer solubility.[22] On the other hand, Winnik and Manners reported a series of 2D assemblies using a PFS core-forming block.[18, 48, 49] In these studies, well-developed and size controllable 2D structures could be achieved using an epitaxial growth mechanism by adding PFS blend unimer to 1D precursors in a selective solvent.[48, 49]

PCL, a well-known biomedical material, has shown great potential in biomedicine for its excellent biocompatibility and biodegradability.[50] Although 2D PCL platelets have been reported, where the uniformity and shape of PCL platelets could be tailored, precise control over the resultant platelet size is still limited.[51-56] Therefore, preparing uniform 2D PCL assemblies with controlled size and dimension is of great importance.

Herein, we synthesise a PCL homopolymer and PCL-*b*-PDMA (PDMA: poly(N,N-dimethyl acrylamide)) block copolymers using ring-opening polymerisation (ROP) and reversible addition fragmentation chain transfer (RAFT) polymerisation, demonstrating a novel strategy for the fabrication of well-defined 2D PCL platelets obtained through the seeded epitaxial growth of PCL blends (PCL homopolymer and PCL-*b*-PDMA block

copolymer) in the presence of 1D short crystalline seeds. More importantly, the size and spatial growth of such 2D multi-block co-micelles could be precisely tailored by controlling the addition of PCL blends with different corona-forming blocks. The epitaxial crystallisation of PCL blends from pre-existing seeds or platelet edges leads to the living CDSA process, thus producing 2D platelets with controlled morphology and size (**Scheme 2.1**).



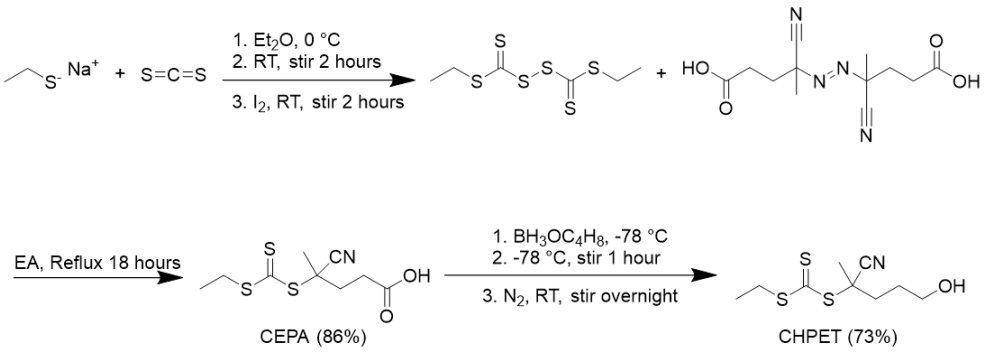
Scheme 2.1 Synthetic strategy of multi-layered platelets with controlled dimensions.

2.3 Results and Discussion

In this chapter, the precise fabrication of uniform two-dimensional PCL-based platelets is investigated *via* living CDSA.

2.3.1 Synthesis of Dual Head Chain Transfer Agent (CTA)

Followed by our group previous study, the first step of this work is the preparation of hydroxyl-functionalised dual-head RAFT chain transfer agent of 2-cyano-5-hydroxypentan-2-yl ethyl carbonotrithioate (CHPET), which contains both reversible addition-fragmentation chain transfer (RAFT) and ring-opening polymerisation (ROP) initiators needed to prepare block copolymers.[22, 57] The synthesis of dual-head chain transfer agent (CTA) CHPET was carried out in a three-step process according to **Scheme 2.2**. An acid terminated precursor, 4-cyano-4-(((ethylthio)carbonothioyl)thio)pentanoic acid (CEPA), was synthesized with 86% yield *via* a modified literature protocol. [58, 59] ^{1}H and ^{13}C NMR spectroscopy confirmed the desired structure (**Figure 2.1**), with the characteristic resonances of the carboxyl group identified in the ^{13}C NMR spectrum at 177.3 ppm (C9) along with retention of the diagnostic resonance for the trithiocarbonate group (C3) at 216.7 ppm. Moreover, in the ^{1}H NMR spectrum the methylene proton (δ = 3.34 (H2) and 2.68 (H5) ppm) appeared next to the trithiocarbonyl and carboxyl functionality, respectively.



Scheme 2.2 Three-step synthesis of dual-head RAFT chain transfer agent CHPET.

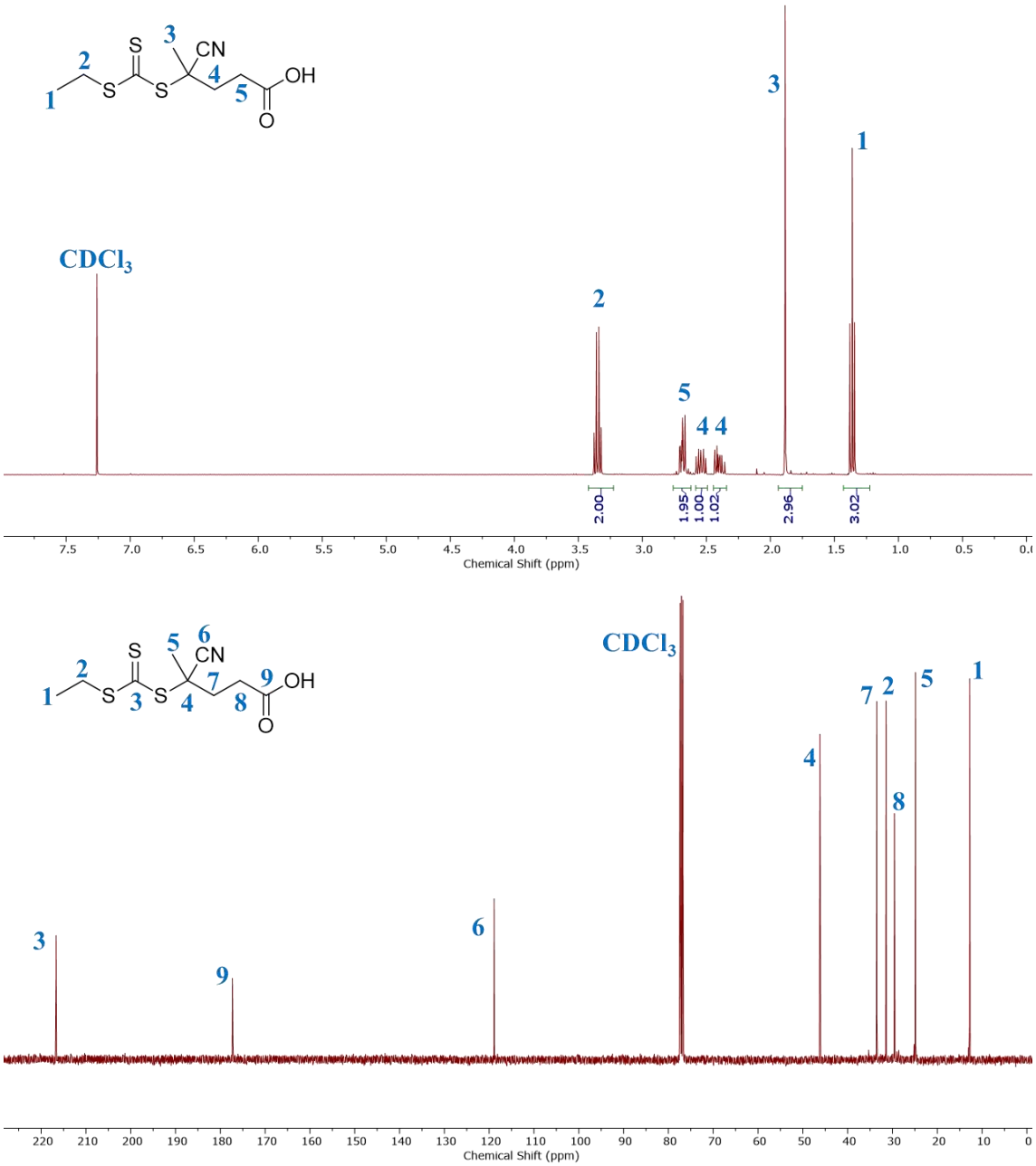


Figure 2.1 ^{1}H NMR (400 MHz) and ^{13}C NMR (100 MHz) spectra of 4-cyano-4-(((ethylthio)carbonothioyl)thio)pentanoic acid (CEPA) in $CDCl_3$.

Subsequent reduction of the acid group to the corresponding alcohol was achieved using a borane tetrahydrofuran complex solution ($BH_3OC_4H_8$), affording CHPET in a 73% yield.[58, 59] The formation of the desired products was confirmed by ^{1}H and ^{13}C NMR spectroscopy (**Figure 2.2**), with the characteristic resonances of the methylene proton and

carbon next to the hydroxyl group identified in the ^{1}H and ^{13}C NMR spectrum at δ = 3.73 (H6) and 61.7 (C9) ppm, respectively.

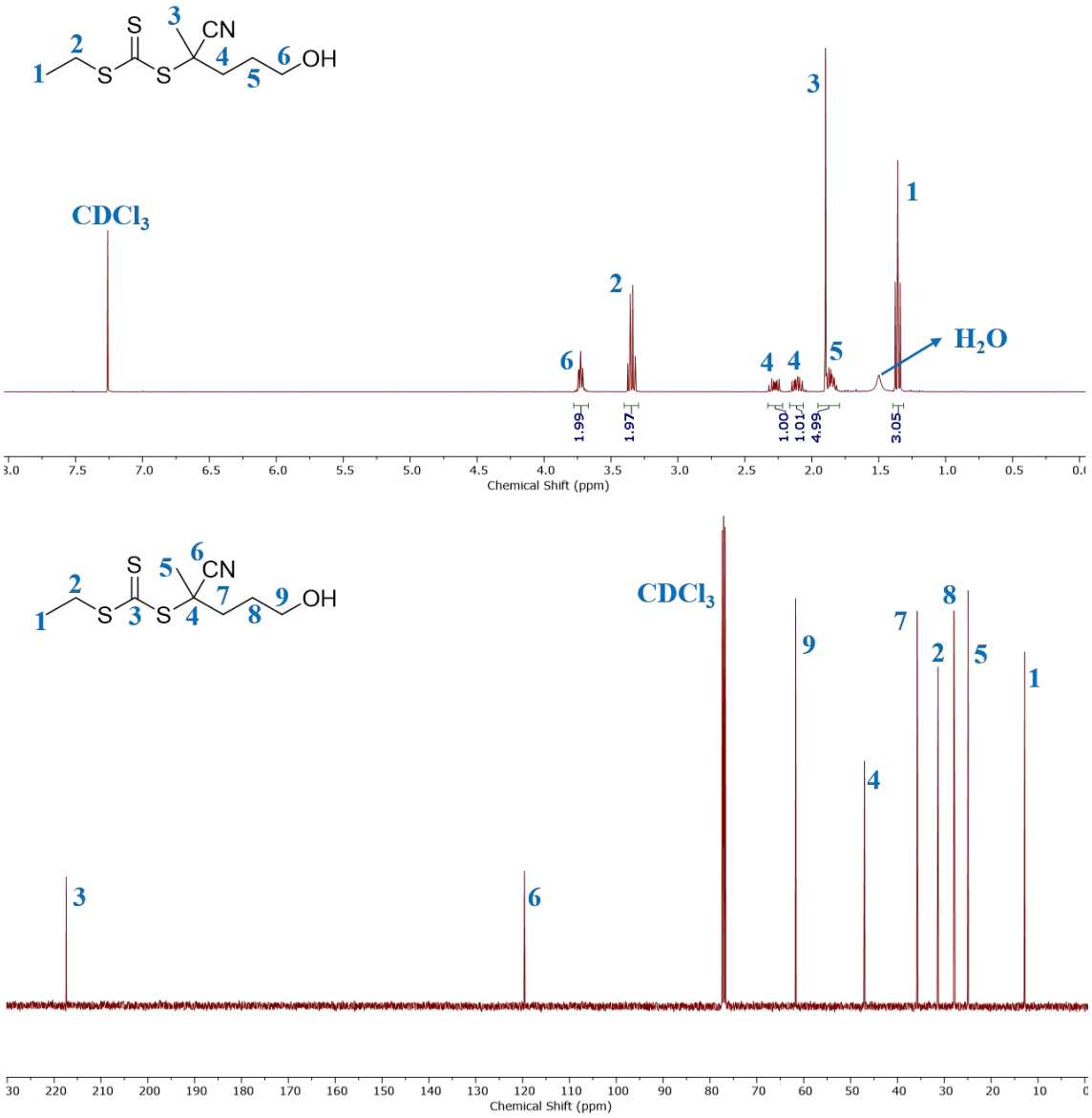
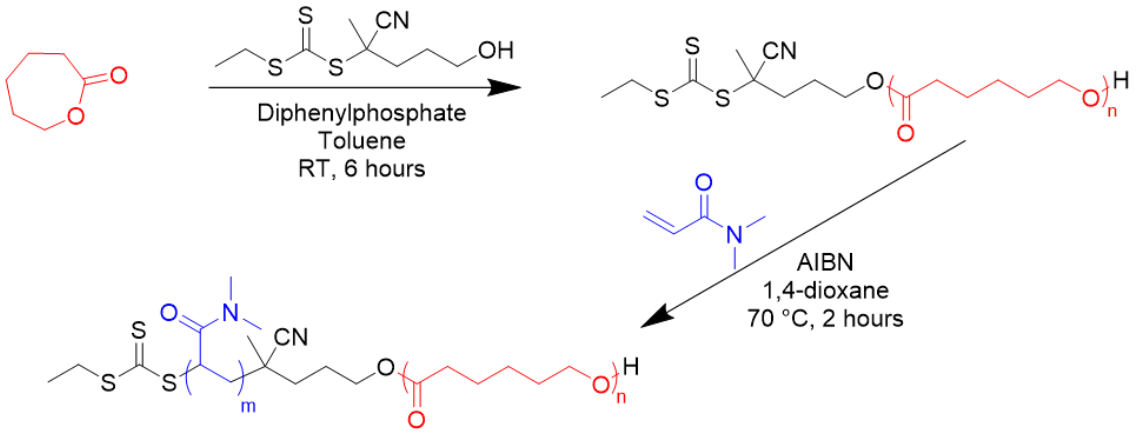


Figure 2.2 ^{1}H NMR (400 MHz) and ^{13}C NMR (100 MHz) spectra of 2-cyano-5-hydroxypentan-2-yl ethyl carbonotrithioate (CHPET) in $CDCl_3$.

2.3.2 Synthesis of Homopolymer and Block Copolymer

After accomplishing the synthesis of dual functional head CTA, PCL homopolymer and PCL-*b*-PDMA block copolymers were synthesized by ROP of ε-caprolactone followed by RAFT polymerisation with DMA monomer (**Scheme 2.3**).



Scheme 2.3 Synthesis of PCL macro CTA and PCL-*b*-PDMA block copolymer by ROP and RAFT polymerisation.

2.3.2.1 Ring Opening Polymerisation of Poly(ε-Caprolactone) (PCL)

The CTA was used as initiator to a grow crystalline block of homopolymer PCL *via* ROP of ε-caprolactone monomer using diphenylphosphate (DPP) as a catalyst. All ROPs were performed in a glove box, to ensure inert atmosphere is achieved and minimise water initiation. After reaction, products were precipitated three times into cold diethyl ether dropwise and collected by centrifugation, and then dried by vacuum. In order to investigate the reaction process, a kinetic experiment for macro-CTA PCL was conducted to access the controlled trend displayed for $\ln([M]_0/[M]_t)$ versus time plots (**Figure 2.3**), showing ROP of ε-caprolactone in toluene followed a first order kinetic profile.

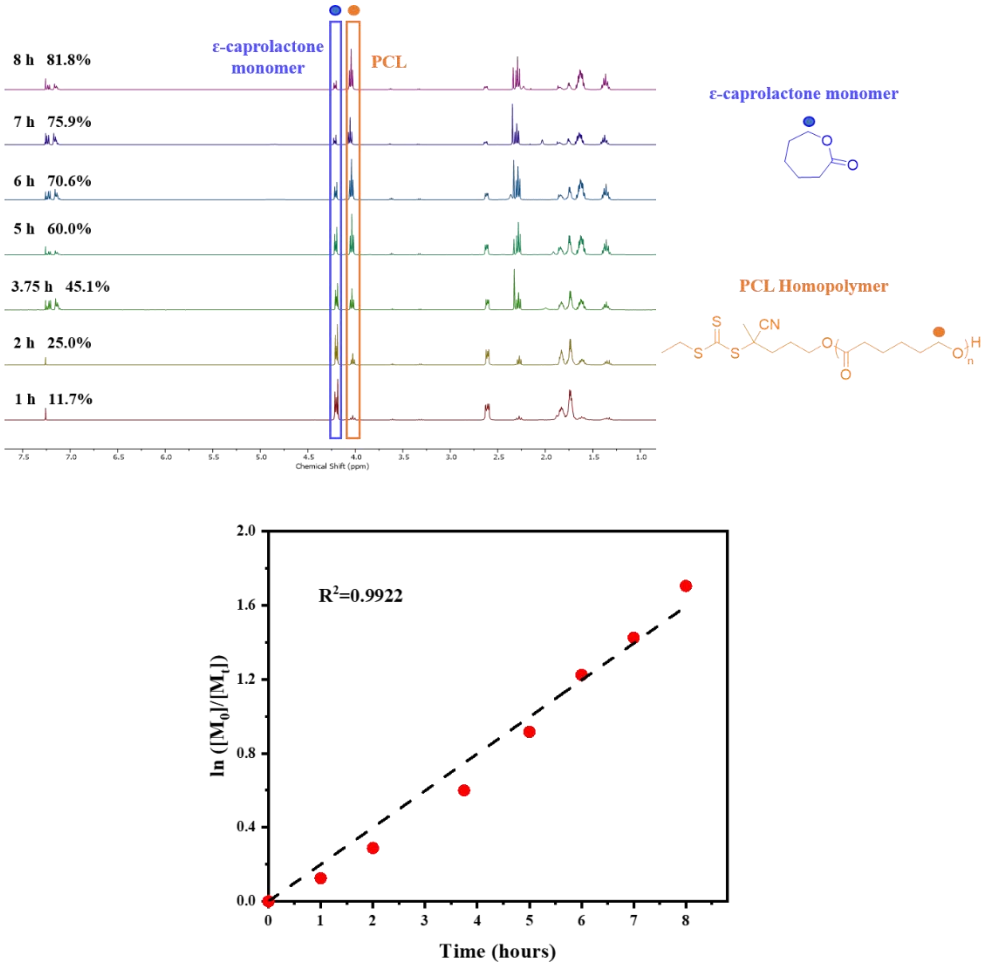


Figure 2.3 Kinetic for the ROP of ε-caprolactone. Top: ^{1}H NMR of ROP kinetic of ε-caprolactone at different reaction time. Bottom: plot of ln of initial monomer concentration by monomer concentration ($\ln([M_0]/[M_t])$) against time for the ROP of ε-caprolactone.

^{1}H NMR spectroscopy indicated the successful polymerisation of PCL with the appearance of a triplet at δ = 4.04 ppm (H11) corresponding to the methylene proton in the polymer backbone. Additionally, the quartet at δ = 3.32 ppm (H2) shows the presence of the methylene protons in the initiator (**Figure 2.4**). The reaction reached 70% conversion after 6 h, achieving a degree of polymerisation (DP) of 50 as calculated by ^{1}H NMR spectroscopy end group analysis. SEC analysis of PCL indicated a number molecular weight (M_n) of 15.2 kDa and a narrow dispersity ($Đ_M$) of 1.05 (**Figure 2.5**). SEC analysis of the refractive index (RI) with a UV detector ($\lambda_{abs.}$ = 309 nm) indicated

that the polymers retained the trithiocarbonate RAFT end-group, with a good overlay of UV and refractive index (RI) traces.

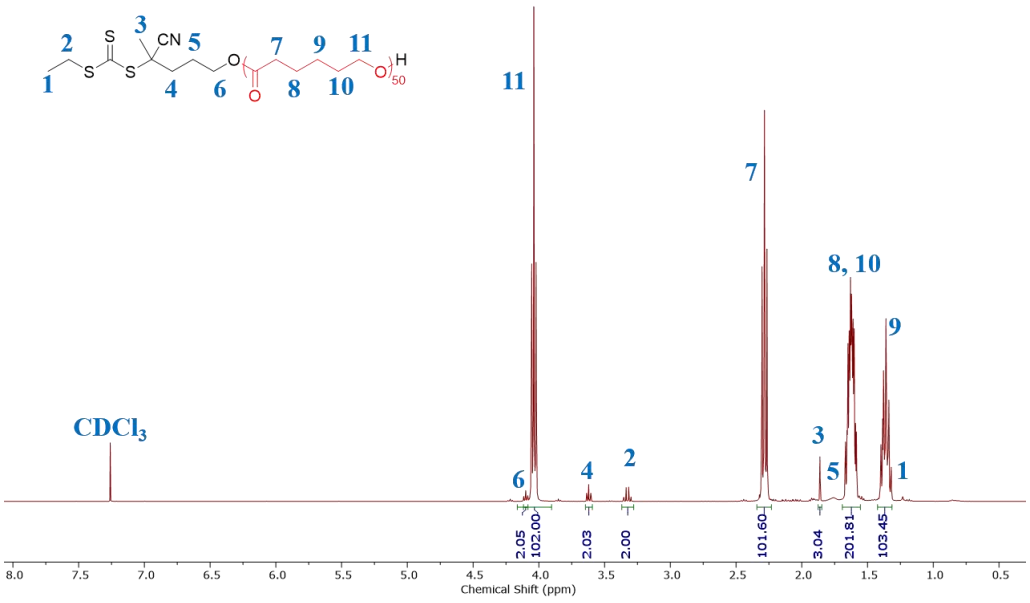


Figure 2.4 ^{1}H NMR spectrum of PCL_{50} in $CDCl_3$ (400 MHz).

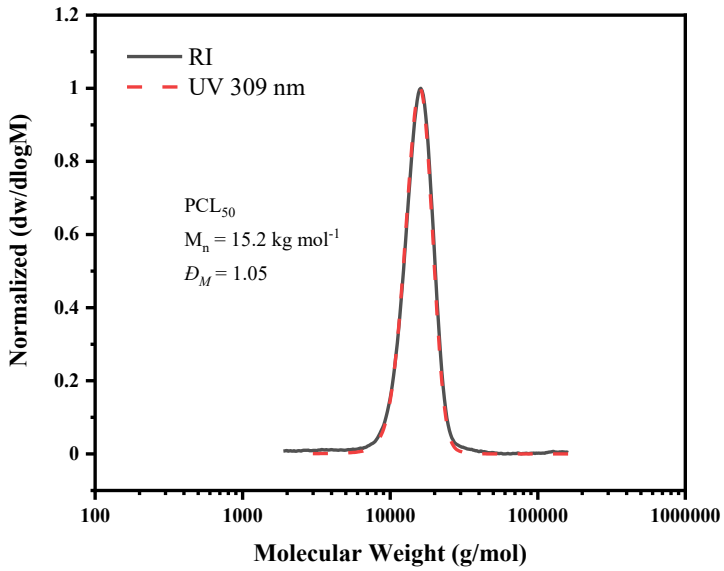


Figure 2.5 SEC chromatogram (RI and UV 309 nm trace) of PCL_{50} using $CHCl_3$ with 0.5% TEA as an eluent. Poly(methyl methacrylate) (PMMA) was used as a standard.

Matrix-assisted laser desorption ionisation - time of flight mass spectrometry (MALDI-ToF MS) showed that the polymerisation was well controlled (**Figure 2.6** and **Table 2.1**). The absence of secondary distribution in the spectrum revealed a high end-group fidelity, no water initiation and minimal transesterification.[60, 61] Furthermore, the experimental molecular weight determined was in good correspondence to the theoretical value, confirming the controlled nature of the polymerisation.

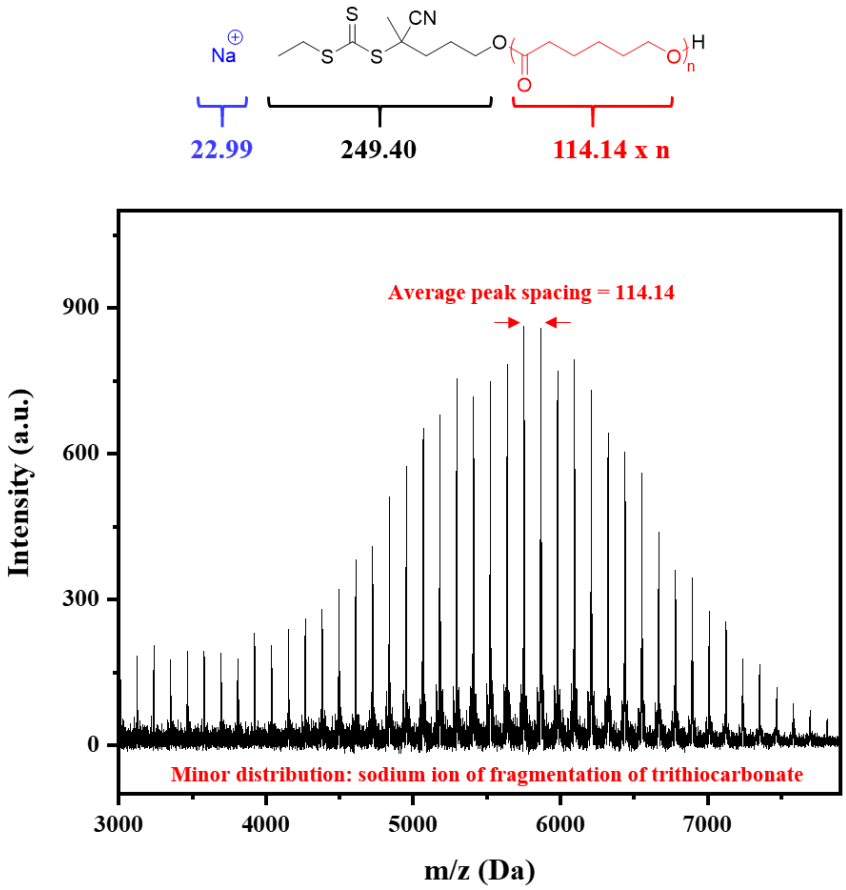


Figure 2.6 MALDI-TOF mass spectrum of PCL_{50}. Minor distribution corresponds to sodium ion of the fragmentation of the trithiocarbonate.[60]

Table 1.1 MALDI-TOF data of PCL_{50}.[a]

DP (n)	M + Na (Theoretical)	Found (Experimental)	DP (n)	M + Na (Theoretical)	Found (Experimental)

41	4952.13	4952.32	**51**	6093.53	6093.99
42	5066.27	5066.53	**52**	6207.67	6208.44
43	5180.41	5180.67	**53**	6321.81	6322.64
44	5294.55	5294.83	**54**	6435.95	6436.70
45	5408.69	5408.84	**55**	6550.09	6550.97
46	5522.83	5523.07	**56**	6664.23	6665.10
47	5636.97	5637.34	**57**	6778.37	6779.27
48	5751.11	5751.49	**58**	6892.51	6893.41
49	5865.25	5865.70	**59**	7006.65	7007.60
50	5979.39	5979.97	**60**	7120.79	7121.71

[a]. Average difference between calculated and found m/z = 0.55.

2.3.2.2 RAFT Polymerisation of PCL-*b*-PDMA

The RAFT polymerisation of DMA monomer was carried out in 1,4-dioxane at 70 °C under nitrogen atmosphere using 2,2-azobis(2-methylpropionitrile) (AIBN) as a radical initiator. ^{1}H NMR spectrum of **Figure 2.7**, showed that the reaction reached 80% conversion after 3 h, giving DP 198 and a $M_{n,\ NMR}$ by NMR of 25.6 kDa, in good agreement with the $M_{n,\ SEC}$ by SEC of 31.8 kDa. SEC analysis using chloroform as an eluent gave a narrow dispersity ($Đ_M$) of 1.09 with a good overlap of the RI and UV traces (λ_{abs} = 309 nm), exhibiting the retention of the trithiocarbonate end group (**Figure 2.8**). Comparison with PCL homopolymer also showed a significant shift in molecular weight, with no observed evidence of low molecular weight oligomers.

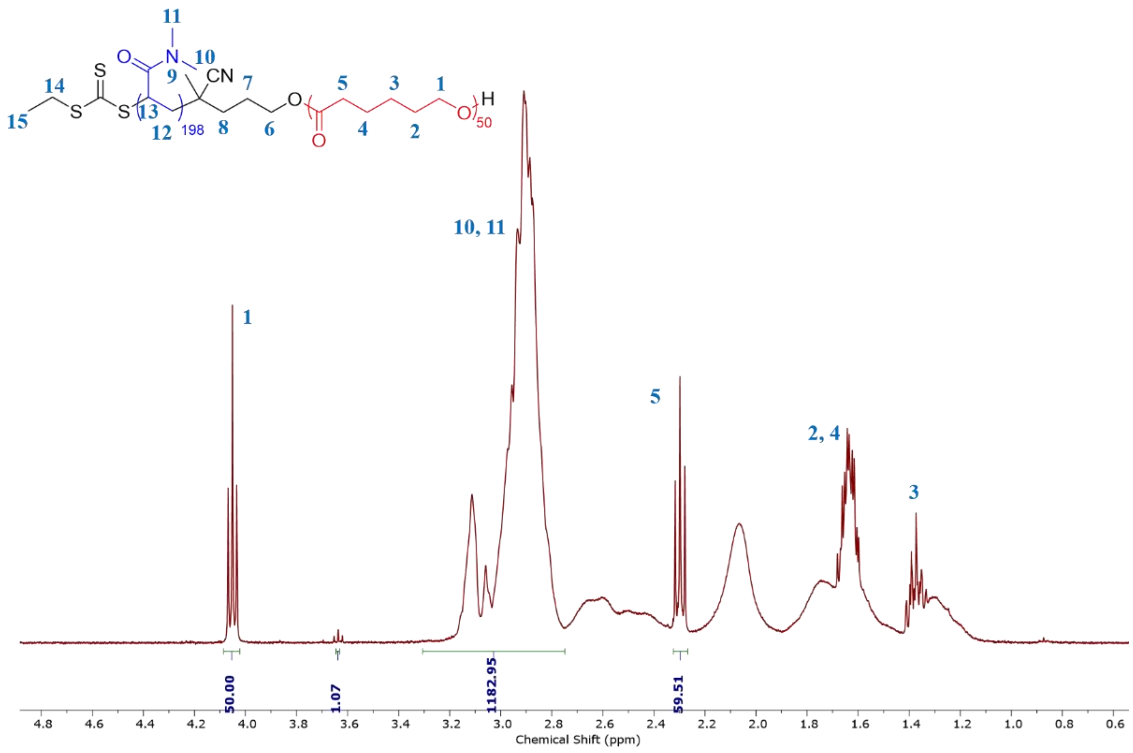


Figure 2.7 ^{1}H NMR spectrum of PCL_{50}-*b*-$PDMA_{198}$ in $CDCl_3$ (400 MHz).

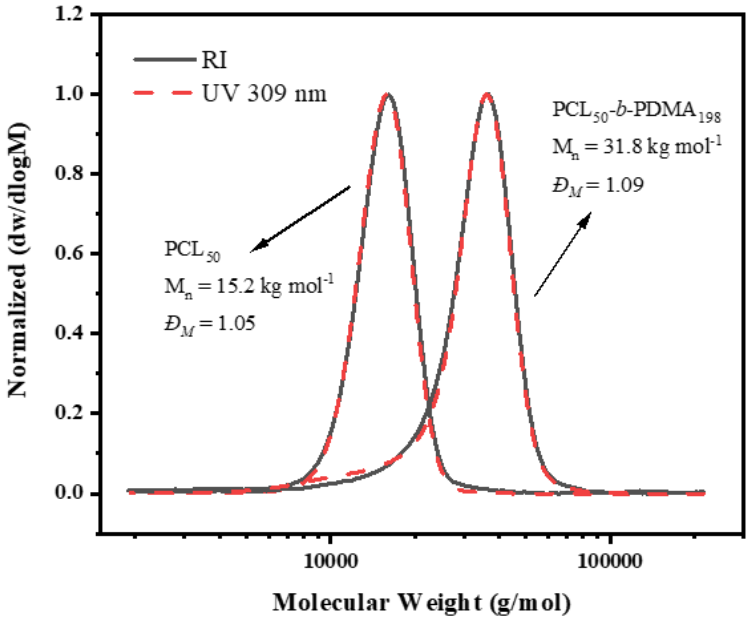
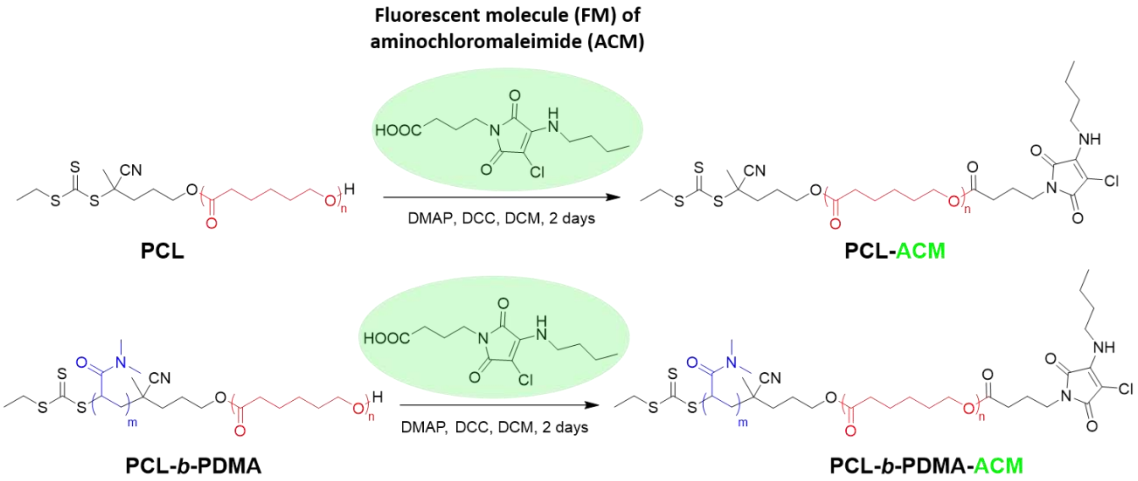


Figure 2.8 SEC chromatogram (RI and UV 309 nm trace) of PCL_{50}-*b*-$PDMA_{198}$ using $CHCl_3$ with 0.5% TEA as an eluent (PMMA standard).

2.3.2.3 Fluorescent Functionalisation of PCL and PCL-*b*-PDMA

Labelling of micellar constructs with fluorescent molecules provides a simple way to readily track and image particles by confocal laser scanning microscopy (CLSM) imaging. To achieve this objective, a fluorescent polymer has been designed (**Scheme 2.4**).



Scheme 2.4 Design of fluorescent functionalised homopolymer and block copolymer.

PCL homopolymer bearing an hydroxyl functional group at the chain end was reacted with a small-molecule fluorophore dye, aminochloromaleimide[62] (ACM, synthesised and donated by Dr. Yujie Xie) using dicyclohexylcarbodiimide (DCC) and 4-dimethylaminopyridine (DMAP) as activating reagents for the coupling reaction. The reaction was carried out in a concentrated solution for an extensive period of time (2 days) using an excess of the carboxylic group functionality to promote quantitative attachment of the ACM to the homopolymer chain end. As observed from the ^{1}H NMR spectrum of PCL-ACM, the triplet was associated with the methyl proton of ABM at δ = 0.96 ppm (H18) (**Figure 2.9**). Further characterisation by SEC (**Figure 2.10**) showed a significant change in the UV trace at 360 nm, confirming that the PCL homopolymer had been successfully functionalised with ACM.

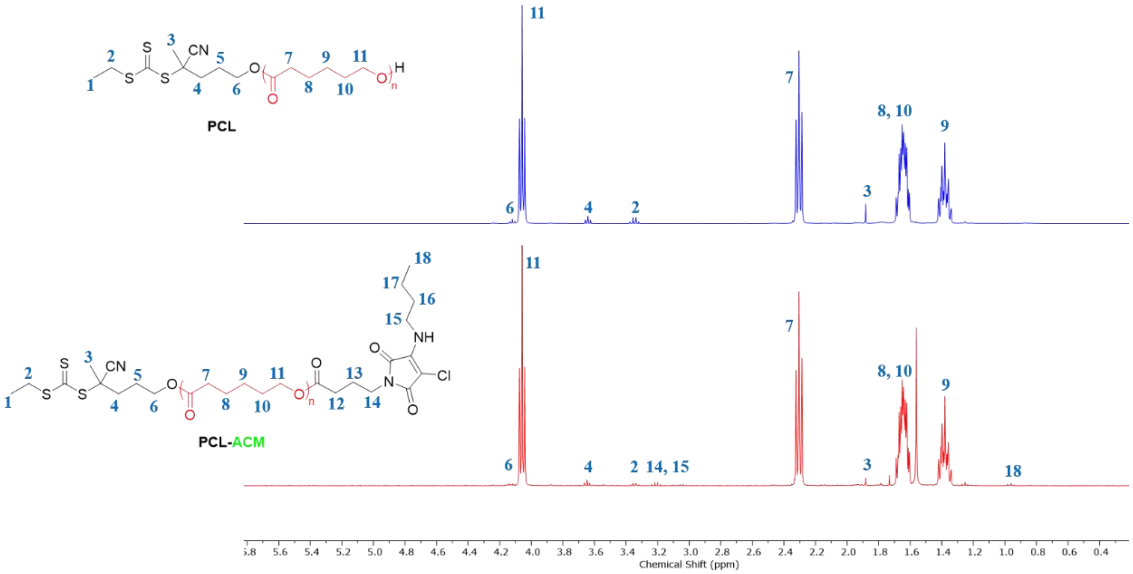


Figure 2.9 ^{1}H NMR spectra of PCL_{50} homopolymer before and after coupling with fluorescent molecule ACM in $CDCl_3$ (400 MHz).

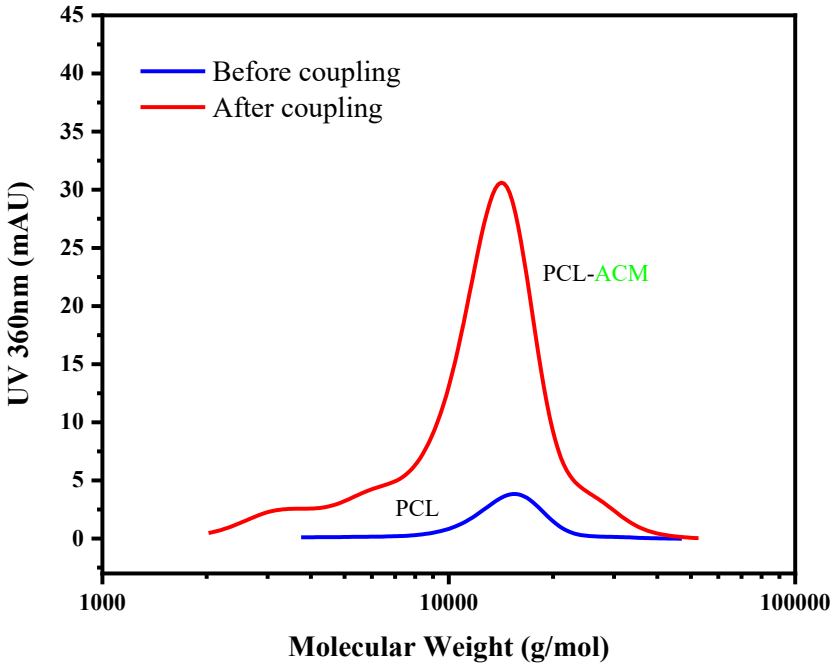


Figure 2.10 SEC chromatogram (UV trace, 360 nm) of PCL_{50} homopolymer before and after coupling with fluorescent molecule ACM using $CHCl_3$ with 0.5% TEA as an eluent with PMMA standards.

Block copolymer (PCL_{50}-*b*-$PDMA_{198}$) also was synthesized following a similar procedure. SEC analysis showed a significant change in the UV trace (λ_{abs} = 360 nm), confirming that PCL_{50}-*b*-$PDMA_{198}$ block copolymer has been successfully functionalised with ACM (**Figure 2.11**).

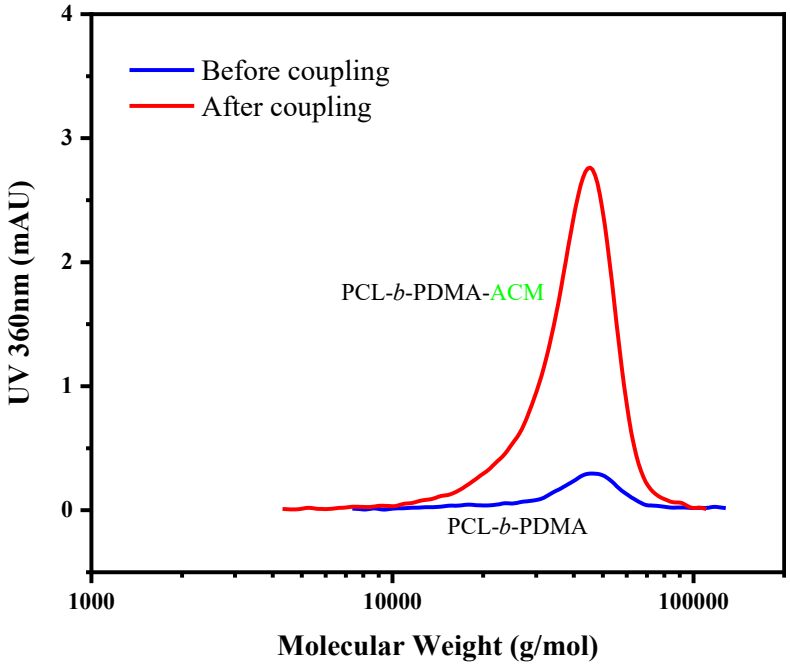


Figure 2.11 SEC chromatogram (UV trace, 360 nm) of block copolymer PCL_{50}-*b*-$PDMA_{198}$ before and after coupling with fluorescent molecule ACM using $CHCl_3$ with 0.5% TEA as an eluent with PMMA standards.

2.3.3 Crystallisation-Driven Self-Assembly (CDSA) of PCL-*b*-PDMA

Initially, the self-nucleation of PCL_{50}-*b*-$PDMA_{198}$ was investigated. Based on previous reports from our group,[57] ethanol was selected as the best solvent to dissolve the corona block. As such, the polymer (5 mg mL^{-1}) was heated in ethanol at 70 °C for 3 h, above both the T_c and T_m of PCL_{50} (T_c = 35 °C and T_m = 60 °C. T_c and T_m represent the temperature of crystallisation and melting, respectively),[57] allowing the PCL block to

melt, followed by slow cooling down to ambient temperature. No Tyndall phenomenon was observed in solution for the first few hours, which indicates a lack of assembly into larger structures. After aging for 1-week, long cylinders with non-uniform lengths were observed by TEM imaging (**Figure 2.12**).

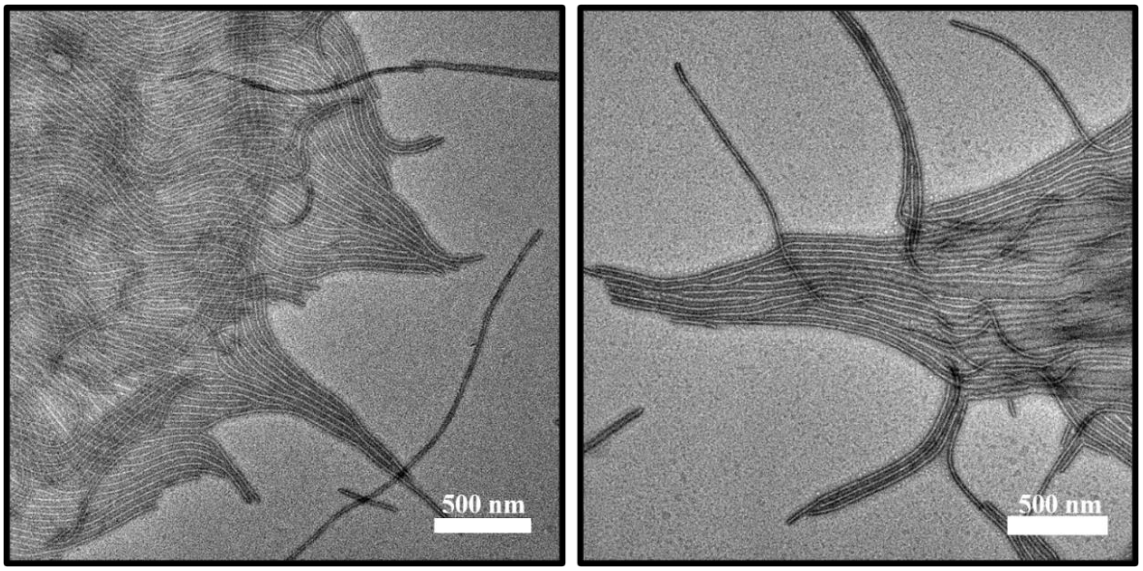


Figure 2.12 Transmission electron microscopy (TEM) images of cylindrical micelles (0.5 mg mL^{-1}) prepared using PCL_{50}-*b*-$PDMA_{198}$ in ethanol, heating at 70 °C for 3 h and subsequently cooling down to room temperature (stained with 1 wt. % uranyl acetate in water). (TEM images collected by Mr. Bo Li.)

In order to obtain well defined structures of controlled size, it is necessary to prepare uniform crystalline seeds that serve as nuclei for the 2D living growth. Sonication of the aged cylindrical micelles was carried out to generate short seeds at 0 °C, using an ice-water bath. Polymer solution was fractured for 10 cycles of 2 min. sonication each with a pause of 20 min. in between to cool down the probe and prevent undesirable crystallisation as result of local heating. After sonication, short and uniform 1D seeds were achieved (L_n = 125.3 nm, L_w = 127.3 nm, L_w/L_n= 1.02), as analysed by TEM (**Figure 2.13**).

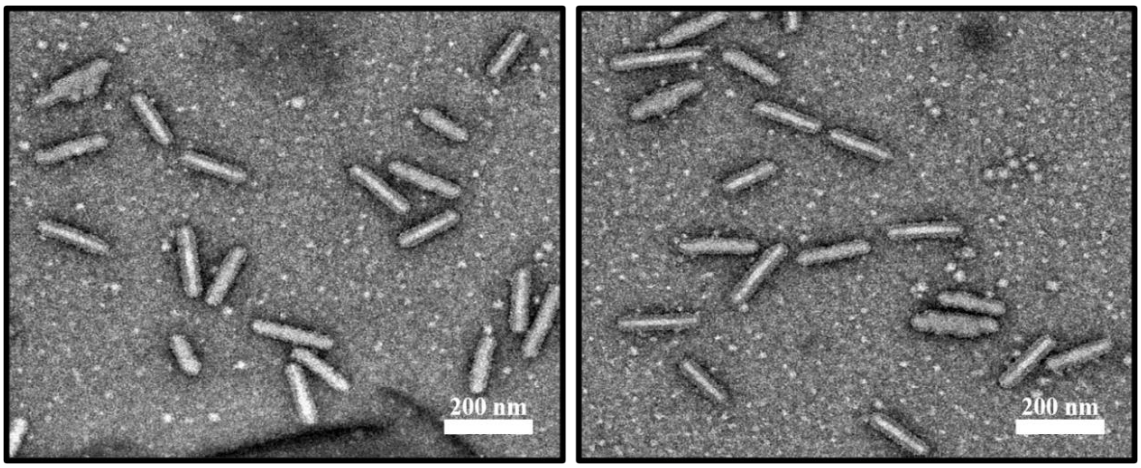


Figure 2.13 TEM micrographs of PCL_{50}-*b*-$PDMA_{198}$ cylinders assembled in ethanol after sonication at 0 °C for 20 min using a sonic probe (stained with 1 wt. % uranyl acetate in water). (TEM images collected by Mr. Bo Li).

2.3.4 Two-Dimensional Epitaxial Growth

Following the successful preparation of crystalline seed micelles of uniform dispersity, 2D structures were achieved through the living seeds growth process. The crystalline seeds can serve as initiation sites for micelle growth on addition of homopolymer and block copolymer blend unimers for the formation of platelets with controlled size.

2.3.4.1 Effect of Homopolymer Amounts on Assemblies Morphologies

In order to exploit the influence of homopolymer concentration on the morphology and dimensions of the resultant PCL_{50}/PCL_{50}-*b*-$PDMA_{198}$ platelets, the homopolymer amount was varied from 0.25 to 5 (with a fixed ratio of unimers to seed of 10) and the formed PCL_{50}/PCL_{50}-*b*-$PDMA_{198}$ platelets were further characterized by CLSM and AFM (**Figure 2.14**). It was observed that, with increasing percentage of homopolymer, the size (length and width) increases. However, when the homopolymer to block copolymer ratio reaches 2, the platelets stop to increase in size, which implies the PCL homopolymer plays a key role on forming and stabling the platelets.

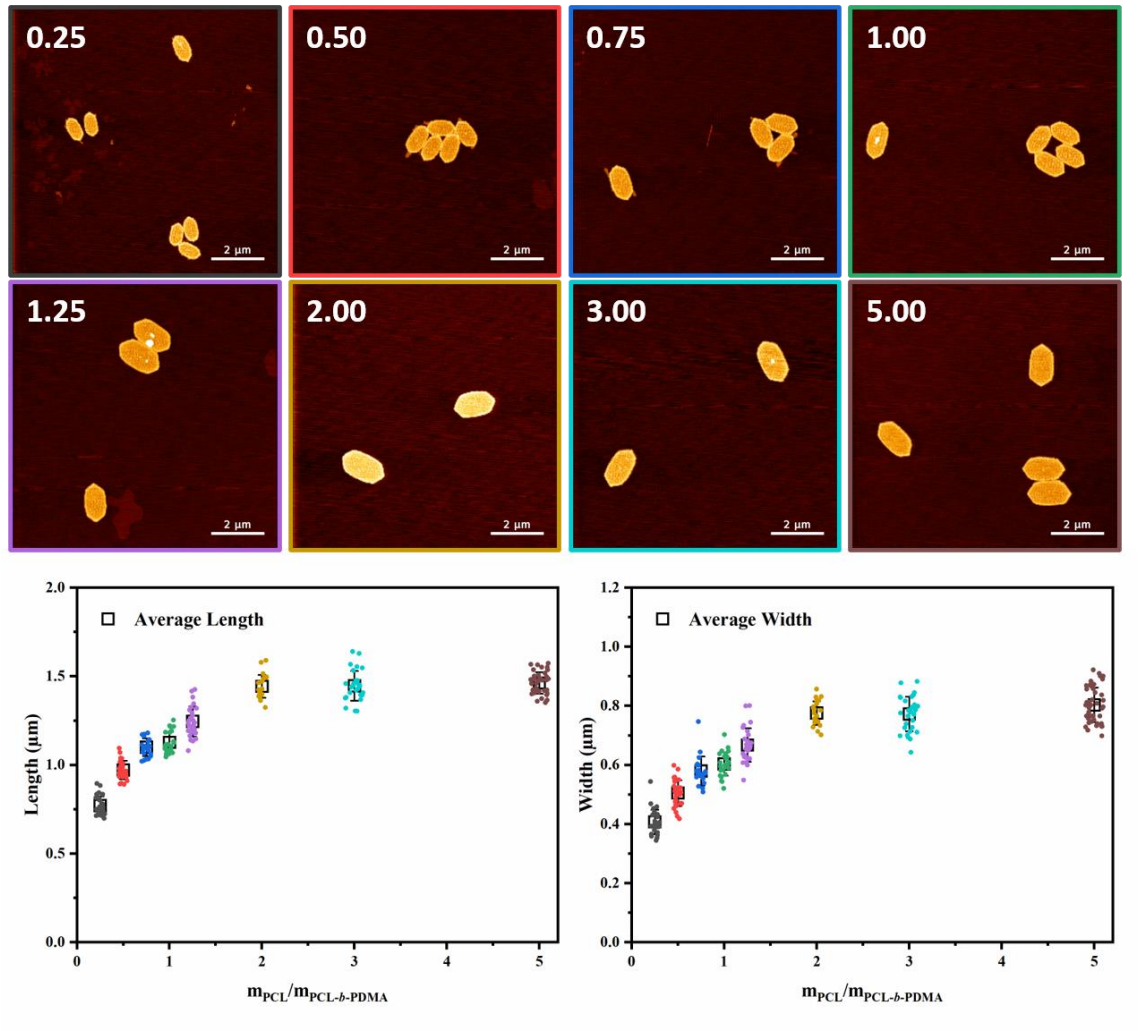
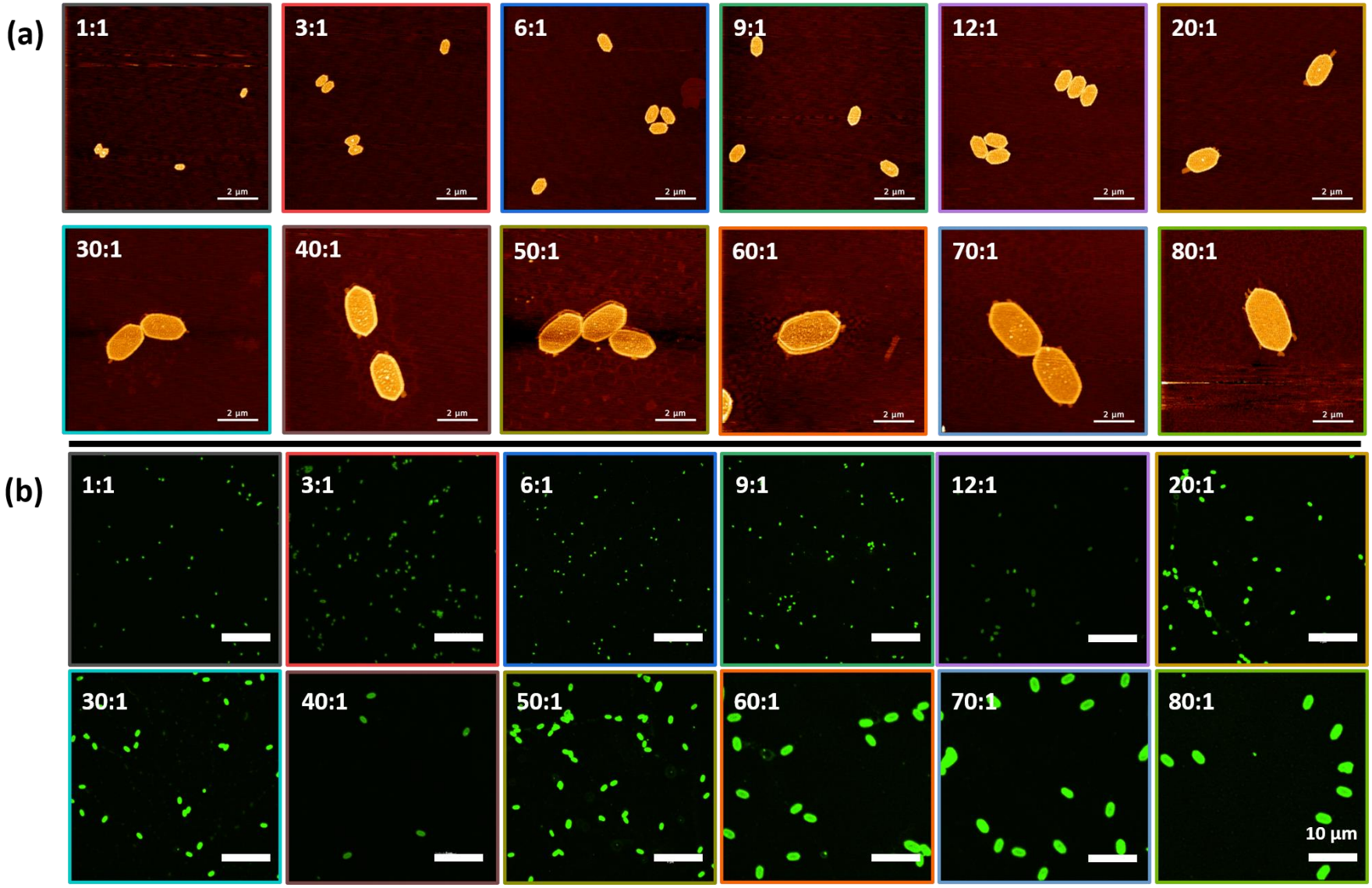


Figure 2.14 Effect of PCL homopolymer concentration on the assemblies by seeded epitaxial growth. m_{PCL}: $m_{PCL\text{-}b\text{-}PDMA}$=0.25, 0.5, 0.75, 1, 1.25, 2, 3 and 5; The crystalline seeds are prepared from PCL_{50}-*b*-$PDMA_{198}$ cylinder. The unimer-to-seed ratio is fixed as 10. Top: AFM images of PCL_{50}/PCL_{50}-*b*-$PDMA_{198}$ blending platelets; Bottom: Plots of 2D assemblies' length versus m_{unimer}/m_{seed}.

2.3.4.2 2D 'living' CDSA

Further investigating the nature of living CDSA in PCL/PCL-*b*-PDMA blending system, a linear relationship between unimers-to-seed ratio by mass (m_{unimer}/m_{seed}) and size (area) was observed up to the addition of 80 mass equivalents, as characterized by AFM (**Figure 2.15**). However, it can be observed that with the increase in the unimers-to-seed ratio the growth rate of length and width decreases, but the ratio of length-to-width always kept a

relatively stable value of ca. 1.85 (1.77~1.91). The micelles were observed to be of consistently low dispersity (no more than 1.02 in all cases, **Table 2.1**). To further confirm the process of 2D living CDSA, followed by the same procedure using PCL-ACM/PCL-*b*-PDMA-ACM blending system, uniform and size-controlled platelets were visualised by CLSM, which confirmed the AFM results.


(a)
1:1
3:1
6:1
9:1
12:1
20:1
30:1
40:1
50:1
60:1
70:1
80:1
2 µm
(b)
1:1
3:1
6:1
9:1
12:1
20:1
30:1
40:1
50:1
60:1
70:1
80:1
10 µm

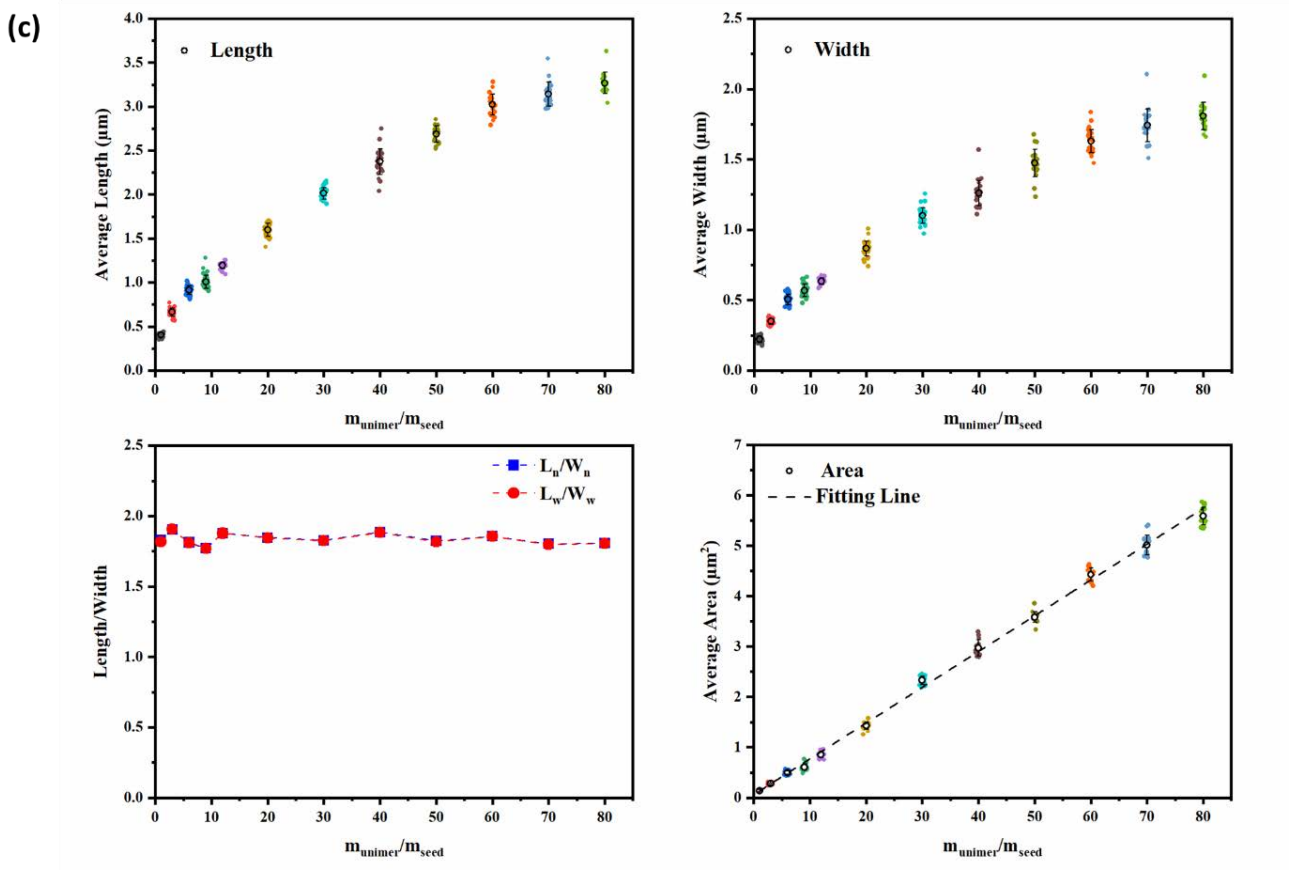


Figure 2.15 (a) AFM images and (b) CLSM images of PCL_{50}/PCL_{50}-*b*-$PDMA_{198}$ (mass ratio=1) blending platelets grown from PCL_{50}-*b*-$PDMA_{198}$ crystalline seeds with m_{unimer}/m_{seed} of 1, 3, 6, 9, 12, 20, 30, 40, 50, 60, 70 and 80; (c) graph showing the linear dependence of 2D platelet length, width, ratio of length-to-width and area upon the unimer-to-seed ratio. (Normally, the concentration of unimers is 10 mg mL^{-1}, when the ratio of unimers to seeds above 20, it changes to 50 mg mL^{-1}) (CLSM images collected by Dr. Yujie Xie.)

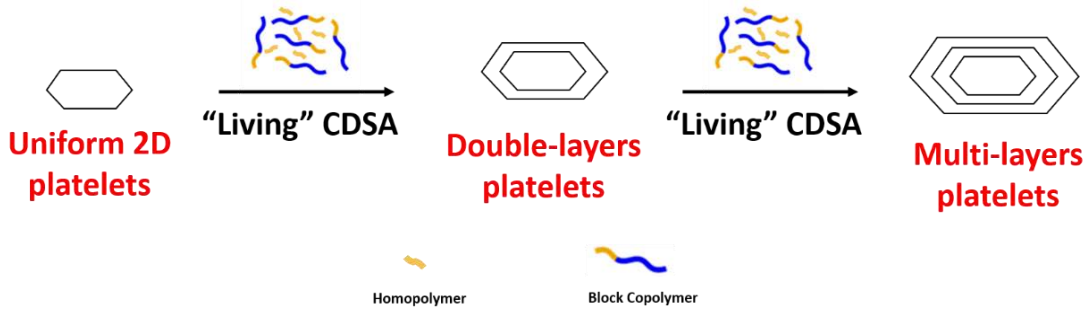
Table 1.2 Length, width and area dispersity of platelet micelles.[a]

$m_{unimers}/m_{seeds}$	Length			Width			Area			Length/Width	
	L_n (nm) [b]	L_w (nm) [c]	L_w/L_n [d]	W_n (nm)	W_w (nm)	W_w/W_n [g]	A_n (10^4 nm^2)	A_w (10^4 nm^2)	A_w/A_n [j]	L_n/W_n [k]	L_w/W_w [l]
1	403.9	405.2	1.00	220.6	223.0	1.02	14.2	14.4	1.02	1.83	1.82
3	663.4	666.5	1.00	348.2	349.5	1.00	27.3	27.4	1.01	1.91	1.91
6	914.7	917.4	1.00	504.3	506.9	1.01	49.6	49.9	1.01	1.81	1.81
9	1008.0	1013.5	1.01	568.9	572.5	1.01	60.6	61.2	1.01	1.77	1.77
12	1192.0	1193.1	1.00	634.8	635.7	1.00	85.3	85.7	1.00	1.88	1.88
20	1597.7	1601.3	1.00	865.1	868.4	1.00	142.4	142.8	1.00	1.85	1.84
30	2012.7	2015.0	1.00	1101.1	1103.8	1.00	232.7	233.0	1.00	1.83	1.83
40	2374.1	2383.0	1.00	1259.4	1265.8	1.01	297.2	298.1	1.00	1.89	1.88
50	2687.1	2690.2	1.00	1472.9	1479.4	1.00	358.1	358.4	1.00	1.82	1.82
60	3023.0	3027.5	1.00	1627.8	1631.9	1.00	443.3	443.7	1.00	1.86	1.86
70	3139.5	3145.4	1.00	1741.0	1748.7	1.00	501.4	502.1	1.00	1.80	1.80
80	3269.3	3273.7	1.00	1808.7	1813.8	1.00	559.1	559.6	1.00	1.81	1.80

[a]. The length, width and area of the platelet was collected by AFM; [b, e, h]. The length, width and area of number average micelle, respectively; [c, f, i]. The length, width and area of weight average micelle, respectively; [d, g, j]. The distribution of micelle length, width and area, respectively; [k, l]. The length-to-width ratio of number and weight average micelle, respectively.

2.3.5 Sequential Growth of Multi-Layered Platelet

After accomplishing 2D epitaxial growth using 1D short seeds, we sought to investigate whether as-prepared platelets could be used as "seed precursors" for subsequent growth on the edge by adding the blend unimers again (**Scheme 2.5**).



Scheme 2.5 Mechanism of preparing multi-layered platelets by sequential seeded growth.

Double layer platelets can be generated by sequential addition of blend unimers. As shown in AFM and TEM images (**Figure 2.16 b)** the 2D platelets contain two regions, an inner layer and an outer layer. To further expand this approach, well-defined triple and quadruple layers platelets were prepared following a similar procedure, as observed by AFM and TEM (**Figure 2.16 c and d)**.

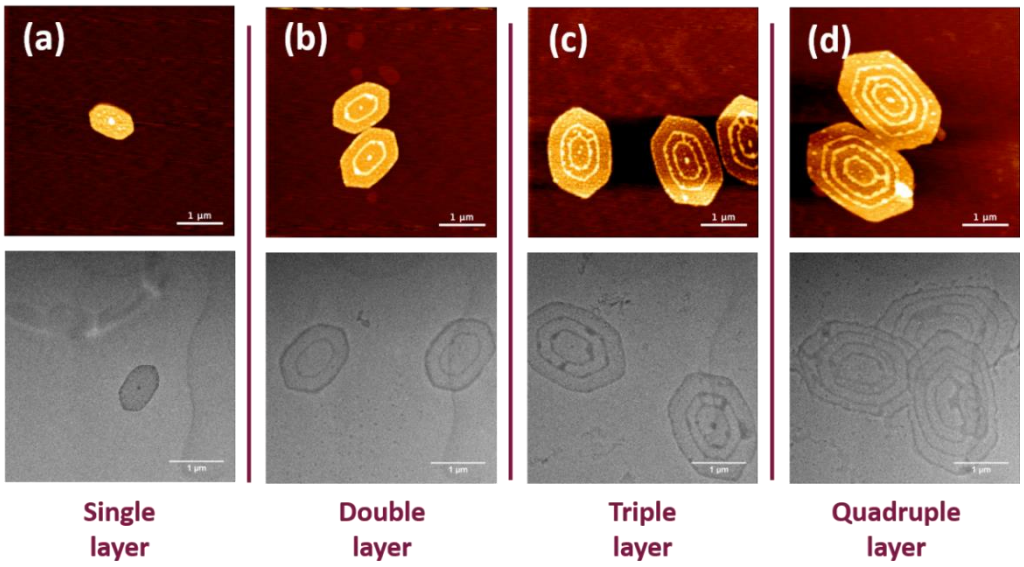
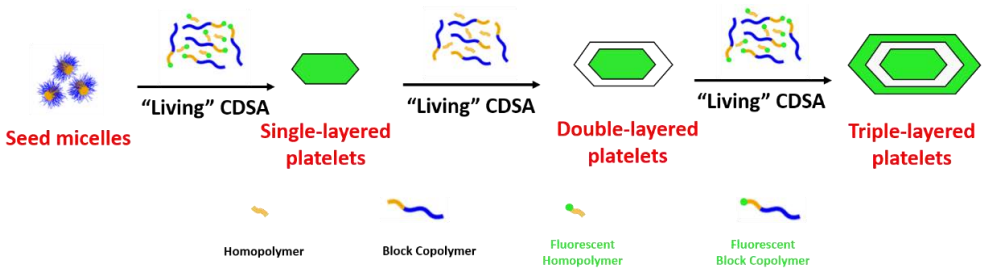


Figure 2.16 AFM (top) and TEM (bottom) images of multi-layered platelets of (a) single, (b) double, (c) triple and (d) quadruple layered after sequential seeded growth. (TEM images collected by Mr Bo Li).

2.3.6 Fluorescent Multi-Layered Platelet

As a proof-of-concept, fluorescent polymers (homopolymer PCL_{50}-ACM and block copolymer PCL_{50}-*b*-$PDMA_{198}$-ACM) were incorporated for *in situ* investigation of the spatially defined segregation of domains by fluorescent emission. **Scheme 2.6** shows the design of centrosymmetric block co-micelles formed by sequential addition of the fluorescent, non-fluorescent and fluorescent polymers to a solution of non-fluorescent seeds.



Scheme 2.6 Mechanism of preparing fluorescent modified multi-layered platelets by sequential seeded growth.

Through different addition of fluorescent or non-fluorescent polymer, various kinds of hollow hexagonal platelets were fabricated and further visualised by CLSM (**Figure 2.17**), demonstrating the formation of complex 2D structures with spatially confined surface functionality. No detectable diffusion of luminescent polymers across the area of the micelles was observed over time (2, 10 and 35 days, **Figure 2.18**), suggesting no chain transformation in the platelet local environment, which further confirms this approach can be used to achieve biocompatible and biodegradable carriers.

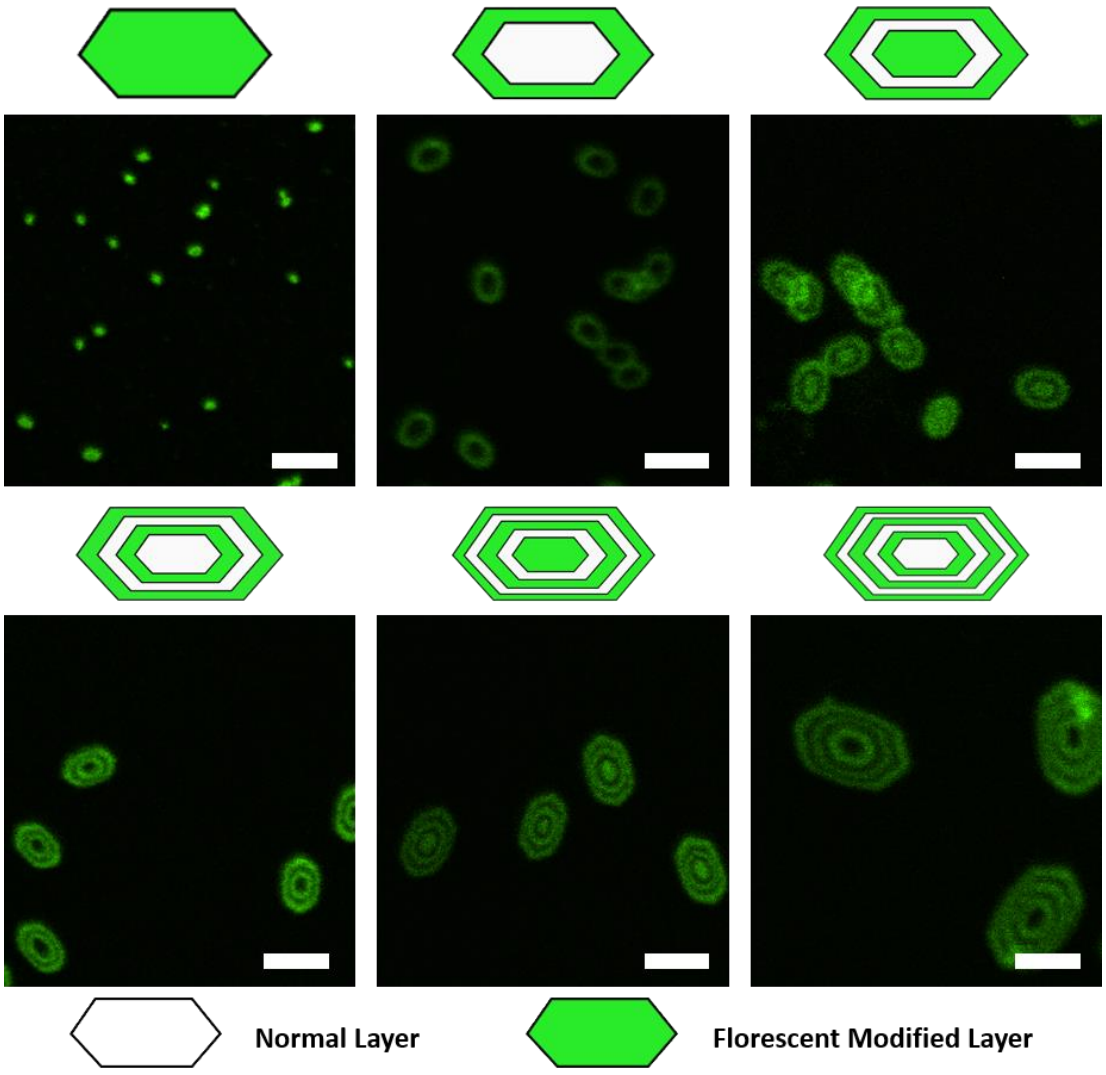


Figure 2.17 CLSM images of fluorescent modified multi-layered platelets by sequential epitaxial growth. (scale bar = 2 μm) (CLSM images collected by Dr. Yujie Xie.)

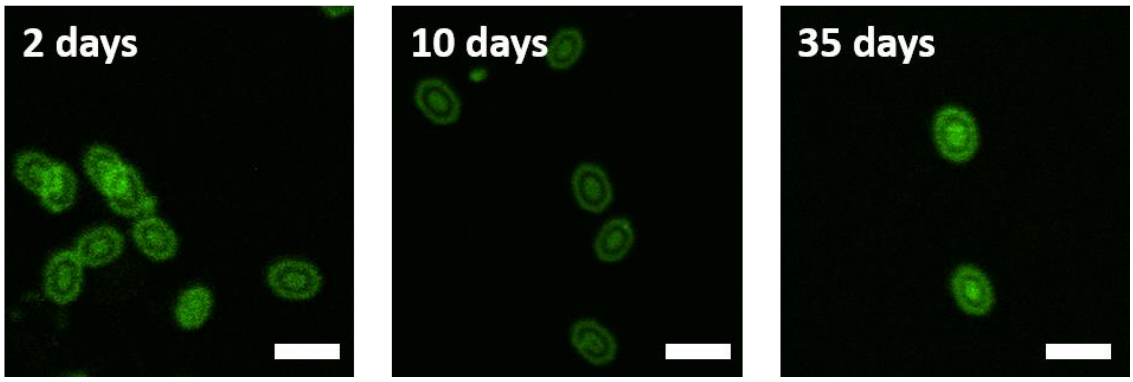


Figure 2.18 CLSM images of fluorescent platelets after different period of time (2, 10 and 35 days). (scale bar = 2 μm) (CLSM images collected by Dr. Yujie Xie.)

2.4 Conclusions

In summary, we have demonstrated a new approach to prepare uniform two-dimensional poly(ε-caprolactone)-based platelets *via* crystallisation-driven self-assembly. Firstly, a seeded growth approach of PCL-based blends unimers was used for the formation of uniform 2D platelet micelles with tuneable size and dimensions, exhibiting living growth with a high ratio of unimers-to-seed up to 80. Moreover, multiblock platelet-like co-micelles were prepared by sequential addition of PCL-based blend unimers to the 1D or 2D precursors. Furthermore, through coupling the PCL-based polymer with a fluorescent dye, it was confirmed that the segmented 2D structures could be spatially confined on the surface, providing possible approaches to customizable platforms for applications in fluorescent imaging or as biocompatible and biodegradable carriers.

2.5 Experimental

2.5.1 Materials

All chemicals and solvents were used as obtained without further purification unless otherwise stated. Sodium ethanethiolate (90%), carbon disulfide (≥99%), solid iodine (≥99%), 4,4'-azobis(4-cyanovaleric acid) (ACVA, 98%) and borane tetrahydrofuran complex solution (1.0 M in THF) were purchased from Sigma Aldrich and Alfa Aesar. The synthesis of dual head CTA of 2-cyano-5-hydroxypentan-2-yl ethyl carbonotrithioate (CHPET) has been followed Varlas et al. and Kang et al. by in previous reports.[58, 59] CTA and diphenylphosphate (DPP, 99%, Sigma Aldrich) were dried over P_2O_5 in desiccator under static vacuum for 1 week before use. ε-caprolactone (99%, ACROS Organics) were vacuum distilled twice over CaH_2 before being introduced in the glovebox and used. 2,2'-azobis(2-methylpropionitrile) (AIBN, 98%, Sigma Aldrich) was recrystallised twice from methanol and stored at 4 °C in the dark. 1,4-dioxane (anhydrous, 99.8%) and N,N-dimethyl acrylamide (DMA, 99%, contains 500 ppm monomethyl ether hydroquinone as inhibitor) were purchased from Sigma Aldrich and passed through a basic alumina plug immediately to remove stabiliser before use. Solvents were purchased from Fisher Scientific. Dry solvents were used directly from a drying and degassing inert solvent tower system. Aminochloromaleimide (ACM) fluorescent dye was synthesised by and taken from Dr. Yujie Xie.[62]

2.5.2 Instrumentation

Nuclear Magnetic Resonance (NMR)

All ^{1}H and ^{13}C NMR spectra were recorded on a Bruker 400 MHz (DPX-400) spectrometer. Chemical shift (δ) are reported in parts per million (ppm) relative to internal

standard tetramethylsilane (TMS) at δ = 0. Samples were prepared in deuterated chloroform ($CDCl_3$) and referenced to residual non-deuterated signal of solvent ($CDCl_3$ @ 7.26 ppm ^{1}H-NMR and 77.2 ppm ^{13}C-NMR). The resonance multiplicities are described as s (singlet), d (doublet), t (triplet), q (quartet) or m (multiplet).

Size Exclusion Chromatography (SEC)

SEC analysis was performed on a Agilent 1260 Infinity II system fitted with RI and ultraviolet (UV) detectors (λ = 309 and 360 nm), equipped with a PLGel 3 μm (50 × 7.5 mm guard column and two PLGel 5 μm (300 × 7.5 mm) mixed-D columns, mobile phase (eluent) using $CHCl_3$ WITH 0.5% triethylamine (TEA). Molecular weight (M_w) and molecular weight distributions ($Đ_M = M_w/M_n$) were calibrated against poly(methyl methacrylate) (PMMA) standards and analysed using Agilent SEC software.

Matrix-Assisted Laser Desorption Ionisation - Time of Flight (MALDI-ToF)

MALDI-ToF mass spectra were obtained using a Bruker Ultraflex II Matrix-assisted laser desorption/ionisation time of flight (MALDI-ToF) mass spectrometer. Typical preparation of samples is as follows; trans-2-[3-(4-tert-butyl-phenyl)-2-methyl-2-propenylidene] malononitrile (DCTB) matrix (20 μL of a 40 mg mL^{-1} HPLC grade THF solution) was added to the sample (20 μL of a 1 mg mL^{-1} HPLC grade THF solution) followed by sodium trifluoroacetate (NaTFA) (20 μL of a 0.1 mg mL^{-1} HPLC grade THF solution) and vortexed before application on a MALDI-ToF plate. Samples were measured in reflectron ion mode and calibrated against SpheriCal (1200 - 8000 g mol^{-1}) standards.

Transmission Electron Microscopy (TEM)*

Dry state transmission electron microscopy (TEM) imaging was performed on JEOL 1400 Bio (1720/GB06) microscopy at an acceleration voltage of 80 kV. CDSA samples

were deposited onto graphene oxide-coated copper grids. Then the grid was stained with an aqueous 1wt. % uranyl acetate (UA) solution to drying and microscopic analysis. For the determination of the average micelles' size at least 100 particles were analysed in each case.

(* The TEM characterization were carried out by Mr Bo Li)

Atomic Force Microscopy (AFM)

AFM samples were prepared by drop casting 10 μL of assemblies in ethanol onto mica silicon wafer which treated by Sigmacote, followed by drying naturally in air. Imaging and analysis were performed on a JPK Nanowizard 4 system in quantitative imaging (QI) mode. The tips for the AFM analysis (PPP-NCHAuD) were purchased from NANOSENSORSTM, with resonance frequency (kHz) in the window of 204 - 497 and force constant in the range of 10 - 130. The AFM pictures and data were analysed and collected using the JPK Data Processing software with QI mode. For determination of the average micelles' size at least 100 particles were analysed in each case.

For micelle contour lengths, widths and areas analysis, ca. 100 micelles in several images were traced manually using the ImageJ software package developed at the US National Institute of Health. The number average micelle length (L_n) and weight average micelle length (L_w) were calculated using blow equation from measurements of the contour lengths (L_i) of individual micelles, where N_i is the number of micelles of length L_i, and n is the number of micelles examined in each sample. The distribution of micelle lengths is characterised by both L_w/L_n.

$$L_n = \frac{\sum_{i=1}^{n} N_i L_i}{\sum_{i=1}^{n} N_i} \qquad L_w = \frac{\sum_{i=1}^{n} N_i L_i^2}{\sum_{i=1}^{n} N_i L_i}$$

The number average micelle width (W_n) and weight average micelle width (W_w) [63]were calculated using blow equation from measurements of the contour widths (W_i) of individual micelles, where N_i is the number of micelles of width W_i, and n is the number of micelles examined in each sample. The distribution of micelle widths is characterised by both W_w/W_n.

$$W_n = \frac{\sum_{i=1}^{n} N_i W_i}{\sum_{i=1}^{n} N_i} \qquad W_w = \frac{\sum_{i=1}^{n} N_i W_i^2}{\sum_{i=1}^{n} N_i W_i}$$

The number average micelle area (A_n) and weight average micelle area (A_w) were calculated using blow equation from measurements of the contour areas (A_i) of individual micelles, where N_i is the number of micelles of length A_i, and n is the number of micelles examined in each sample. The distribution of micelle lengths is characterised by both A_w/A_n.

$$A_n = \frac{\sum_{i=1}^{n} N_i A_i}{\sum_{i=1}^{n} N_i} \qquad A_w = \frac{\sum_{i=1}^{n} N_i A_i^2}{\sum_{i=1}^{n} N_i A_i}$$

Confocal Laser Scanning Microscopy (CLSM)*

FV3000 (Olympus) confocal microscope with a IX-81 inverted base (Olympus) and the 20x and 60x oil lens (Olympus) was used for imaging. The FV3000 system was driven with the FV31S-SW Viewer software platform (Olympus) with scan rates of 1 μs pixel^{-1} at 515 by 512 pixels to 1024 by 1024 pixel^{-1}.

(* The CLSM characterization were carried out by Dr.Yujie Xie)

2.5.3 Experimental Procedures

2.5.3.1 Synthesis of 4-cyano-4-(((ethylthio)carbonothioyl)thio)pentanoic acid (CEPA)

Following a previously reported procedure,[58, 59] to an oven-dried round bottom flask, sodium ethanethiolate (10 g, 119 mmol, 1 eq) was added followed by the addition of dry diethyl ether (500 mL) with the resulting solution cooled to 0 ˚C. Carbon disulfide (7.74 mL, 131 mmol, 1.1 eq) was subsequently added dropwise over 10 min. producing a thick yellow precipitate of sodium S-ethyl trithiocarbonate. After 2 h of stirring at room temperature, solid iodine (15.1 g, 59.4 mmol, 0.5 eq) was added and the resultant reaction mixture was stirred for a further 2 h at room temperature. The reaction mixture was then washed with sodium thiosulfate solution (1 M, 3 × 100 mL), deionized water (3 × 100 mL) and finally with saturated sodium chloride solution (3 × 100 mL). The organic phase was dried over $MgSO_4$, filtered and evaporated to remove solvent, leaving a residue of bis-(ethylsulfanylthiocarbonyl) disulfide (15.6 g, 56.8 mmol).

A solution of 4,4'-azobis(4- cyanovaleric acid) (ACVA) (23.9 g, 85.2 mmol, 1 eq) and bis-(ethylsulfanylthiocarbonyl) disulfide (15.6 g, 56.8 mmol, 0.67 eq) in ethyl acetate (500 mL) was heated to 80 ˚C overnight at reflux under a N_2 atmosphere. After removal of the volatile solvents in vacuo, purification was carried out using silica gel column chromatography (hexane : dichloromethane = 1:3) affording 4-cyano-4-(((ethylthio) carbonothioyl)thio)pentanoic acid (CEPA) as an orange red oil (24.4 g, 97.7 mmol, 86%).

^{1}H NMR (400 MHz, $CDCl_3$): δ (ppm): 3.34 (q, 2H, $SC\boldsymbol{H_2}CH_3$), 2.68 (m, 2H, $C(CN)(CH_3)CH_2C\boldsymbol{H_2}$), 2.33-2.60 (m, 2H, $C(CN)(CH_3)C\boldsymbol{H_2}CH_2$), 1.89 (s, 3H, $C(CN)(C\boldsymbol{H_3})$ CH_2CH_2), 1.36 (t, 3H, $SCH_2C\boldsymbol{H_3}$).

^{13}C NMR (100 MHz, $CDCl_3$): δ (ppm): 216.7 (***C***=S), 177.3 (***C***=O), 118.9 (C(***C***N)(CH_3)CH_2CH_2), 46.2 (***C***(CN)(CH_3)CH_2CH_2), 33.4 (C(CN)(CH_3)***C***H_2CH_2), 31.4 (S***C***H_2CH_3), 29.5 (C(CN)(CH_3)CH_2***C***H_2), 24.8 (C(CN)(***C***H_3)CH_2CH_2), 12.8 (SCH_2***C***H_3).

2.5.3.2 Synthesis of 2-cyano-5-hydroxypentan-2-yl ethyl carbonotrithioate (CHPET)

To a flame-dried three-neck round bottom flask, 4-cyano-4-(((ethylthio)carbonothioyl)thio)pentanoic acid (CEPA) (14.1 g, 53.6 mmol, 1 eq) was added followed by the addition of dry tetrahydrofuran (500 mL) with the resulting solution cooled to -78 ˚C (mixture of dry ice and acetone). Borane tetrahydrofuran complex solution (1 M, 56.3 mL, 56.3 mmol, 1 eq) was subsequently added in a dropwise fashion over 30 min. Reaction mixture was left to stir for 1 h, after which the cooling bath was removed and the reaction stirred overnight at ambient temperature under a N_2 atmosphere. After 18 h of stirring, methanol (100 mL) was added in five portions and stirred for 10 min. after each addition or until no further bubbling was observed. After removal of the volatile solvents in vacuo, the organic residue was dissolved in diethyl ether (250 mL) and washed with saturated $NaHCO_3$ solution (3 × 250 mL) and then with brine (250 mL). Further extraction using diethyl ether from the collected aqueous layers was carried out. Combined organic layers were then dried over $MgSO_4$, filtered and evaporated to dryness. Purification was carried out using silica gel column chromatography (petroleum ether 40/60: ethyl acetate = 1:1) affording 2-cyano-5-hydroxypentan-2-yl ethyl carbonotrithioate (CHPET) as an orange red oil (9.7 g, 39.1 mmol, 73%). Then, the CTA CHPET was dried by static vacuum with P_2O_5 in the desiccator for one week to get rid of water.

^{1}H NMR (400 MHz, $CDCl_3$): δ (ppm): 3.73 (t, 2H, C***H₂***OH), 3.34 (q, 2H, SC***H₂***CH_3), 2.00-2.35 (m, 2H, C(CN)(CH_3)C***H₂***CH_2), 1.90 (s, 3H, C(CN)(C***H₃***)CH_2CH_2), 1.86 (m, 2H, C(CN)(CH_3)CH_2C***H₂***), 1.36 (t, 3H, SCH_2C***H₃***).

^{13}C NMR (100 MHz, $CDCl_3$): δ (ppm): 217.4 (***C***=S), 119.6 (C(***C***N)(CH_3)CH_2CH_2), 61.7 (***C***H_2OH), 47.0 (***C***(CN)(CH_3)CH_2CH_2), 35.8 (C(CN)(CH_3)***C***H_2CH_2), 31.3 (S***C***H_2CH_3), 27.9 (C(CN)(CH_3)CH_2***C***H_2), 24.9 (C(CN)(***C***H_3)CH_2CH_2), 12.8 (SCH_2***C***H_3).

2.5.3.3 Synthesis of Poly(ε-Caprolactone) (PCL)

In a nitrogen-filled glove box with oxygen and water content lower than 0.1 ppm, solutions of diphenylphosphate (DPP, 17 mg, 0.068 mmol, 1 eq) in dry toluene (2.5 mL) and dual-head CTA (17 mg, 0.068 mmol, 1 eq) in dry toluene (1 mL) were added to ε-caprolactone (543.3 ug, 4.76 mmol, 70 eq) dissolved in dry toluene (1.5 mL). After stirring for 6 hours at room temperature, the solution was removed from the glove box, precipitated three times into cold diethyl ether dropwise and collected by centrifugation. It should be noted that the polymers must have no evidence of high or low molecular weight shoulders by SEC before proceeding with RAFT polymerisations and self-assembly.

^{1}H NMR (400 MHz, $CDCl_3$): δ (ppm): 4.10 (t, 2H, C***H₂***OCO), 4.04 (t, 100H, CH_2C***H₂***O), 3.62 (m, 2H, C(CN)C***H₂***CH_2), 3.32 (q, 2H, SC***H₂***CH_3), 2.28 (100H, OCOC***H₂***CH_2), 1.86 (s, 3H, C(CN)(C***H₃***)CH_2), 1.72-1.54 (200H, OCOCH_2C***H₂***CH_2C***H₂***), 1.45-1.28 (100H, OCOCH_2CH_2C***H₂***CH_2).

SEC (Chloroform, PMMA standard): M_n = 15.2 kg mol^{-1}, $Đ_M$ = 1.05.

DSC results: T_c = 35 °C, T_m = 60 °C.

2.5.3.4 Synthesis of PCL-*b*-PDMA

PCL_{50} (100 mg, 0.0168 mmol, 1eq), DMA (399.7 mg, 4.0320 mmol, 240 eq) and AIBN (0.276 mg, 0.00168 mmol, 0.1 eq) were dissolved in 1,4-dioxane (1 mL) and placed in an ampoule. The solution was then freeze-pump-thawed three times and heated for 2 h at 70 ˚C. The reaction was quenched by immersion of the ampoule in liquid nitrogen and the polymer was precipitated in ice-cold diethyl ether three times before being dried under vacuum and analysed.

SEC (Chloroform, PMMA standard): M_n = 31.8 kg mol^{-1}, $Đ_M$ = 1.09.

2.5.3.5 Synthesis of PCL-ACM

Aminochloromaleimide (ACM), synthesised according to a previous method,[26] was coupled to the PCL polymer backbone by esterification. In a typical coupling reaction, PCL (100 mg, 0.0168 mmol, 1 eq), ACM (14.55 mg, 0.0504 mmol, 3 eq), 4-dimethylaminopyridine (DMAP) (2.05 mg, 0.0168 mmol, 1 eq) and N,N′-dicyclohexylcarbodiimide (DCC) (34.66 mg, 0.168 mmol, 10 eq) were mixed together in an ampoule with 2 mL DCM. The solution was left stirring at room temperature for 2 days. The solution was filtered and the filtrate precipitated in diethyl ether three times and the resultant polymer was dried in vacuo.

2.5.3.6 Synthesis of PCL-*b*-PDMA-ACM

Aminochloromaleimide (ACM), synthesised according to a previous method,[26] was coupled to the PCL-*b*-PDMA polymer backbone by esterification. In a typical coupling reaction, PCL-*b*-PDMA (200 mg, 0.0078mmol, 1 eq), ACM (6.64 mg, 0.023 mmol, 3 eq), 4-dimethylaminopyridine (DMAP) (0.95 mg, 0.0078 mmol, 1 eq) and N,N′-dicyclohexylcarbodiimide (DCC) (16.09 mg, 0.078 mmol, 10 eq) were mixed together in an ampoule with 2 mL DCM. The solution was left stirring at room temperature for 2

days. The solution was filtered and the filtrate precipitated in diethyl ether three times and the resultant polymer was dried in vacuo.

2.5.3.7 Crystallisation-Driven Self-Assembly of PCL-*b*-PDMA Cylinder

Block copolymer PCL-*b*-PDMA (20 mg) was added to 4 mL of ethanol (5.0 mg mL^{-1}) in a vial. The samples were heated at 70 °C without stirring on a heating block for 3 h before cooling to room temperature. The sample was aging for 5 days to yield micron-long polydisperse cylinders.

2.5.3.8 Preparation of PCL-*b*-PDMA Seeds Solution

The crystalline cylinders were sonicated using a Bandelin Sonopuls sonication probe in an ice water bath for total 20 min. Polymer solution was fractured for 10 cycles of 2 min sonication each with interval of 20 min to yield short crystalline seeds. For determination of the average seeds' length at least 100 particles were analysed.

2.5.3.9 Living Epitaxial Growth of 2D Platelet

PCL homopolymer with block copolymer PCL-*b*-PDMA, or PCL-ACM homopolymer with block copolymers PCL-*b*-PDMA-ACM dissolved in THF or DMF (10 mg mL^{-1} or 50 mg mL^{-1}) was added to a dispersion of crystalline seeds (0.01 mg mL^{-1}) in a screw cap vial. After shaking the vials for 5 s, the solution was aged for 2 days at room temperature. The unimer-to-seed ratio was altered by adding different volumes of unimer solution to the dispersion of seed micelles (When the ratio of unimers to seeds above 20, the concentration of unimers changes to 50 mg mL^{-1}). The of contour lengths, widths and areas were measured from AFM and CLSM images.

2.5.3.10 Sequential Growth of Multi-Layered Platelet

PCL homopolymer block copolymers PCL-*b*-PDMA dissolved in THF (10 mg mL^{-1}) was added to a dispersion of as prepared platelets seeds and each time aged for 2 days before analysis by AFM and TEM images.

2.5.3.11 Growth of Fluorescent Multi-Layered Platelet

The blending unimers of PCL homopolymer block copolymers PCL-*b*-PDMA (or PCL-ACM and PCL-*b*-PDMA-ACM) dissolved in THF (10 mg mL^{-1}) was added alternatively to a dispersion of as prepared platelets seeds and aged for 2 days before analysis by AFM and CLSM images.

2.6 References

1. H. Luo, Q. Tang, J. Zhong, Z. Lei, J. Zhou and Z. Tong, *Macromol. Chem. Phys.*, 2019, **220**.
2. W.-N. He and J.-T. Xu, *Prog. Polym. Sci.*, 2012, **37**, 1350-1400.
3. Y. Su, H. Luo and Z. Tong, *Macromol. Chem. Phys.*, 2020, **221**.
4. X. X. Ke, L. Wang, J. T. Xu, B. Y. Du, Y. F. Tu and Z. Q. Fan, *Soft Matter*, 2014, **10**, 5201-5211.
5. B. Fan, L. Liu, J. H. Li, X. X. Ke, J. T. Xu, B. Y. Du and Z. Q. Fan, *Soft Matter*, 2016, **12**, 67-76.
6. W.-N. He, B. Zhou, J.-T. Xu, B.-Y. Du and Z.-Q. Fan, *Macromolecules*, 2012, **45**, 9768-9778.
7. W.-N. He, J.-T. Xu, B.-Y. Du, Z.-Q. Fan and F.-L. Sun, *Macromol. Chem. Phys.*, 2012, **213**, 952-964.
8. N. Petzetakis, M. P. Robin, J. P. Patterson, E. G. Kelley, P. Cotanda, P. H. Bomans, N. A. Sommerdijk, A. P. Dove, T. H. Epps and R. K. O'Reilly, *ACS Nano*, 2013, **7**, 1120-1128.
9. Z. Tong, R. Zhang, P. Ma, H. Xu, H. Chen, Y. Li, W. Yu, W. Zhuo and G. Jiang, *Langmuir*, 2017, **33**, 176-183.
10. H. Luo, Y. Lin, Q. Tang, W. Hu, Y. Wang, Z. Lei and Z. Tong, *Macromol. Chem. Phys.*, 2019, **220**.
11. Z. Tong, J. Zhou, J. Zhong, Q. Tang, Z. Lei, H. Luo, P. Ma and X. Liu, *ACS Appl. Mater. Interfaces*, 2018, **10**, 20014-20024.
12. Y. Mai and A. Eisenberg, *Chem. Soc. Rev.*, 2012, **41**, 5969-5985.
13. Y. Mai and A. Eisenberg, *J. Am. Chem. Soc.*, 2010, **132**, 10078-10084.
14. R. Vyhnalkova, A. H. Muller and A. Eisenberg, *Langmuir*, 2014, **30**, 5031-5040.

15. R. Vyhnalkova, A. H. Muller and A. Eisenberg, *Langmuir*, 2014, **30**, 13152-13163.

16. J. Cai, C. Li, N. Kong, Y. Lu, G. Lin, X. Wang, Y. Yao, I. Manners and H. Qiu, *Science*, 2019, **366**, 1095-1098.

17. M. C. Arno, M. Inam, A. C. Weems, Z. Li, A. L. A. Binch, C. I. Platt, S. M. Richardson, J. A. Hoyland, A. P. Dove and R. K. O'Reilly, *Nat. Commun.*, 2020, **11**, 1420.

18. Z. M. Hudson, C. E. Boott, M. E. Robinson, P. A. Rupar, M. A. Winnik and I. Manners, *Nat. Chem.*, 2014, **6**, 893-898.

19. A. M. Oliver, J. Gwyther, M. A. Winnik and I. Manners, *Macromolecules*, 2017, **51**, 222-231.

20. E. L. Kynaston, A. Nazemi, L. R. MacFarlane, G. R. Whittell, C. F. J. Faul and I. Manners, *Macromolecules*, 2018, **51**, 1002-1010.

21. U. Tritschler, J. Gwyther, R. L. Harniman, G. R. Whittell, M. A. Winnik and I. Manners, *Macromolecules*, 2018, **51**, 5101-5113.

22. M. Inam, J. R. Jones, M. M. Perez-Madrigal, M. C. Arno, A. P. Dove and R. K. O'Reilly, *ACS Cent. Sci.*, 2018, **4**, 63-70.

23. F. Xu, P. Zhang, J. Zhang, C. Yu, D. Yan and Y. Mai, *ACS Macro Lett.*, 2018, **7**, 1062-1067.

24. Z. Li, Y. Zhang, L. Wu, W. Yu, T. R. Wilks, A. P. Dove, H.-m. Ding, R. K. O'Reilly, G. Chen and M. Jiang, *ACS Macro Lett.*, 2019, DOI: 10.1021/acsmacrolett.9b00221, 596-602.

25. C. E. Boott, E. M. Leitao, D. W. Hayward, R. F. Laine, P. Mahou, G. Guerin, M. A. Winnik, R. M. Richardson, C. F. Kaminski, G. R. Whittell and I. Manners, *ACS Nano*, 2018, **12**, 8920-8933.

26. W. Yu, M. Inam, J. R. Jones, A. P. Dove and R. K. O'Reilly, *Polym. Chem.*, 2017, **8**, 5504-5512.
27. S. Shin, F. Menk, Y. Kim, J. Lim, K. Char, R. Zentel and T. L. Choi, *J. Am. Chem. Soc.*, 2018, **140**, 6088-6094.
28. J. C. Foster, S. Varlas, B. Couturaud, Z. Coe and R. K. O'Reilly, *J. Am. Chem. Soc.*, 2019, **141**, 2742-2753.
29. J. R. Finnegan, X. He, S. T. G. Street, J. D. Garcia-Hernandez, D. W. Hayward, R. L. Harniman, R. M. Richardson, G. R. Whittell and I. Manners, *J. Am. Chem. Soc.*, 2018, **140**, 17127-17140.
30. A. M. Oliver, J. Gwyther, C. E. Boott, S. Davis, S. Pearce and I. Manners, *J. Am. Chem. Soc.*, 2018, **140**, 18104-18114.
31. N. Petzetakis, A. P. Dove and R. K. O'Reilly, *Chem. Sci.*, 2011, **2**, 955-960.
32. A. Pitto-Barry, N. Kirby, A. P. Dove and R. K. O'Reilly, *Polym. Chem.*, 2014, **5**, 1427-1436.
33. Y. Gao, H. Qiu, H. Zhou, X. Li, R. Harniman, M. A. Winnik and I. Manners, *J. Am. Chem. Soc.*, 2015, **137**, 2203-2206.
34. H. Wang, X. Wang, M. A. Winnik and I. Manners, *J. Am. Chem. Soc.*, 2008, **130**, 12921-12930.
35. X. Li, Y. Gao, R. Harniman, M. Winnik and I. Manners, *J. Am. Chem. Soc.*, 2016, **138**, 12902-12912.
36. L. Sun, N. Petzetakis, A. Pitto-Barry, T. L. Schiller, N. Kirby, D. J. Keddie, B. J. Boyd, R. K. O'Reilly and A. P. Dove, *Macromolecules*, 2013, **46**, 9074-9082.
37. M.-S. Hsiao, S. F. M. Yusoff, M. A. Winnik and I. Manners, *Macromolecules*, 2014, **47**, 2361-2372.

38. L. Sun, A. Pitto-Barry, N. Kirby, T. L. Schiller, A. M. Sanchez, M. A. Dyson, J. Sloan, N. R. Wilson, R. K. O'Reilly and A. P. Dove, *Nat. Commun.*, 2014, **5**, 5746.

39. Z.-X. Du, J.-T. Xu and Z.-Q. Fan, *Macromolecules*, 2007, **40**, 7633-7637.

40. Z.-X. Du, J.-T. Xu and Z.-Q. Fan, *Macromol. Rapid Commun.*, 2008, **29**, 467-471.

41. C. Jiang, H. Huang, C. Ma, T. He and F. Zhang, *J. Colloid Interface Sci.*, 2013, **411**, 53-60.

42. C. Jiang, Z. Wang, H. Huang and T. He, *Langmuir*, 2011, **27**, 4351-4357.

43. W. Y. Chen, C. Y. Li, J. X. Zheng, P. Huang, L. Zhu, Q. Ge, R. P. Quirk, B. Lotz, L. Deng, C. Wu, E. L. Thomas and S. Z. D. Cheng, *Macromolecules*, 2004, **37**, 5292-5299.

44. G. Rizis, T. G. van de Ven and A. Eisenberg, *Angew. Chem. Int. Ed.*, 2014, **53**, 9000-9003.

45. G. Rizis, T. G. van de Ven and A. Eisenberg, *ACS Nano*, 2015, **9**, 3627-3640.

46. B. Fan, R.-Y. Wang, X.-Y. Wang, J.-T. Xu, B.-Y. Du and Z.-Q. Fan, *Macromolecules*, 2017, **50**, 2006-2015.

47. M. Inam, G. Cambridge, A. Pitto-Barry, Z. P. L. Laker, N. R. Wilson, R. T. Mathers, A. P. Dove and R. K. O'Reilly, *Chem. Sci.*, 2017, **8**, 4223-4230.

48. A. Nazemi, X. He, L. R. MacFarlane, R. L. Harniman, M. S. Hsiao, M. A. Winnik, C. F. Faul and I. Manners, *J. Am. Chem. Soc.*, 2017, **139**, 4409-4417.

49. H. Qiu, Y. Gao, C. E. Boott, O. E. Gould, R. L. Harniman, M. J. Miles, S. E. Webb, M. A. Winnik and I. Manners, *Science*, 2016, **352**, 697-701.

50. H. Tian, Z. Tang, X. Zhuang, X. Chen and X. Jing, *Prog. Polym. Sci.*, 2012, **37**, 237-280.

51. X.-Y. Wang, R.-Y. Wang, B. Fan, J.-T. Xu, B.-Y. Du and Z.-Q. Fan, *Macromolecules*, 2018, **51**, 2138-2144.

52. H. Qi, T. Zhou, S. Mei, X. Chen and C. Y. Li, *ACS Macro Lett.*, 2016, **5**, 651-655.

53. Z. Tong, Y. Li, H. Xu, H. Chen, W. Yu, W. Zhuo, R. Zhang and G. Jiang, *ACS Macro Lett.*, 2016, **5**, 867-872.

54. B. Li, B. Wang, R. C. M. Ferrier and C. Y. Li, *Macromolecules*, 2009, **42**, 9394-9399.

55. M. Su, H. Huang, X. Ma, Q. Wang and Z. Su, *Macromol. Rapid Commun.*, 2013, **34**, 1067-1071.

56. B. Dong, T. Zhou, H. Zhang and C. Y. Li, *ACS Nano*, 2013, **7**, 5192-5198.

57. M. C. Arno, M. Inam, Z. Coe, G. Cambridge, L. J. Macdougall, R. Keogh, A. P. Dove and R. K. O'Reilly, *J. Am. Chem. Soc.*, 2017, **139**, 16980-16985.

58. S. Varlas, P. G. Georgiou, P. Bilalis, J. R. Jones, N. Hadjichristidis and R. K. O'Reilly, *Biomacromolecules*, 2018, **19**, 4453-4462.

59. H. U. Kang, Y. C. Yu, S. J. Shin and J. H. Youk, *J. Polym. Sci. A Polym. Chem.*, 2012, **51**, 774-779.

60. C. Ladavi re, P. Lacroix-Desmazes and F. d. r. Delolme, *Macromolecules*, 2009, **42**, 70-84.

61. O. I. Strube, L. Nothdurft, M. Drache and G. Schmidt-Naake, *Macromol. Chem. Phys.*, 2011, **212**, 574-582.

62. Y. Xie, J. T. Husband, M. Torrent-Sucarrat, H. Yang, W. Liu and R. K. O'Reilly, *Chem. Commun.*, 2018, **54**, 3339-3342.

63. J. Schmelz, M. Karg, T. Hellweg and H. Schmalz, *ACS Nano*, 2011, **5**, 9523-9534.

Chapter three – Precision surface modification of poly(*ε*-caprolactone) assemblies *via* photo RAFT polymerisation

3.1 Abstract

The modification of surfaces with precise chemistries is of great importance in a broad range of fields from nanotechnology, to energy, and environmental chemistry. The surface modification of 2D materials allows the achievement of multifunctional assemblies for many applications. Herein, we demonstrate a facile method to prepare poly(ε-caprolactone)-based platelets, in which the height can be precisely altered by photo-RAFT polymerisation owing to the extended corona polymer chain. Meanwhile, the fluorescent monomer could be further polymerised on the surface of such platelets, leading to t visual tracking of these structures by confocal microscopic. Furthermore, through adjusting the RAFT end group (trithiocarbonate group) in specific regions, the surface of the platelets could be spatially functionalised by selectively increasing their height and imparting fluorescent properties. This study provides a suitable platform for precisely controlled surface functionalisation of soft materials with potential applications in a wide variety of areas.

3.2 Introduction

Self-assembly of macromolecules has emerged as a highly effective strategy for the construction of artificial architectures from simple building blocks, allowing precise control of highly ordered assemblies from randomly oriented molecules. Assemblies with increasing complexity in molecular packing often exhibit unique morphology which offer great potential for a variety of applications. A variety of one-dimensional (1D) and two-dimensional (2D) structures have been investigated using CDSA, including cylindrical micelles[1-12] and platelet micelles.[13-18] More complex hierarchical structures have been studied with great control over morphology and dimensions, such as branched cylindrical micelles,[19, 20] scarf-like micelles,[21-27] multi-armed micelles,[28] patchy platelet,[29, 30] and cylindrical networks.[31] To date, the most controlled approach in the dimensional and morphological modulation of crystallisable block copolymer nanostructures involves the use of living growth, where crystalline micelles grow *via* an epitaxial growth mechanism by addition of molecularly dissolved polymer unimers to seeds. The ends of the crystalline seeds remain active to the addition of unimers to produce well defined structures.

Nowadays, assemblies with single intrinsic properties cannot meet the requirement of the practical world. Therefore, surface modification endows new properties independent of those of the original substrate, leading to applications in membranes, semi-conductive sensors, microfluidic, biomedical devices and many other fields.[32-45] Sargent and co-workers reported an N-aryl-substituted tetrahydro-bipyridine film modified copper catalyst,[46] which can improve the stabilisation of an 'atop-bound' CO intermediate, thereby favouring further reduction from CO_2 to valuable chemical ethylene (**Figure 3.1 a**). Creton and co-workers investigated comb-like random copolymer brushes consisted of poly(ethylene glycol)-*b*-poly(dimethylsiloxane) (PEG-*b*-PDMS) grafted on rough

silicon wafers,[41] exhibiting adaptive adhesion properties to self-tune their adhesion behaviour (**Figure 3.2 b**). Seymour *et al.* synthesised a series of poly(alkyl methacrylate) brush-grafted silica nanoparticles,[40] applying in oil lubricant additives for friction and wear reduction (**Figure 3.1 c**). Im and co-workers demonstrated a spin coating approach of depositing dense $MAPbBr_3$ perovskite thin-films on a TiO_2/FTO substrate,[33] exhibiting superior power conversion efficiency of 10.4% in solar cell (**Figure 3.1 d**).

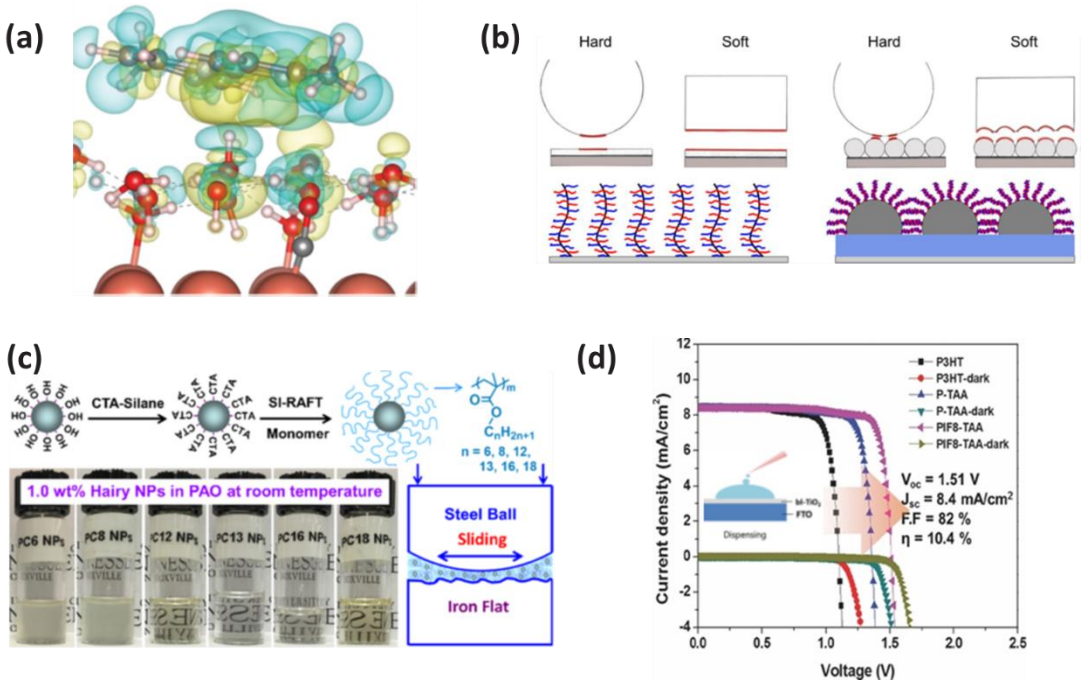


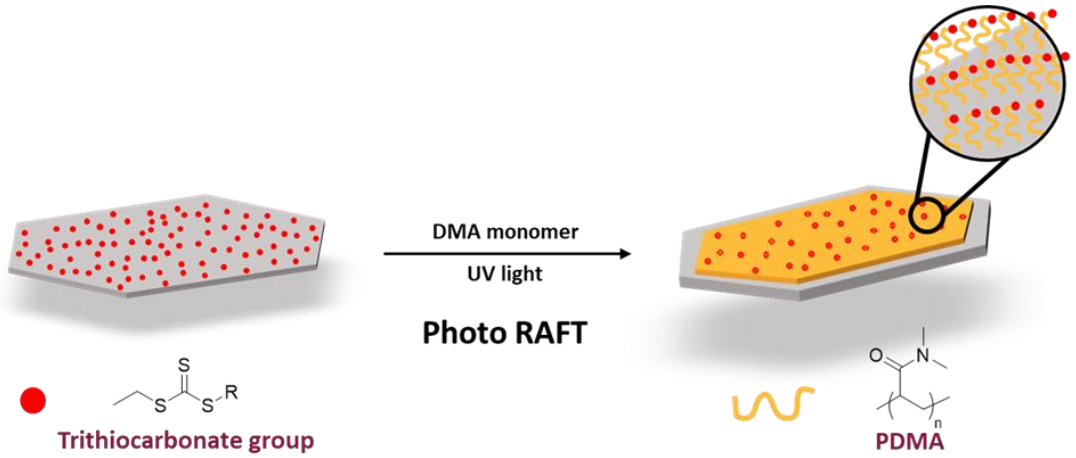
Figure 3.1 The applications of surface modified materials. (a) CO_2 catalysis,[46] (b) adhesion,[41] (c) lubrication,[40] and (d) energy storage.[33]

However, fewer examples on the precise tailoring of the surface of a substrate have been investigated, due to difficulties in controlling the functionalisation process of the methods currently used. To overcome this challenge, Manners and co-workers presented tailored multifunctional micellar brushes through crystallisation driven growth from a surface of immobilisation seeds, which can be used in catalysis and antibacterial applications.[47] The density, length, and coronal chemistry of the micellar brushes can be precisely tuned through the crystallisation-driven growth. Though promising, the above approaches are

mainly focused on a rigid substrate and hard template of inorganic chemistry while the control over the surface of soft materials still remains as a key challenge in the field of polymer-based nanomaterials.

Light induced surface-initiated polymerisations have received extensive attention as an effective approach for the surface functionalisation of polymer brushes. The self-assembled monolayer of initiators is general distributed on the surface of the substrate, tethering polymer chains to the substrate at one end while providing temporal and spatial control.[48] Hawker and co-workers reported a facile method to fabricate complex and arbitrary three-dimensional structures with polymer brushes from a uniform initiating layer *via* visible light mediated living radical polymerisation.[49]

Inspired by these studies, we herein report a selective and efficient method to tailor the surface of PCL-based platelets (described in **Chapter Two**) by photo-RAFT polymerisation (**Scheme 3.1**). Uniform platelets with different height thickness were prepared by adjusting the equivalents of DMA monomer (mass ratio of monomer to platelet), extending the DMA corona block DP on the platelet, enabling control over the surface chemistry as well as the height of the platelet. A fluorescent monomer can also be polymerised by the same strategy and readily tracked by CSLM. More importantly, a specific region (containing RAFT group layer) of a platelets surface could be selectively functionalised to polymerisation, with height change and fluorescent property observed. This approach provides a novel strategy to precisely control the surface functionalisation of soft materials.



Scheme 3.1 Strategy of surface modification of platelets prepared by CDSA *via* photo-RAFT polymerisation. Red dots: Light responsive group for photo RAFT. Yellow line: Extended corona after photo RAFT.

3.3 Results and Discussion

3.3.1 Photo RAFT Polymerisation on Platelets Surface

Based on established assembly methods as previously described (**Chapter Two**), PCL/PCL-*b*-PDMA platelets were obtained using epitaxial seeded growth. The assemblies of PCL/PCL-*b*-PDMA platelets were observed by AFM (**Figure 3.1**), exhibiting a uniform height of 10 nm across the platelets.

Photo RAFT polymerisation of DMA (100 eq, mass ratio of monomer to platelet) on the surface of platelets was carried out under 405 nm UV light irradiation for 4 h at room temperature (N_2 atmosphere), and subsequently dialysed in ethanol to remove unreacted monomer. AFM analysis indicated that the height of platelets increased to 20 nm and the platelet morphology were maintained (**Figure 3.2**), revealing a successful surface functionalisation *via* photo RAFT.

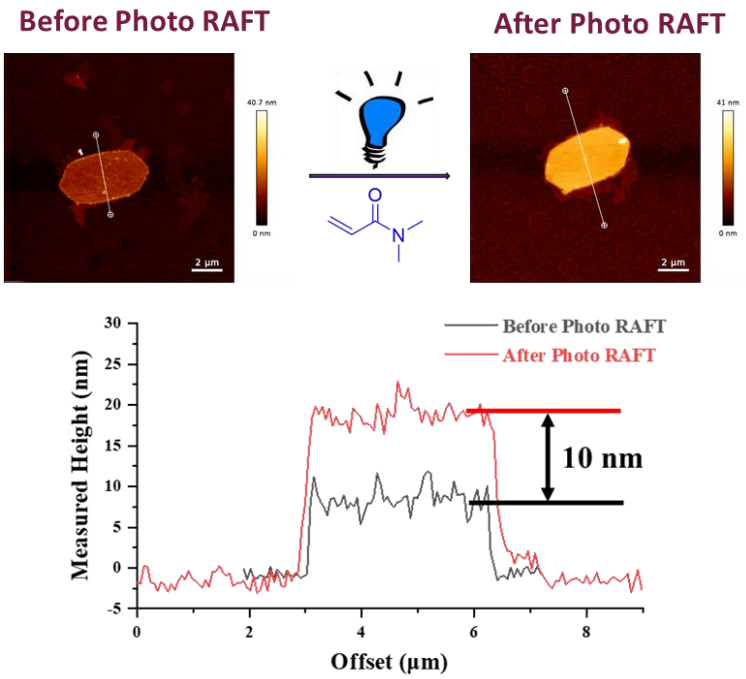


Figure 3.2 AFM images and height profiles of platelet before (left) and after (right) photo RAFT polymerisation; below: height measured at selected region (line).

In order to prove the successful photo RAFT on the surface of the platelets, SEC was used to confirm the molecular weight and distribution of the chain extended diblocks by dissolving the assembles in chloroform. Due to the platelet assemblies composed by PCL homopolyer and PCL-b-PDMA block copolymer blends, the SEC chromatogram would be a bimodal curve. A clear shift integrally in molecular weight of the bimodal distributions was confirmed by SEC refractive index analysis with good overlap of the UV trace (λ_{abs} = 309 nm), showing the successful polymerisation and retention of the RAFT end group (**Figure 3.3**).

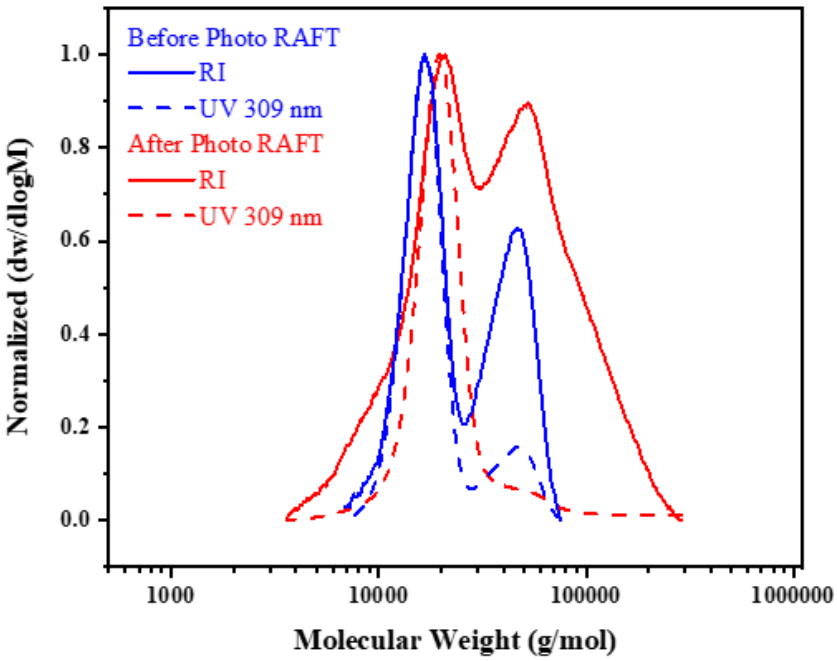
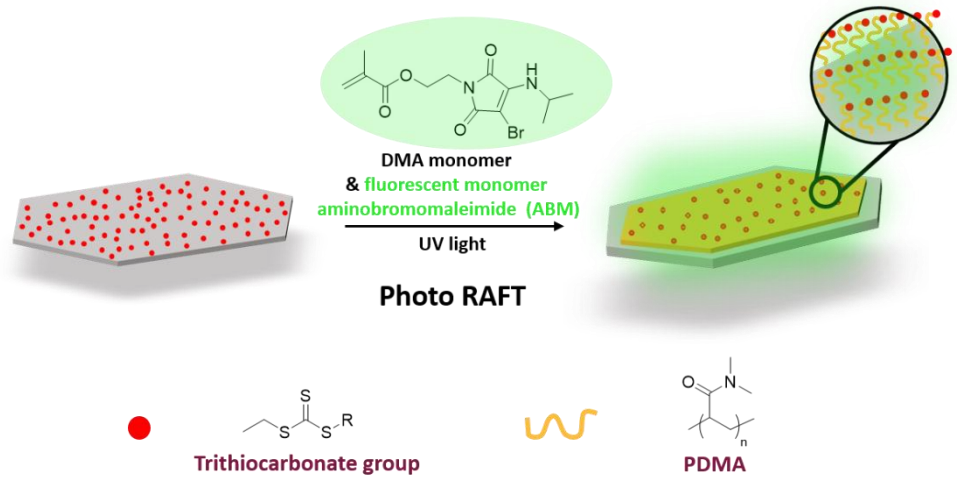


Figure 3.3 SEC chromatogram of PCL/PCL-*b*-PDMA platelets before and after photo RAFT polymerisation using $CHCl_3$ with 0.5% TEA as an eluent with PMMA standards. (Blue line present the molecular weight distribution of original platelets; Red line presents the molecular weight distribution of platelets after photo RAFT)

3.3.2 Photo RAFT of Fluorescent Monomer

To further confirm this approach, the PCL/PCL-*b*-PDMA platelets were photo RAFT polymerised with the fluorescent monomer aminobromomaleimide (ABM) for *in situ* observation of the surface modification of CDSA platelets (**Scheme 3.2**). After photo RAFT polymerisation, the fluorescent functionalised platelets maintained their original shape, as visualised by CLSM. The overlap of emission channel and bright field channel in confocal microscopy confirmed that the fluorescent dye was distributed uniformly on the surface of the platelets (**Figure 3.4**).



Scheme 3.2 Strategy of fluorescence modification of PCL/PCL-*b*-PDMA platelet *via* photo RAFT polymerisation.

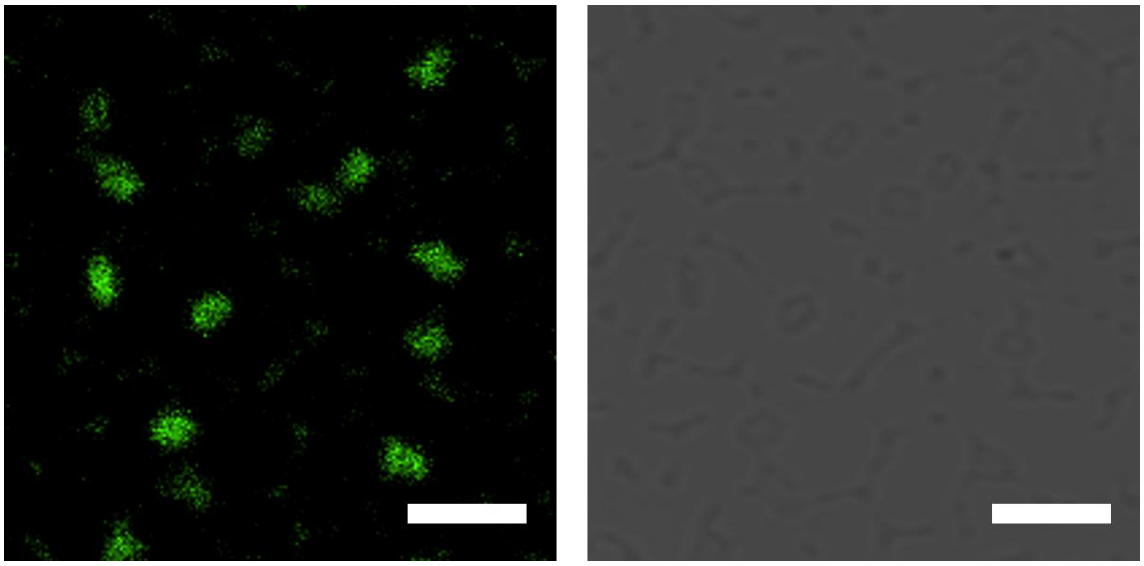


Figure 3.4 CLSM images of platelets after photo RAFT with fluorescent dye. Left: confocal field; Right: bright field. (Scale bar = 3 μm) (CLSM images collected by Dr. Yujie Xie.)

3.3.3 Photo RAFT with Different DMA Monomer Concentration

After successful surface modification with homologous monomer and fluorescent monomer by photo RAFT, the investigation of the effect of monomer concentration over the platelet height was carried out. This was undertaken using a similar procedure as outlined above, but with varying amounts of DMA monomer, various modified platelets have been achieved (**Figure 3.5**). From AFM analysis, the height of the platelets changed as expected, and increased in a linear relationship between platelet height and monomer concentration. The height of platelet can be up to 20 nm when the concentration of DMA monomer is below 100 equivalents (mass ratio of monomer to platelet). Interestingly, when the concentration of DMA increased to more than 100 equivalents, the height remained of about 22 nm without any further increase. (**Figure 3.6**). This phenomenon can be probably ascribed to two reasons. Firstly, the polymeric chain is too long to stand, and chain ends could bend and aggregate on the surface of the platelets. Secondly, with the increasing degree of polymerisation, the active polymer chains are very bulky which limits the active RAFT group to further react with free monomer.

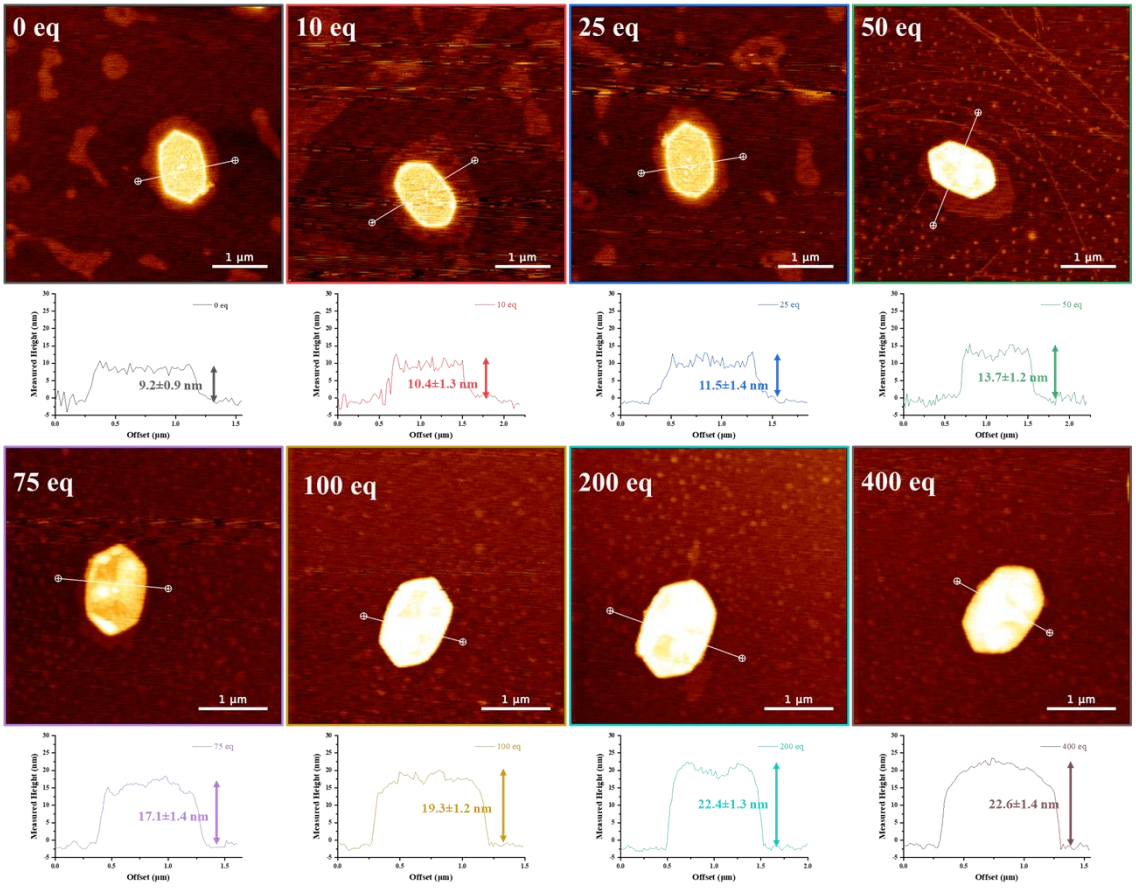


Figure 3.5 AFM images of platelets reacted with different concentration of DMA (0, 10, 25, 50, 75, 100, 200 and 400 equivalent) before and after photo RAFT.

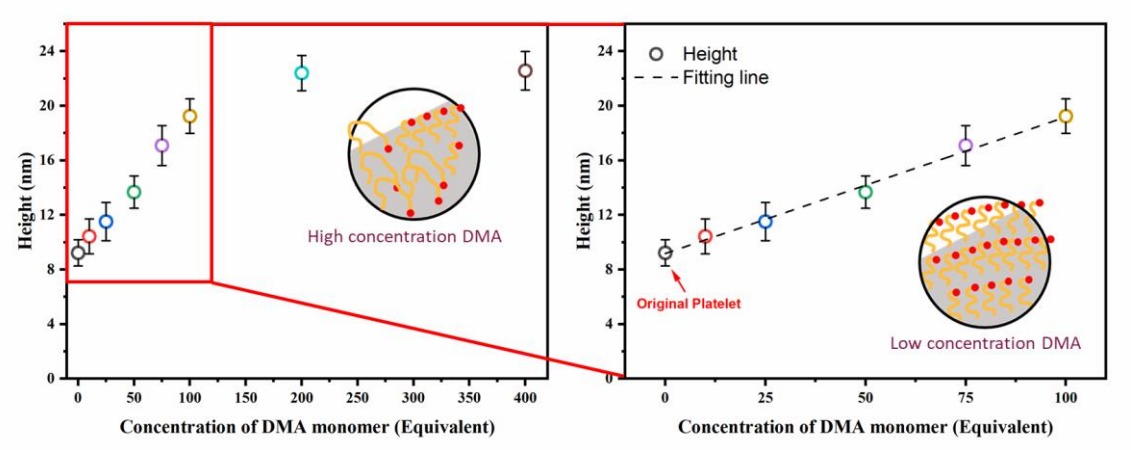


Figure 3.6 Plots of platelets height against the concentration of DMA monomer.

3.3.4 Photo RAFT with Different Monomers

Encouraged by the promising results that platelets assembled *via* CDSA could act as a template for surface decoration, we sought to investigate whether heterogeneous monomers could also be applied in this system. Such a method would polymerise with tens of different monomers and will be the focus of future work. In the current work, four monomers were investigated including homologous monomer DMA, and heterogeneous monomer N-isopropylacrylamide (NIPAm), 4-vinylpyridine (4VP), and 2-(dimethylamino)ethyl methacrylate (DMAEMA). Analysis by SEC (**Figure 3.7**) found that NIPAm and 4VP monomers did not polymerise on the surface of the platelet by photo RAFT. Compared to NIPAm and 4-VP, the addition of heterogeneous DMAEMA monomer was successfully achieved by photo RAFT, although a significant increase in molecular weight, higher than expected, was detected by SEC analysis, requiring further investigation of the photo-RAFT for this system using DMAEMA (**Figure 3.7 d**).

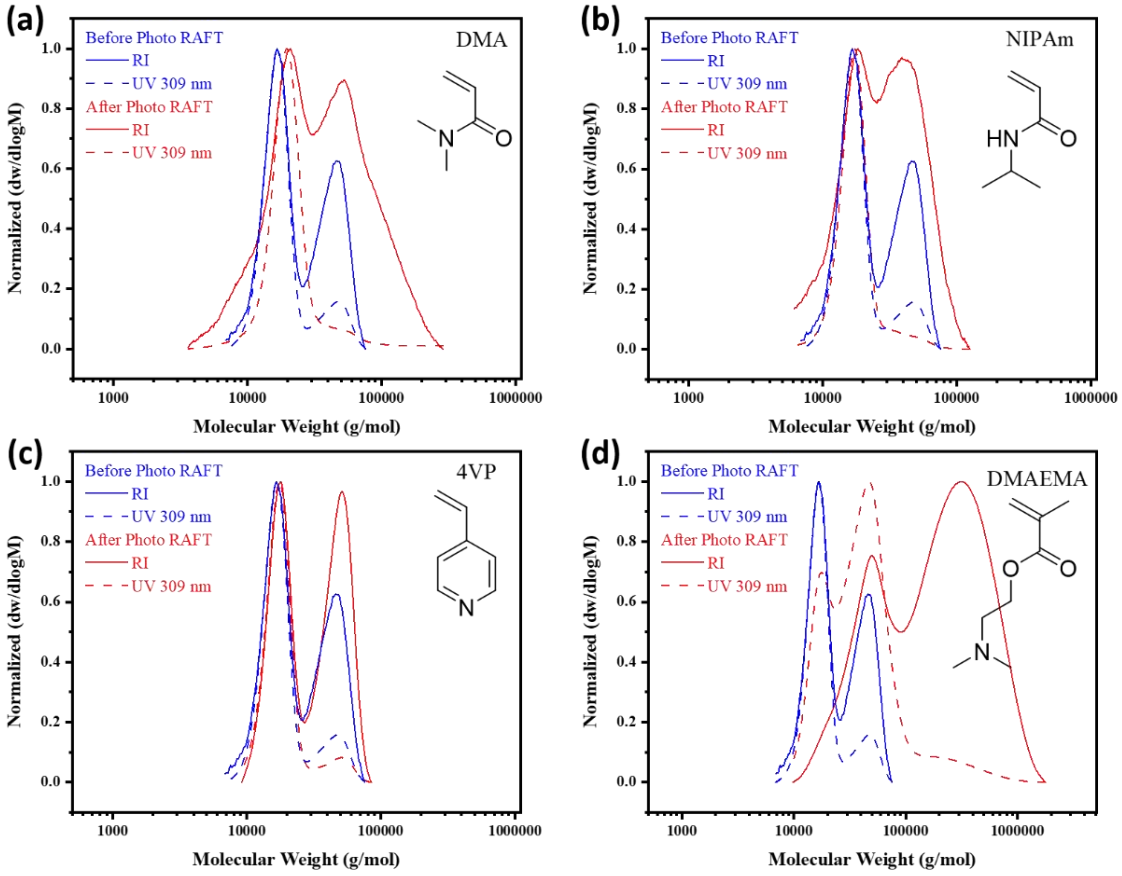
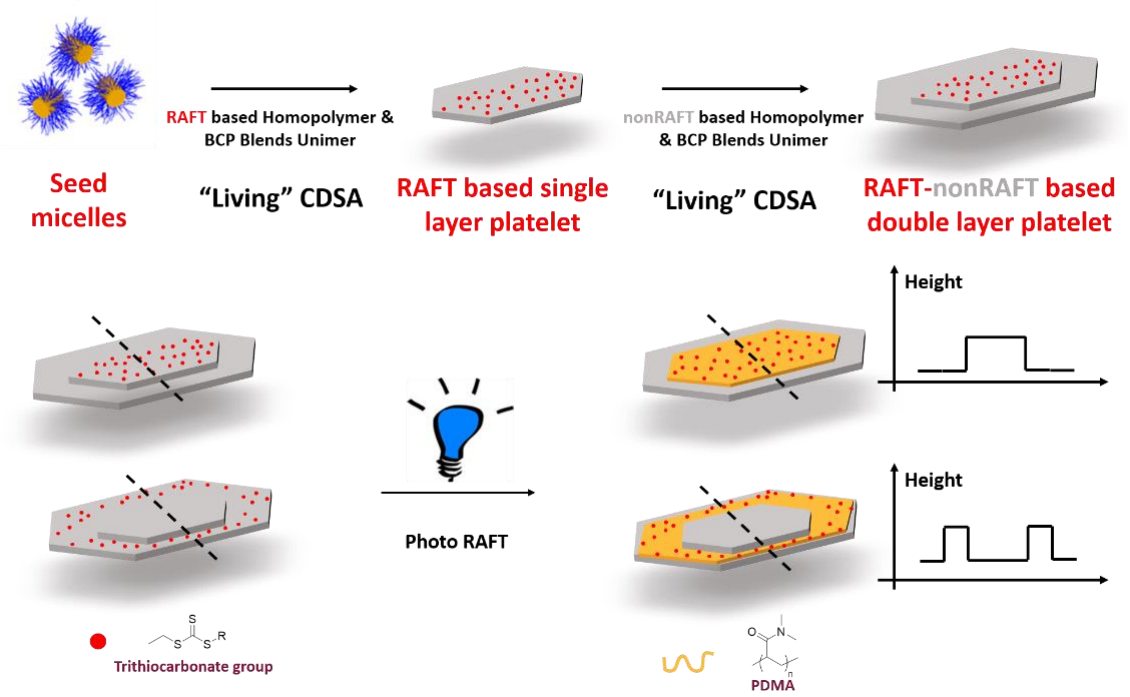


Figure 3.7 SEC chromatogram of PCL/PCL-*b*-PDMA platelets reacted with different monomer (a) DMA, (b) NIPAm, (c) 4VP, and (d) DMAEMA before and after photo RAFT polymerisation using $CHCl_3$ with 0.5% TEA as an eluent with PMMA standards.

3.3.5 Spatial Selective Modification on the Surface of Platelets

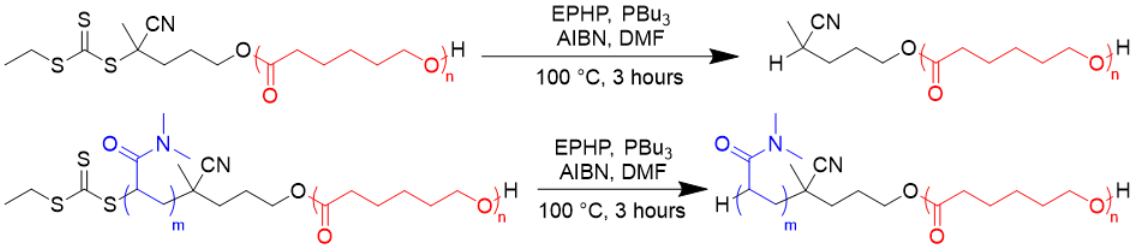
Based on the above study of surface decoration on the whole surface *via* photo RAFT, we sought to selective functionalise a specific region of the platelet using this strategy. Modulating the RAFT active group of different layers of the platelets is a facile way to trace and image particles by AFM height analysis and CLSM imaging, providing the ability to surface polymerisation only on layer containing the RAFT group (**Scheme 3.3**).



Scheme 3.3 Route of spatial selective modification on the surface of platelets.

3.3.5.1 Removal of Trithiocarbonate End Group

Removal of the RAFT group offers a simple route to construct complex hierarchal structures for post spatial modification on the surface of platelets. To achieve this objective, the end group removed polymer was designed (**Scheme 3.4**). The removal of RAFT end group in polymers (PCL homopolymer and PCL-*b*-PDMA block copolymer) was attempted using 1-ethylpiperidine hypophosphite (EPHP), mixed with tributylphosphine (PBu_3) and 2,2′-Azobis(2-methylpropionitrile) (AIBN) in DMF, degassed and heated to 100°C for three hours. The product polymer was isolated by precipitation into cold diethyl ether (0 °C).



Scheme 3.4 Design of RAFT group removed homopolymer and block copolymer.

Using a previously reported method, the RAFT group was substituted by a hydrogen atom and all functionality was effectively removed from this end of the polymer. To confirm the successful removal of the end group, ^{1}H NMR spectra were compared before and after the reaction. Removal of the trithiocarbonate group resulted in the disappearance of the signal of methylene proton at 3.35 ppm (H10) (**Figure 3.8**). Further characterisation by SEC confirmed disappearance of the the UV trace at 309 nm, indicating successful removal of the RAFT end-group (**Figure 3.9**).

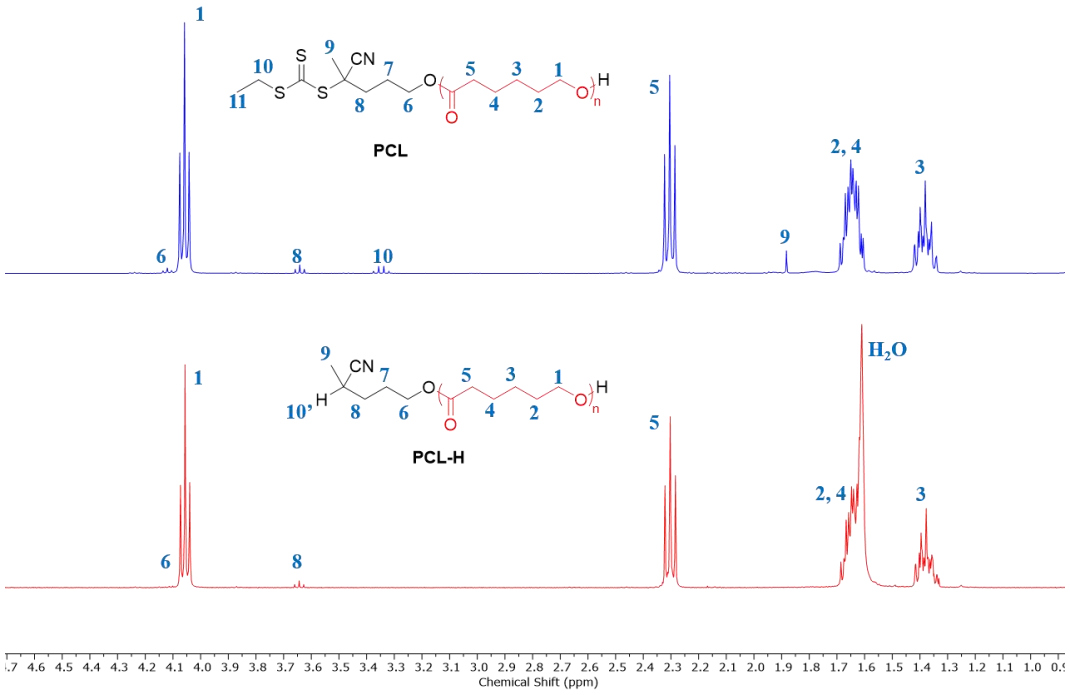


Figure 3.8 ^{1}H NMR spectrum of PCL_{50} homopolymer before and after removing end group in $CDCl_3$ (400 MHz).

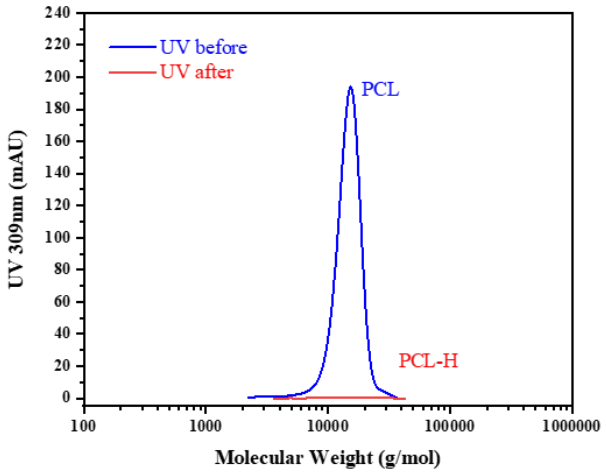


Figure 3.9 SEC chromatogram (UV trace, 309 nm) of PCL_{50} homopolymer before and after removing end group using $CHCl_3$ with 0.5% TEA as an eluent with PMMA standards.

Block copolymer (PCL_{50}-*b*-$PDMA_{198}$) was synthesized following a similar procedure. SEC analysis showed a significant change in the UV trace at 309 nm, confirming that the end group of PCL_{50}-*b*-$PDMA_{198}$ block copolymer was successfully removed (**Figure 3.10**).

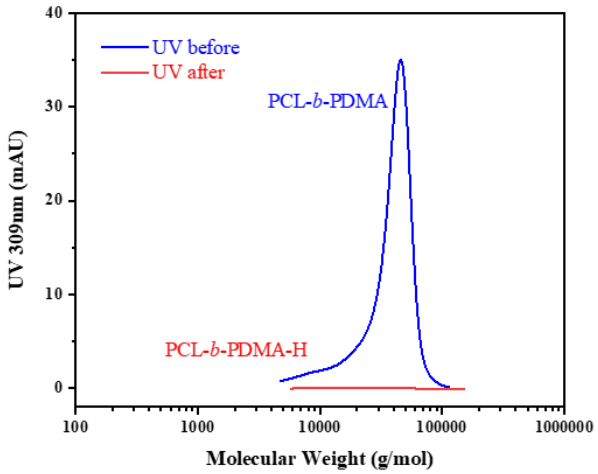
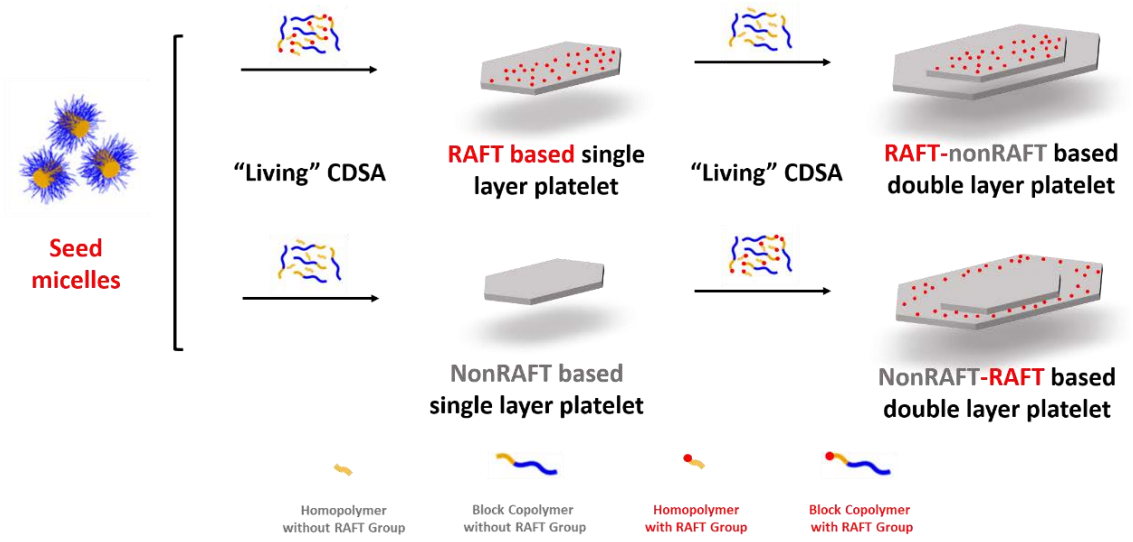


Figure 3.10 SEC chromatogram (UV trace, 309 nm) of block copolymer PCL_{50}-*b*-$PDMA_{198}$ before and after removing end group using $CHCl_3$ with 0.5% TEA as an eluent with PMMA standards.

3.3.5.2 Growth of Multi-Layered Platelets

Following the procedure of multi-layered platelet assembly using seeded growth described in **Chapter two**, the well-defined double layered platelets can be produced by sequential addition of the blend unimers (RAFT or non-RAFT based polymer) (**Scheme 3.5**). As shown in AFM images (**Figure 3.11**), the double-layered platelets were observed, containing an inner layer and an outer layer, but just one layer possessing RAFT group for photo RAFT polymerisation.



Scheme 3.5 Design of alternate RAFT or nonRAFT layered platelet.

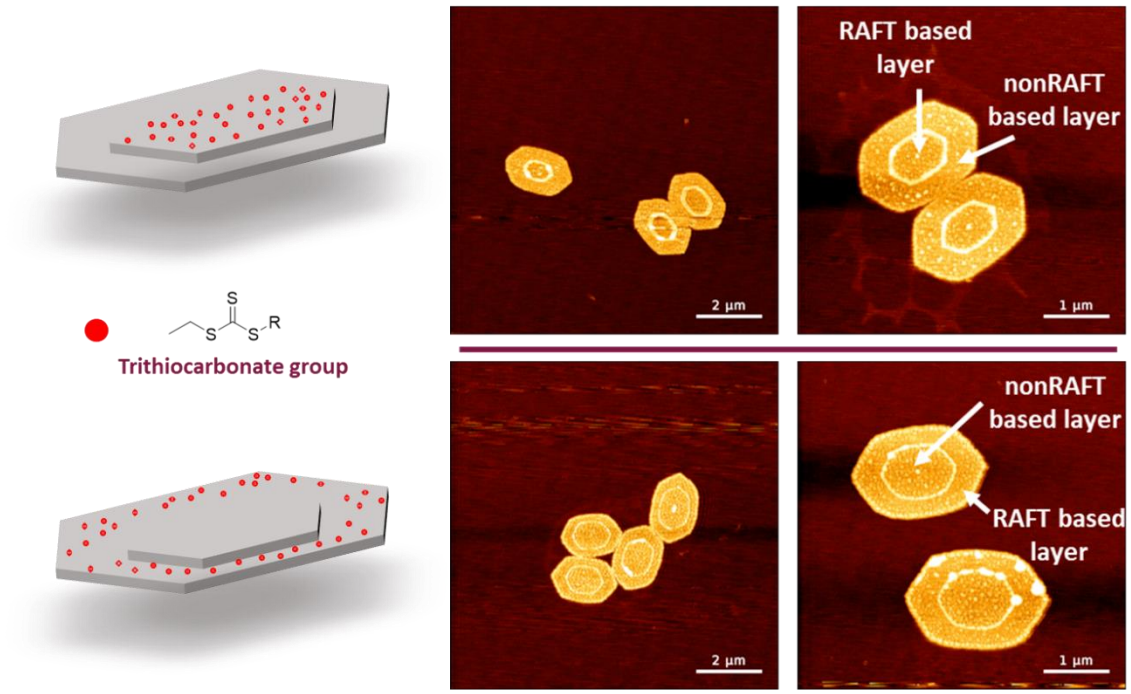


Figure 3.11 AFM images and height profiles of double-layered platelet. Top: inner layer - RAFT layer, outer layer - nonRAFT layer; Bottom: inner layer - nonRAFT layer, outer layer - RAFT layer.

3.3.5.3 Photo RAFT on the Surface of Multi-Layered Platelets

Following the preparation of specific double layered platelet, photo RAFT polymerisation was carried out in the mixture of platelets and DMA monomer. From AFM analysis, when the inner layer possessed the RAFT group, the height of inner layer increased to 23 nm and the outer layer remained at the original height. In contrast, when the RAFT group was located in the outer layer, the height of outer layer is about 6 nm higher than that of inner layer, demonstrating the success of selective surface modification (**Figure 3.12 and 3.13**).

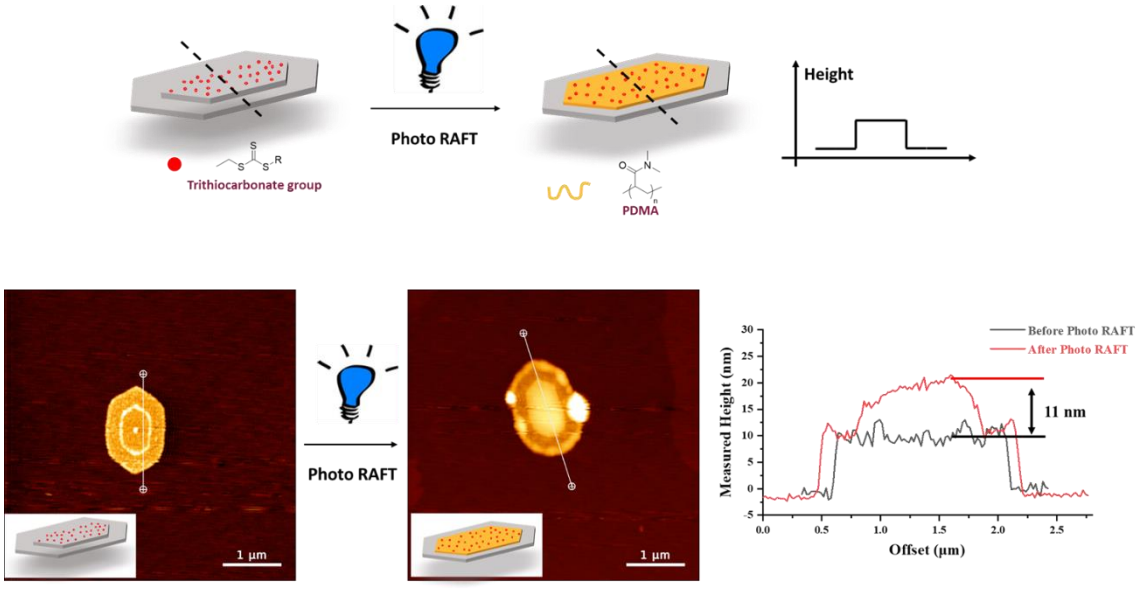


Figure 3.12 AFM images and height profiles of double-layered platelet (inner layer: RAFT layer, outer layer: nonRAFT layer) before and after photo RAFT with DMA.

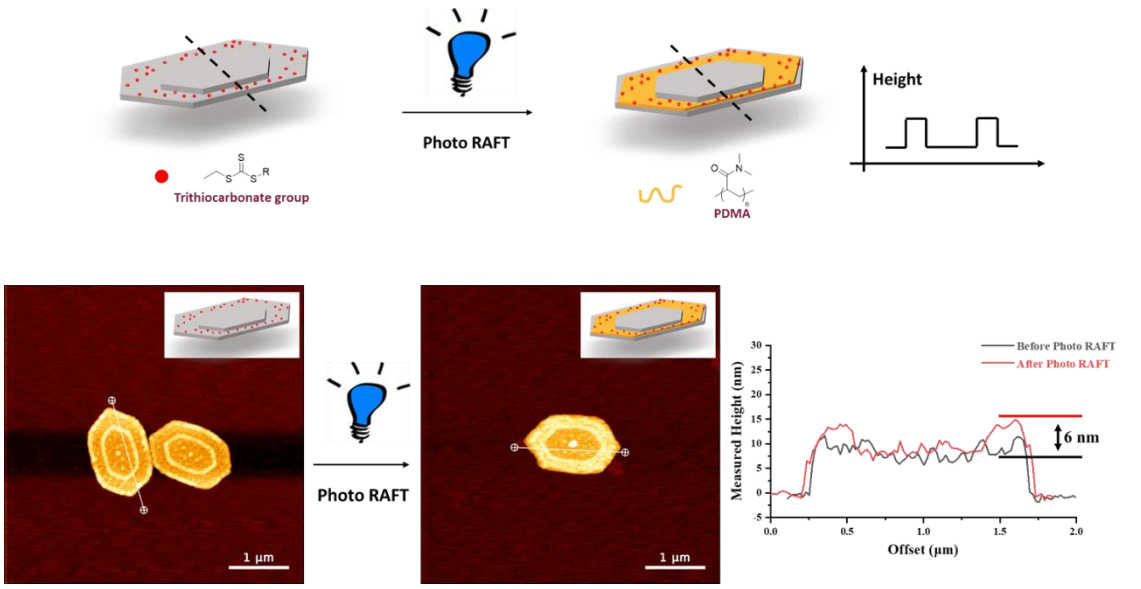
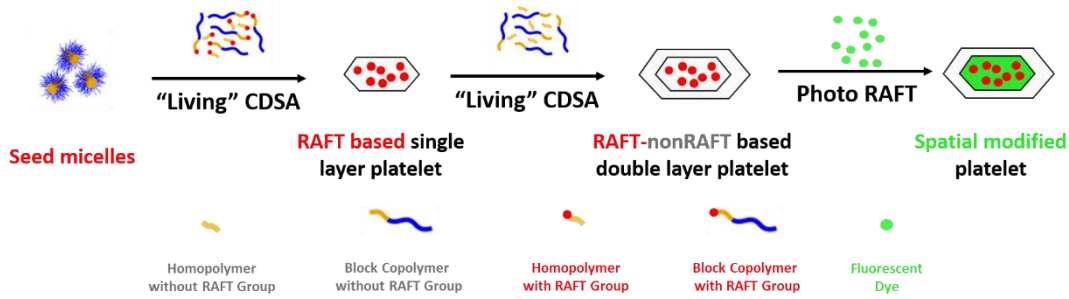


Figure 3.13 AFM images and height profiles of double-layered platelet (inner layer: nonRAFT layer, outer layer: RAFT layer) before and after photo RAFT with DMA.

3.3.5.4 Photo RAFT with Fluorescent Dye on the Surface of Multi-Layered Platelets

As a proof of concept, a fluorescent dye was incorporated by photo RAFT for *in situ* investigation of the spatially defined segregation of domains by fluorescent emission. **Scheme 3.6** shows the design of centrosymmetric block co-micelles formed by sequentially addition of RAFT and nonRAFT based polymer to a solution of seeds, and then polymerised with fluorescent dye by photo RAFT.



Scheme 3.6 Route of spatial selective functionalisation with fluorescent dye on the surface of platelets.

Visualisation by CLSM (**Figure 3.14**), the green hollow hexagonal platelets and green central-bright platelets were fabricated, proving the formation of complex hierarchical structure with spatially defined by post surface modification.

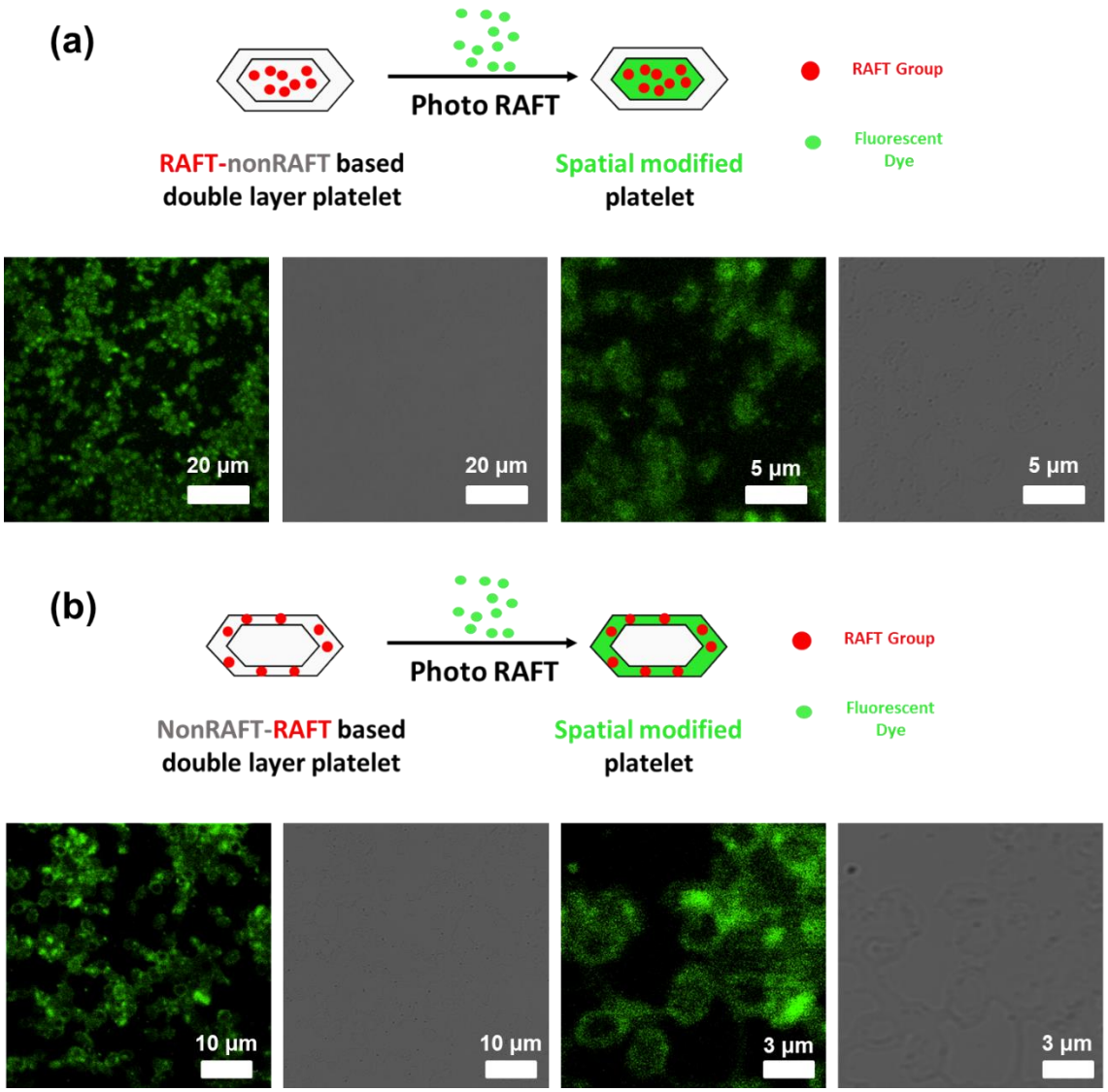


Figure 3.14 CLSM images of double-layered platelet before and after photo RAFT with fluorescent dye. (a) Inner layer: RAFT layer, outer layer: nonRAFT layer; (b) Inner layer: nonRAFT layer, outer layer: RAFT layer. (CLSM images collected by Dr. Yujie Xie.)

3.4 Conclusions

In summary, we demonstrated a facile method to modify the surface of platelets *via in situ* photo RAFT polymerisation. The post modification approach was firstly achieved on the surface of the platelets *via* photo RAFT polymerisation with DMA as a monomer and a fluorescent dye. Moreover, uniform platelets with different heights were prepared by modulating the equivalent of DMA monomer, exhibiting a good control and a linear relationship between surface growth height and concentration of DMA, up to 100 equivalents of DMA monomer.

Furthermore, through removal of the active RAFT chain end, specific double layered platelets were synthesised with a selected layer containing the RAFT group for post photo RAFT polymerisation. The segmented complex hierarchical structure could be selectively functionalised on the surface, leading to a spatially controlled change in platelets height and the introduction of fluorescent properties, offering a new route for surface modification in a controlled fashion with great selectivity.

3.5 Experimental

3.5.1 Materials

Chemicals and solvents were purchased from Sigma-Aldrich, Acros, Fluka, TCI, Fisher Chemical, Alfa Aesar or VWR. Various kinds of platelets were prepared from Chapter two. 2,2'-azobis(2-methylpropionitrile) (AIBN, 98%, Sigma Aldrich) was recrystallised twice from methanol and stored at 4 °C in the dark. N,N-dimethyl acrylamide (DMA, 99%, contains 500 ppm monomethyl ether hydroquinone as inhibitor) were purchased from Sigma Aldrich and passed through a basic alumina plug immediately to remove stabiliser before use. 1-ethylpiperidine hypophosphite (EPHP) and tributylphosphine (PBu_3) were purchased from Sigma Aldrich. Solvents were purchased from Fisher Scientific. Aminobromomaleimide (ABM) fluorescent dye was synthesised by and taken from Dr. Yujie Xie.[50]

3.5.2 Instrumentation

Light Apparatus Setup

The light source for the photo RAFT polymerisation reactions (TruOpto OSV5X3CAC1E) was purchased from Rapid Electronics and had an output power of 800 mW at 12 V DC operating at a wavelength of 400 - 410 nm. This was fitted to a custom-built setup fitted with a dimmer switch for controlling the output light intensity.

Size Exclusion Chromatography (SEC)

SEC analysis was performed on a Agilent 1260 Infinity II system fitted with RI and ultraviolet (UV) detectors ($\lambda = 309$ nm), equipped with a PLGel 3 μm (50 × 7.5 mm guard column and two PLGel 5 μm (300 × 7.5 mm) mixed-D columns, mobile phase (eluent) using $CHCl_3$ WITH 0.5% triethylamine (TEA). Molecular weight (M_w) and molecular

weight distributions ($Đ_M = M_w/M_n$) were calibrated against poly(methyl methacrylate) standards and analysed using Agilent SEC software.

Atomic Force Microscopy (AFM)

AFM samples were prepared by drop casting 10 μL of assemblies in ethanol onto mica silicon wafer which treated by Sigmacote, followed by drying naturally in air. Imaging and analysis were performed on a JPK Nanowizard 4 system in quantitative imaging (QI) mode. The tips for the AFM analysis (PPP-NCHAuD) were purchased from NANOSENSORSTM, with resonance frequency (kHz) in the window of 204 - 497 and force constant in the range of 10 - 130. The AFM pictures and data were analysed and collected using the JPK Data Processing software with QI mode. For determination of the average micelles' height at least 20 particles were analysed in each case.

Confocal Laser Scanning Microscopy (CLSM)*

FV3000 (Olympus) confocal microscope with an IX-81 inverted base (Olympus) and the 20x and 60x oil lens (Olympus) was used for imaging. The FV3000 system was driven with the FV31S-SW Viewer software platform (Olympus) with scan rates of 1 μs pixel^{-1} at 515 by 512 pixels to 1024 by 1024 pixel^{-1}.

(* The CLSM characterization were carried out by Dr.Yujie Xie)

3.5.3 Experimental procedures

3.5.3.1 Photo RAFT polymerisation on platelets surface

The DMA monomer was added into as-prepared PCL/PCL-*b*-PDMA platelets solution (1eq for weight mass) and degassed under a nitrogen flow with a rubber plug for 30 min in ice bath. Then the solution was placed in the crosslinker and irradiated with 405 nm

light under 25 °C for 4 h. The solution was then dialysed in ethanol to remove unreacted DMA monomer.

3.5.3.2 Synthesis of PCL-H

The removal of the trithiocarbonate end group was performed following procedure by Beth and Thomas et al.[51, 52] PCL, 1-ethylpiperidine hypophosphite (EPHP), tributylphosphine (PBu_3) and AIBN (molar mass ratio = 1 eq : 10 eq : 2 eq : 0.33 eq) were dissolved in DMF and degassed by three freeze-pump-thaw cycles in an ampoule. The mixture solution was stirred for 3 h at 100 °C, over the course of which the solution became colourless from yellow. After precipitating into cold diethyl ether three times and being dried under vacuum, the nonRAFT group (-H) terminated polymers as a white powder, were obtained and analyzed.

SEC (Chloroform, PMMA standard): M_n = 14.8 kg mol^{-1}, $Đ_M$ = 1.12.

3.5.3.3 Synthesis of PCL-*b*-PDMA-H

The removal of the trithiocarbonate end group was performed following procedure by Beth and Thomas et al.[51, 52] PCL-*b*-PDMA, , 1-ethylpiperidine hypophosphite (EPHP), tributylphosphine (PBu_3) and AIBN (molar mass ratio = 1 eq : 10 eq : 2 eq : 0.33 eq) were dissolved in DMF and degassed by three freeze-pump-thaw cycles in an ampoule. The mixture solution was stirred for 3 h at 100 °C, over the course of which the solution became colourless from yellow. After precipitating into cold diethyl ether three times and being dried under vacuum, nonRAFT group (-H) terminated polymers as a white powder, were obtained and analyzed.

SEC (Chloroform, PMMA standard): M_n = 35.6 kg mol^{-1}, $Đ_M$ = 1.18.

3.5.3.4 Epitaxial growth of platelets

PCL homopolymer with block copolymers PCL-*b*-PDMA, or PCL-H homopolymer with block copolymers PCL-*b*-PDMA-H dissolved in DMF (10 mg mL^{-1}) was added to a dispersion of crystalline seeds (0.01 mg mL^{-1}) and aged for 2 days before analysis by AFM.

3.5.3.5 Sequential growth of multi-layered platelets

The blend of PCL homopolymer and block copolymer PCL-*b*-PDMA (or PCL-H and PCL-*b*-PDMA-H) dissolved in THF (10 mg mL^{-1}) was added to a dispersion of as prepared platelets seeds (0.01 mg mL^{-1}) and aged for 2 days before analysis by AFM.

3.6 References

1. M. C. Arno, M. Inam, Z. Coe, G. Cambridge, L. J. Macdougall, R. Keogh, A. P. Dove and R. K. O'Reilly, *J. Am. Chem. Soc.*, 2017, **139**, 16980-16985.
2. C. E. Boott, J. Gwyther, R. L. Harniman, D. W. Hayward and I. Manners, *Nat. Chem.*, 2017, **9**, 785-792.
3. C. E. Boott, E. M. Leitao, D. W. Hayward, R. F. Laine, P. Mahou, G. Guerin, M. A. Winnik, R. M. Richardson, C. F. Kaminski, G. R. Whittell and I. Manners, *ACS Nano*, 2018, **12**, 8920-8933.
4. J. B. Gilroy, T. Gadt, G. R. Whittell, L. Chabanne, J. M. Mitchels, R. M. Richardson, M. A. Winnik and I. Manners, *Nat. Chem.*, 2010, **2**, 566-570.
5. J. B. Gilroy, D. J. Lunn, S. K. Patra, G. R. Whittell, M. A. Winnik and I. Manners, *Macromolecules*, 2012, **45**, 5806-5815.
6. Y. He, J. C. Eloi, R. L. Harniman, R. M. Richardson, G. R. Whittell, R. T. Mathers, A. P. Dove, R. K. O'Reilly and I. Manners, *J. Am. Chem. Soc.*, 2019, **141**, 19088-19098.
7. A. M. Oliver, J. Gwyther, C. E. Boott, S. Davis, S. Pearce and I. Manners, *J. Am. Chem. Soc.*, 2018, **140**, 18104-18114.
8. M. E. Robinson, D. J. Lunn, A. Nazemi, G. R. Whittell, L. De Cola and I. Manners, *Chem. Commun.*, 2015, **51**, 15921-15924.
9. L. Sun, N. Petzetakis, A. Pitto-Barry, T. L. Schiller, N. Kirby, D. J. Keddie, B. J. Boyd, R. K. O'Reilly and A. P. Dove, *Macromolecules*, 2013, **46**, 9074-9082.
10. J. R. Finnegan, X. He, S. T. G. Street, J. D. Garcia-Hernandez, D. W. Hayward, R. L. Harniman, R. M. Richardson, G. R. Whittell and I. Manners, *J. Am. Chem. Soc.*, 2018, **140**, 17127-17140.

11. T. Fukui, J. D. Garcia-Hernandez, L. R. MacFarlane, S. Lei, G. R. Whittell and I. Manners, *J. Am. Chem. Soc.*, 2020, **142**, 15038-15048.

12. X. Wang, G. Guerin, H. Wang, Y. Wang, I. Manners and M. A. Winnik, *Science*, 2007, **317**, 644-647.

13. M. C. Arno, M. Inam, A. C. Weems, Z. Li, A. L. A. Binch, C. I. Platt, S. M. Richardson, J. A. Hoyland, A. P. Dove and R. K. O'Reilly, *Nat. Commun.*, 2020, **11**, 1420.

14. Y. Cha, C. Jarrett-Wilkins, M. A. Rahman, T. Zhu, Y. Sha, I. Manners and C. Tang, *ACS Macro Lett.*, 2019, **8**, 835-840.

15. S. Ganda, M. Dulle, M. Drechsler, B. Förster, S. Förster and M. H. Stenzel, *Macromolecules*, 2017, **50**, 8544-8553.

16. X. He, M. S. Hsiao, C. E. Boott, R. L. Harniman, A. Nazemi, X. Li, M. A. Winnik and I. Manners, *Nat. Mater.*, 2017, **16**, 481-488.

17. Z. M. Hudson, C. E. Boott, M. E. Robinson, P. A. Rupar, M. A. Winnik and I. Manners, *Nat. Chem.*, 2014, **6**, 893-898.

18. S. Pearce, X. He, M.-S. Hsiao, R. L. Harniman, L. R. MacFarlane and I. Manners, *Macromolecules*, 2019, **52**, 6068-6079.

19. C. N. Jarrett-Wilkins, R. A. Musgrave, R. L. N. Hailes, R. L. Harniman, C. F. J. Faul and I. Manners, *Macromolecules*, 2019, **52**, 7289-7300.

20. X. Li, Y. Gao, R. Harniman, M. Winnik and I. Manners, *J. Am. Chem. Soc.*, 2016, **138**, 12902-12912.

21. L. Jia, A. Petretic, G. Molev, G. Guerin, I. Manners and M. A. Winnik, *ACS Nano*, 2015, **9**, 10673-10685.

22. X. H. Jin, M. B. Price, J. R. Finnegan, C. E. Boott, J. M. Richter, A. Rao, S. M. Menke, R. H. Friend, G. R. Whittell and I. Manners, *Science*, 2018, **360**, 897-900.

23. E. L. Kynaston, A. Nazemi, L. R. MacFarlane, G. R. Whittell, C. F. J. Faul and I. Manners, *Macromolecules*, 2018, **51**, 1002-1010.

24. G. Rizis, T. G. van de Ven and A. Eisenberg, *Angew. Chem. Int. Ed.*, 2014, **53**, 9000-9003.

25. D. Tao, Z. Wang, X. Huang, M. Tian, G. Lu, I. Manners, M. A. Winnik and C. Feng, *Angew. Chem. Int. Ed.*, 2020, **59**, 8232-8239.

26. J. Xu, H. Zhou, Q. Yu, G. Guerin, I. Manners and M. A. Winnik, *Chem. Sci.*, 2019, **10**, 2280-2284.

27. Q. Yu, M. G. Roberts, S. Pearce, A. M. Oliver, H. Zhou, C. Allen, I. Manners and M. A. Winnik, *Macromolecules*, 2019, **52**, 5231-5244.

28. H. Qiu, G. Cambridge, M. A. Winnik and I. Manners, *J. Am. Chem. Soc.*, 2013, **135**, 12180-12183.

29. A. Nazemi, X. He, L. R. MacFarlane, R. L. Harniman, M. S. Hsiao, M. A. Winnik, C. F. Faul and I. Manners, *J. Am. Chem. Soc.*, 2017, **139**, 4409-4417.

30. H. Qiu, Y. Gao, C. E. Boott, O. E. Gould, R. L. Harniman, M. J. Miles, S. E. Webb, M. A. Winnik and I. Manners, *Science*, 2016, **352**, 697-701.

31. H. Qiu, Z. M. Hudson, M. A. Winnik and I. Manners, *Science*, 2015, **347**, 1329-1332.

32. I. S. Yang, M. R. Sohn, S. D. Sung, Y. J. Kim, Y. J. Yoo, J. Kim and W. I. Lee, *Nano Energy*, 2017, **32**, 414-421.

33. J. H. Heo, D. H. Song and S. H. Im, *Adv. Mater.*, 2014, **26**, 8179-8183.

34. T. Ozel, B. A. Zhang, R. Gao, R. W. Day, C. M. Lieber and D. G. Nocera, *Nano Lett.*, 2017, **17**, 4502-4507.

35. C. Yan, J. Huang, K. Sun, S. Johnston, Y. Zhang, H. Sun, A. Pu, M. He, F. Liu, K. Eder, L. Yang, J. M. Cairney, N. J. Ekins-Daukes, Z. Hameiri, J. A. Stride, S. Chen, M. A. Green and X. Hao, *Nat. Energy*, 2018, **3**, 764-772.

36. G. Sun, S. Cho, C. Clark, S. V. Verkhoturov, M. J. Eller, A. Li, A. Pavia-Jimenez, E. A. Schweikert, J. W. Thackeray, P. Trefonas and K. L. Wooley, *J. Am. Chem. Soc.*, 2013, **135**, 4203-4206.

37. W. Zong, G. W. Li, J. M. Cao, X. Lei, M. L. Hu, H. Sun, C. Griesinger and R. X. Tan, *Angew. Chem. Int. Ed.*, 2016, **55**, 3690-3693.

38. O. Azzaroni, A. A. Brown and W. T. Huck, *Angew. Chem. Int. Ed.*, 2006, **45**, 1770-1774.

39. O. Roling, L. Stricker, J. Voskuhl, S. Lamping and B. J. Ravoo, *Chem. Commun.*, 2016, **52**, 1964-1966.

40. B. T. Seymour, R. A. E. Wright, A. C. Parrott, H. Gao, A. Martini, J. Qu, S. Dai and B. Zhao, *ACS Appl. Mater. Interfaces*, 2017, **9**, 25038-25048.

41. A. Synytska, E. Svetushkina, D. Martina, C. Bellmann, F. Simon, L. Ionov, M. Stamm and C. Creton, *Langmuir*, 2012, **28**, 16444-16454.

42. R. A. Wright, K. Wang, J. Qu and B. Zhao, *Angew. Chem. Int. Ed.*, 2016, **55**, 8656-8660.

43. H. Yamaguchi, M. Kikuchi, M. Kobayashi, H. Ogawa, H. Masunaga, O. Sakata and A. Takahara, *Macromolecules*, 2012, **45**, 1509-1516.

44. B. A. Humphreys, E. J. Wanless and G. B. Webber, *J. Colloid Interface Sci.*, 2018, **516**, 153-161.

45. F. Polzer, D. A. Kunz, J. Breu and M. Ballauff, *Chem. Mater.*, 2010, **22**, 2916-2922.

46. F. Li, A. Thevenon, A. Rosas-Hernandez, Z. Wang, Y. Li, C. M. Gabardo, A. Ozden, C. T. Dinh, J. Li, Y. Wang, J. P. Edwards, Y. Xu, C. McCallum, L. Tao, Z. Q. Liang, M. Luo, X. Wang, H. Li, C. P. O'Brien, C. S. Tan, D. H. Nam, R. Quintero-Bermudez, T. T. Zhuang, Y. C. Li, Z. Han, R. D. Britt, D. Sinton, T. Agapie, J. C. Peters and E. H. Sargent, *Nature*, 2020, **577**, 509-513.

47. J. Cai, C. Li, N. Kong, Y. Lu, G. Lin, X. Wang, Y. Yao, I. Manners and H. Qiu, *Science*, 2019, **366**, 1095-1098.

48. Q. Fu, T. G. McKenzie, J. M. Ren, S. Tan, E. Nam and G. G. Qiao, *Sci. Rep.*, 2016, **6**, 20779.

49. J. E. Poelma, B. P. Fors, G. F. Meyers, J. W. Kramer and C. J. Hawker, *Angew. Chem. Int. Ed.*, 2013, **52**, 6844-6848.

50. Y. Xie, J. T. Husband, M. Torrent-Sucarrat, H. Yang, W. Liu and R. K. O'Reilly, *Chem. Commun.*, 2018, **54**, 3339-3342.

51. T. D. Michl, K. E. S. Locock, N. E. Stevens, J. D. Hayball, K. Vasilev, A. Postma, Y. Qu, A. Traven, M. Haeussler, L. Meagher and H. J. Griesser, *Polym. Chem.*, 2014, **5**, 5813-5822.

52. B. L. Moore, A. Lu, D. A. Longbottom and R. K. O'Reilly, *Polym. Chem.*, 2013, **4**.

Chapter Four – Conclusions and Outlook

In this thesis, we precisely designed a series of poly(*ε*-caprolactone)-based 2D assemblies *via* living CDSA and achieved the selective surface modification for 2D platelets using photo RAFT polymerisation. The self-assembly PCL-based 2D micelles was investigated with high level of control. It has been proved that precisely controlled platelets could be obtained by varying the addition of unimer-to-seed ratio. Multi-layered platelet-like co-micelles were prepared by sequential addition of PCL-based blend unimers to the 1D or 2D precursors. Subsequently, the PCL-based polymers were modified to attach a fluorescent dye, spatially altering the platelets surface. Such designed approach offers a customizable 2D polymeric platform with controlled size and surface chemistry for applications in fluorescent imaging, biocompatible/biodegradable carriers and nanotechnologies/engineering areas.

We then expanded the scope of surface modification on the PCL-based platelets *via* the photo RAFT polymerisation technique. It was demonstrated that the height of the assemblies could be precisely tuned. A fluorescent monomer could be polymerised using the same strategy allowing readily tracking of the platelets by CSLM. More importantly, specific regions of platelet could be spatially selectively functionalised. As a general and adaptable *in-situ* modification approach, it is potentially interesting to further explore the different heterogeneous monomers with a diverse range of chemistries/functional groups which could open the doors to applications in biology, energy, and information storage.

Several questions raised in this thesis remain to be answered. The behaviour and kinetic of platelets assembly needs to be better understand, in order for the full manipulation of the assemblies in morphology and size. In addition, the affecting factor of surface polymerisation and the reason of limited compatibility to different monomers needs further explored. A more complete understanding of mechanism of surface modification may allow it to be overcome.